THE PERFORMANCE OF TUNED LIQUID DAMPERS WITH DIFFERENT TANK GEOMETRIES

THE PERFORMANCE

OF TUNED LIQUID DAMPERS WITH DIFFERENT TANK GEOMETRIES

By

XIAOCONG DENG, B.Eng.

A Thesis

Submitted to the School of Graduate Studies

in Partial Fulfillment of the Requirements

for the Degree

Master of Applied Science

McMaster University

MASTER OF APPLIED SCIENCE (2007) McMaster University

(Civil Engineering) Hamilton, Ontario

TITLE: The Performance of Tuned Liquid Dampers with Different Tank Geometries

AUTHOR: Xiaocong Deng, B.ENG. (McMaster University)

SUPERVISOR: Dr. Michael J. Tait

NUMBER OF PAGES: xvi, 178

Abstract

Tuned Liquid Dampers (TLDs) are increasingly being used to suppress the dynamic vibration of tall buildings. An equivalent mechanical model is essential for rapid analysis and design of a TLD. The most common TLD tank geometries are circular, annular and rectangular. Rectangular tanks are utilized for 1-D and 2-D TLDs, whereas circular and annular are usually applied to axisymmetric structures. The amount of fluid that participates in the sloshing motion is directly influenced by the tank geometry. Although not commonly used, a TLD having a curved-bottom tank is expected to perform more effectively due to its relatively large value of effective mass. The main objective of this study is to develop mechanical models for seven TLDs with different tank geometries including the curved-bottom case, and to theoretically investigate the performance of rectangular, vertical-cylindrical and horizontal-cylindrical TLDs.

Potential flow theory, linear long wave theory, Lagrange's equations and virtual work method are employed to develop the equivalent mechanical model parameters of TLDs with rectangular, vertical-cylindrical, horizontal-cylindrical, hyperboloid, triangular, sloped-bottom, and parabolic tank geometries. A rectangular, vertical-cylindrical and horizontal-cylindrical TLD are selected for further study using a single-degree-of-freedom (SDOF) model and a two degree of freedom structure-TLD system model applying the derived equivalent mechanical parameters.

The dynamic characteristics of the TLDs as a SDOF system are investigated. The mechanical model is verified by comparing calculated values with experimental results for a rectangular TLD. The free surface motion, sloshing force and energy dissipation are

found to be dependent upon the excitation amplitude. Analytical results also indicate that the horizontal-cylindrical TLD possesses the greatest normalized sloshing force and energy dissipation among the TLDs considered.

The performances of various TLDs installed in a structure are studied in terms of effective damping, efficiency and robustness. Tuning ratio, structural response amplitude, mass ratio and liquid depth are adjusted to investigate their affect on the performance of the studied TLDs. Performance charts are developed and subsequently used to present the results. It is found that small liquid depth ratio and large mass ratio can lead to a robust structure-TLD system with small relative motion ratio between the structure and the vibration absorber. Comparisons of performance between the three TLDs are made and it can be concluded that the horizontal-cylindrical TLD is the most robust and effective device with the smallest relative motion ratio.

KEYWORDS: Conical, Dynamic Vibration Absorber, Horizontal-Cylindrical, Hyperboloid, Liquid Sloshing, Mechanical Model, Parabolic, Rectangular, Structure-TLD System, Structural Vibration Sloped-Bottom, Tank, Triangular, Tuned Liquid Damper, Vertical-Cylindrical

Acknowledgements

I would like very much to express my gratitude to my supervisor, Dr. Michael Tait for his support, guidance and encouragement throughout this study.

I would like to thank my colleagues, Marcus Cassolato and Jamie Hamelin for their helpful discussions and support.

I would like to acknowledge the financial support and scholarship provided by the Civil Engineering Department and the Centre for Effective Design of Structures.

To my parents, grandma, niece, brother and sister, thank you for your continuous and unconditional love.

To my good friends, Shou-Jin, Jian, Li-Li, Yu-Jian and Zhi-Xin, thank you for your support and encouragement.

Table of Contents

List of Tables

List of Figures

Nomenclature

List of Symbols

a	Radius of a vertical-cylindrical tank and geometrical parameter related to liquid depth for a horizontal-cylindrical tank
b	Tank width
C_L	Loss coefficient
c^*	Generalized damping of a TLD
E_d	Energy dissipation by sloshing liquid
F_d	Sloshing force
g	Gravitational acceleration
H	Height measured from the free surface to the x-axis of a horizontal-cylindrical tank
h	Liquid depth
$J_i()$	Bessel function of order i
j	Number of screen(s)
k^*	Generalized stiffness of a TLD
KE	Kinetic energy
L	Tank length
M^*	Generalized mass of the primary structure
m_w	Total liquid mass
m^*	Generalized mass of a TLD
m_0	Non-participating portion of liquid mass
m_{eff}	Effective mass of the liquid
n	Integer value associated with different modes/ harmonics
PE	Potential energy
q_0	Wave amplitude at the end-walls (Generalized coordinate)
R	Radius of a horizontal-cylindrical and radius of the free surface for a hyperboloid tank
R_η	Relative motion ratio between the structure and dynamic vibration absorber

S Damping screen solidity ratio

s Length of sloping region (slope-bottom tank)

T Period of excitation

u Horizontal velocity component

w Vertical velocity component

X Horizontal displacement excitation

X_0 Horizontal excitation amplitude

x_j Damping screen location

β Forcing frequency ratio

ζ TLD damping ratio (% critical)

ζ_{eff} Effective damping ratio (% critical)

ζ_{eq} Equivalent viscous damping ratio (% critical)

$\zeta_{eff\text{-}opt}$ Optimum effective damping ratio (% critical)

ζ_s Structural effective damping ratio (% critical)

η Free surface amplitude (wave height from still water level)

λ Frequency parameters for a horizontal-cylindrical tank

μ Mass ratio

μ_w Total mass ratio

σ_s RMS structural response motion

$\sigma_{s\text{-}target}$ RMS target structure response motion

σ_η RMS free surface motion

ϕ Velocity potential

Ψ Efficiency

Ω Tuning ratio

ω Excitation frequency

Subscripts

r Rectangular TLD

vc Vertical-cylindrical TLD

hc	Horizontal-cylindrical TLD
h	Hyperboloid TLD
t	Triangular TLD
s	Sloped-bottom TLD
p	Parabolic TLD
eff	Effective
opt	Optimal
w	Water

Superscript

*	Generalized property

Chapter 1 Introduction and Literature Review

1.1 Introduction

Slender, flexible and lightly damped structures are often sensitive to dynamic excitation, such as wind and earthquake forces, which can result in an unacceptably large dynamic response. Various serviceability limit state criteria have been proposed to limit wind-induced building accelerations. For instance, NBCC (2005) indicates that 10 to 30 milli-g has been generally considered as an acceptable range for one-in-ten-year average hourly peak accelerations for many tall buildings. Different devices have been employed to suppress wind-induced vibrations in order to satisfy serviceability limit state criteria. They include passive, semi-active and active control energy dissipating devices. A dynamic vibration absorber (DVA), which reduces the dynamic response of a structure by modifying its frequency response behaviour, belongs to the category of passive control energy dissipating devices.

1.1.1 Tuned Mass Damper

A commonly used type of DVA is the tuned mass damper (TMD), which consists of a mass, a spring and a dashpot as shown in Figure 1.1a, where the structure is represented by a single-degree-of-freedom (SDOF) system with mass, M_s, stiffness, K_s, and damping ratio, ζ_s. The natural frequency of a TMD is tuned to the natural frequency of the structure so that when the structure is at resonance the TMD vibrates out of phase, thus exerting an inertial force onto the primary structure anti-phase to the excitation force, which suppresses the structure's motion. In order to minimize the response of a structure

under external excitation, a TMD must be properly designed. The optimal design parameters for a linear TMD attached to an undamped structure are well-understood and formulated (Warburton 1982). The performance of a TMD can be evaluated in terms of effective damping, ζ_{eff}, which is a function of the tuning ratio, Ω, mass ratio, μ, and damping ratio, ζ_A, of a structure-TMD system. The tuning ratio equals the natural frequency of the damper divided by the natural frequency of the structure. The mass ratio is the ratio of the mass of the damper to the mass of the structure. Figures 1.2a to 1.2c show the relationship between the effective damping and these three parameters, respectively. It can be seen in Figure 1.2a that the level of effective damping increases as the mass ratio is increased. Figure 1.2b is the variation of ζ_{eff} with Ω for an optimally damped TMD and Figure 1.2c is the variation of ζ_{eff} with ζ_A for an optimally tuned TMD, for a particular mass ratio value. These plots show that the mass ratio, tuning ratio and damping ratio significantly influence the performance of a TMD. Figure 1.3 shows performance charts of the effective damping and root-mean-square (RMS) relative motion ratio, respectively, for a linear TMD, as functions of Ω and ζ_A for a particular value of μ. RMS relative motion ratio is defined as the ratio of the RMS motion between the absorber and the primary structure. These charts allow the performance of a TMD to be rapidly examined. In this study, the performance of a DVA is evaluated by effective damping, efficiency and robustness. Effective damping of a DVA is defined as the additional damping provided by the DVA to a SDOF system with the same dynamic properties as the original primary structure of the structure-DVA system (Vickery and Davenport 1970). Efficiency of a DVA is defined here as the ratio of effective damping of a DVA to

that of an equivalent optimized linear TMD with the same liquid mass ratio. Robustness is defined as the insensitivity of efficiency or effective damping to variations in the tuning ratio and (or) level of applied excitation.

Applications of TMDs include the Centerpoint Tower in Sydney (Australia), the Canadian National (CN) Tower in Toronto, the John Hancock Tower in Boston, the Citicorp Center in New York and Shenzhen Bridge in Hong Kong. In addition, a total of 11 applications of TMD installations in Japan have been reported on (Tamura 1998).

1.1.2 Tuned Liquid Damper

Another type of DVA is the tuned liquid damper (TLD). It is increasingly being used to suppress the resonant motion of tall buildings due to its low cost, ease of implementation and efficiency. The TLD was first employed in 1902 by Frahm to reduce the rolling motion of large ships (Den Hartog 1956), and has also been applied to space satellites (Carrier and Miles 1960). Research on the application of TLDs to civil engineering structures began in the 1980s (Bauer 1984, Modi and Welt 1987, Kareem and Sun 1987). A TLD, shown in Figure 1.1b, is a rigid tank that is partially filled with a liquid (often water). The liquid in a TLD supplies not only the mass, but also the damping through viscous action at the interface of tank and liquid. Additionally, gravity of the liquid acts as an equivalent spring. As a TLD and TMD are both dynamic vibration absorbers, they mitigate dynamic motion by modifying the frequency response of a structure. Figure 1.4 shows the frequency response of both a structure and a structure-TLD system. It can be seen from Figure 1.4 that the resonant response is significantly reduced after a TLD is installed in the structure. For random excitation, the effective

damping is determined by equating the area under the frequency response function of a structure-TLD system to that of an equivalent SDOF system (see Figure 1.1c). As shown earlier in Figure 1.2a, an increase in the mass ratio leads to an increase in the effective damping. As a result, it reduces the area under the frequency response function, which is related to the RMS response of the structure. However, not all the liquid in a TLD tank participates in the sloshing motion, which results in a reduction in the mass ratio. One way to resolve this problem is to modify the tank geometry of the TLD. The most common TLD tank geometries are vertical-cylindrical, annular and rectangular (Modi and Welt 1987, Kareem and Sun 1987). Another type of liquid damper widely studied is tuned liquid column damper (TLCD) (Xu et al.1992) as shown in Figure 1.5.

Based on potential flow theory, the velocity profile of sloshing liquid in a rectangular tank is obtained. The dimensionless velocity at different locations of a tank is shown in Figure 1.6. As a curved-bottom tank possesses a larger effective mass by reducing the inactive water near the tank end-walls, it is postulated that a TLD with a curved-bottom tank may be a more effective vibration absorber compared to a rectangular tank (Gardarsson et al. 2001). Similar to a TMD, the damping ratio of a TLD influences the effective damping. The inherent damping of a TLD indicates the amount of energy the TLD can dissipate. Usually the inherent damping is significantly lower than the optimal damping value that permits the effective damping to achieve its maximum value. For small excitation amplitudes, an effective way to achieve optimal damping is to insert screens inside the TLD tank. The addition of screens has been considered for both rectangular and vertical-cylindrical TLDs.

TLD applications include The Suites at 1 King West in Toronto, Nanjing TV Tower in China and the European Court of Justice in Luxembourg. In addition, Tamura (1998) documented a total of 12 TLD applications in Japan. Full-scale monitoring of the wind-induced response of four buildings equipped with TLDs has been conducted, and the results show that TLDs can significantly improve the serviceability of tall buildings (Tamura 1995).

1.2 Literature Review

TMD theory is not directly applicable to TLD analysis and design due to its nonlinear response behaviour. Initial research on TLDs began with the development of analytical models, which can simulate the dynamic response of a TLD and a structure-TLD system. In addition, equivalent mechanical models of TLDs were constructed to simplify the complex sloshing motion inside the tank and to allow the application of TMD theory.

1.2.1 Analytical Models

1.2.1.1 Shallow Water Tuned Liquid Dampers

In early TLD applications, shallow water depths were utilized to resolve the problem of insufficient inherent damping induced by the boundary layers. Shallow water depths introduce wave breaking, which results in significant energy dissipation leading to, or even exceeding, the required amount of damping. A number of analytical models for shallow water TLDs were developed based on nonlinear long wave theory, which is able to capture the nonlinear dynamic response behaviour. The governing equations of wave

motion are simplified by integrating or averaging through the liquid depth (Shimizu and Hayama 1987, Lepelletier and Raichlen 1988). Fujino (1992) utilized Shimizu and Hayama's model to study the response of a structure-TLD system, and Sun (1992) expanded on this model by incorporating the influence of wave breaking. The drawback of the shallow water TLD is that a large number of TLDs are required to achieve a sufficient mass ratio and the response behaviour of the TLD is highly nonlinear.

Alternative strategies and devices have been studied to increase the inherent damping of TLDs, such as using high viscosity liquid, adding floating surface particles and inserting energy dissipating devices (Isaacson and Premasiri 2001, Ju 2004). Fediw et al. (1995) modelled a TLD equipped with screens by dividing the TLD into a number of subtanks. In this model, the governing equations for linear long wave theory are solved by applying the boundary condition of equal velocity and head loss at the screen. Kaneko and Ishikawa (1999) developed a model of a TLD with a submerged net, based on nonlinear long wave theory introduced by Lepelletier and Raichlen (1988). Staggered-grid finite-difference and Runge-Kutta methods were applied to compute the average horizontal velocity component and the wave height, taking the effect of a submerged net into consideration. It was found that the nonlinear model can capture the dynamic response of a TLD over a large range of excitation amplitudes (Tait 2004).

1.2.1.2 Intermediate and Deep Water Tuned Liquid Dampers

The response behaviour of intermediate and deep water TLDs is more linear than that of shallow water TLDs, however, less liquid participates in the sloshing motion and the inherent damping decreases. Thus, energy dissipating devices are usually required to

provide sufficient damping. In order to resolve the problem of reduced mass ratio, due to the loss of participating liquid, the geometry of a TLD can be modified. Potential flow theory is often utilized to describe the sloshing motion in intermediate and deep water TLDs. Coupled mode nonlinear simultaneous ordinary differential equations for sloshing motion in both a rectangular (Kaneko and Yoshida, 1999) and vertical-cylindrical TLD (Kaneko and Mizota, 1999) were formulated, taking into account a submerged net at the centre of the TLD. In these two models, the Galerkin method was applied to obtain the sloshing force. Energy dissipation due to the submerged net was obtained by using the relationship between the pressure loss, wave height and the average horizontal velocity component at the net.

With the assumption of small wave amplitude, the nonlinear terms in the governing equations of sloshing motion can be neglected and a simple approach to investigate sloshing motion in a tank is attained. Budiansky (1960) applied Lagrange's equations to formulate the generalized properties of the sloshing motion in a horizontal-cylindrical tank. Warnitchai and Pinkaew (1998) applied the same technique to develop a mathematical model of liquid sloshing in a rectangular tank, which includes the effects of an energy dissipating device at the centre of the tank, assuming viscous and velocity squared damping. All of the analytical models mentioned above can be used to evaluate the response wave amplitude, sloshing force and energy dissipation of a TLD.

1.2.2 Equivalent Mechanical Models

Equivalent mechanical models of the liquid dynamics inside a rigid tank include mass-spring dashpot and pendulum models (Graham 1951 and 1952, and Bauer 1960,

1961 and 1962). Simple equivalent mechanical models of TLDs are essential for the preliminary design and investigation of their performance. Although the properties of TLDs are amplitude dependent, they have been successfully studied using linear TMD analogy.

1.2.2.1 Semi-empirical Equivalent Mechanical Models

Several semi-empirical equivalent mechanical models have been developed. Sun et al. (1995) determined the nonlinear properties of a TLD, which include the natural frequency, effective mass and damping, using the concept of virtual mass and virtual damping. Yu (1999) constructed a model with nonlinear damping, nonlinear stiffness and constant mass, based on energy dissipation equivalence of experimental and theoretical results. Tait (2004) expanded on this model to permit the evaluation of the amplitude dependent effective mass and the damping due to a number of energy dissipating devices inside the tank.

1.2.2.2 Theoretical Equivalent Mechanical Models

Equivalent mechanical models of TLDs are also developed theoretically without the need of conducting any shaking table experiments. Graham and Rodriguez (1952) constructed an equivalent mechanical model of the fluid sloshing motion inside a rectangular tank. This model consists of a rigid mass representing the inactive portion of the liquid and a series of masses and springs representing the equivalent mass and stiffness of each sloshing mode. The natural frequency is obtained using potential flow theory, while the properties of the mechanical model are obtained by equating the force

exerted by the mechanical system to the pressure forces exerted by the liquid inside the tank. Similarly, Bauer (1964) constructed an equivalent mechanical model for a vertical-cylindrical tank. In the 1990s, theoretical equivalent mechanical models of various TLDs emerged. Chang and Qu (1998) calculated the generalized properties for a number of different dynamic vibration absorbers and developed models to evaluate the performance of the corresponding structure-TLD systems. However, no energy dissipating devices were included in these models. Cai et al. (1999) introduced a model of a vertical-cylindrical TLD with baffles. In this model, the effective mass is obtained by matching the kinetic energy of the sloshing motion to that of the equivalent mechanical model; while the damping due to the baffles is formulated using virtual work principles. Recently, Tait (2007) extended Warnitchai's approach by permitting the evaluation of the damping due to multiple energy dissipating devices at any location inside a rectangular tank using the concept of virtual work. In addition, a co-ordinate relationship was applied to convert the generalized TLD properties to equivalent properties for developing an equivalent TLD mechanical model and a structure-TLD model, which are capable of simulating the dynamic response of a TLD and a structure-TLD system, respectively, under random or sinusoidal excitation.

1.2.3 Application of TMD Theory to TLD

It is noted that the equivalent mechanical model and simplification of damping (linearization of the velocity squared damping and neglecting viscous damping) (Tait 2007) result in the applicability of the optimal design criteria for the well-studied TMD to a TLD. Earlier, Chang and Qu (1998) applied similar concepts to formulate optimum

parameters of various types of DVAs with no energy dissipating devices. Linearization of nonlinear damping has been performed for several different types of DVAs. Gao and Kwok (1997) linearized the velocity squared damping of a TCLD equipped with an orifice by minimizing the error between the linear and nonlinear damping forces. Vickery et al. (2001) linearized the velocity squared damping and constant force damping by matching the energy dissipation rate to that of a linear viscously damped SDOF system. Before the concepts of linearization of damping and equivalent mechanical modelling were introduced, the optimum damping of a TLD was studied both experimentally and analytically. Fujino et al. (1988) found that there exists an optimal damping that minimizes the response of the structure by conducting experiments on a structure-TLD system, using liquids with different viscosities. Gao and Kwok (1997) conducted a parametric study using a numerical search technique to determine the optimal values of tuning ratio and damping ratio for a structure-TLCD system.

A theoretical equivalent mechanical model, which can simulate the response of a TLD with different tank geometries and energy dissipating devices under different types of loading, is of interest. This particular type of model for a TLD permits the direct application of TMD theory. Therefore, it is essential for rapid design and preliminary investigation of TLD performance. However, such models are not currently available, except for a rectangular TLD (Tait 2007). In addition, most of the modelling focuses on sinusoidal excitation. In this thesis, TLDs under both sinusoidal and random excitation will be studied.

1.3 Research Scope and Objectives

An equivalent mechanical model of a rectangular TLD with inserted screens has been developed (Tait 2007) and is adopted here. In this thesis, equivalent mechanical models for TLDs with different tank geometries are developed using potential flow theory and linear long wave theory, respectively, under the assumption of small response amplitude. In addition, the performance of rectangular, vertical-cylindrical and horizontal-cylindrical TLDs is investigated theoretically for a structure-TLD system under random excitation.

1.4 Organization of Thesis

Chapter 2 presents the derivation of the properties of an equivalent mechanical model for TLDs with commonly used and new tank geometries applying potential flow theory, Lagrange's equations, Morison's formula and the method of virtual work. Subsequently, the effective mass, damping ratio and natural frequency of each TLD are studied and compared.

Chapter 3 presents the derivation of the properties of an equivalent mechanical model for a triangular, sloped-bottom, parabolic and rectangular TLD based on linear long wave theory. Comparisons of the TLD properties are subsequently made.

Chapter 4 reports the dynamic characteristics of a rectangular, vertical-cylindrical and horizontal-cylindrical TLD as an SDOF system excited sinusoidally. Dynamic characteristics—response amplitude, sloshing force and energy dissipation—of a TLD are investigated first, followed by comparisons of their dynamic response behaviour.

Chapter 5 investigates the performance of three TLDs for a structure-TLD system under random excitation in terms of effective damping, efficiency and robustness. The effects of the various parameters on the performance of the TLDs are examined, and comparisons of TLD performance are made.

Chapter 6 presents the major conclusions drawn from this research work and recommendations for future studies on TLDs.

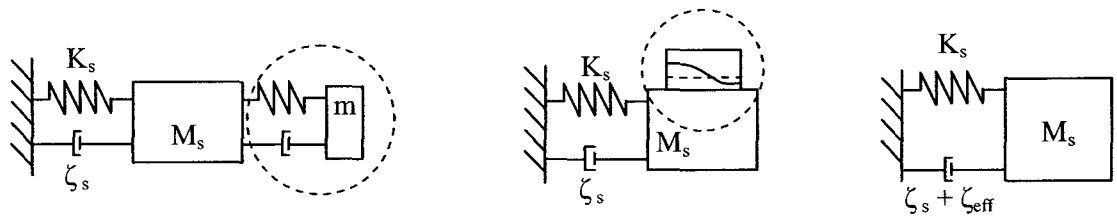

Figure 1.1 (a) TMD (b) TLD (c) Equivalent SDOF System

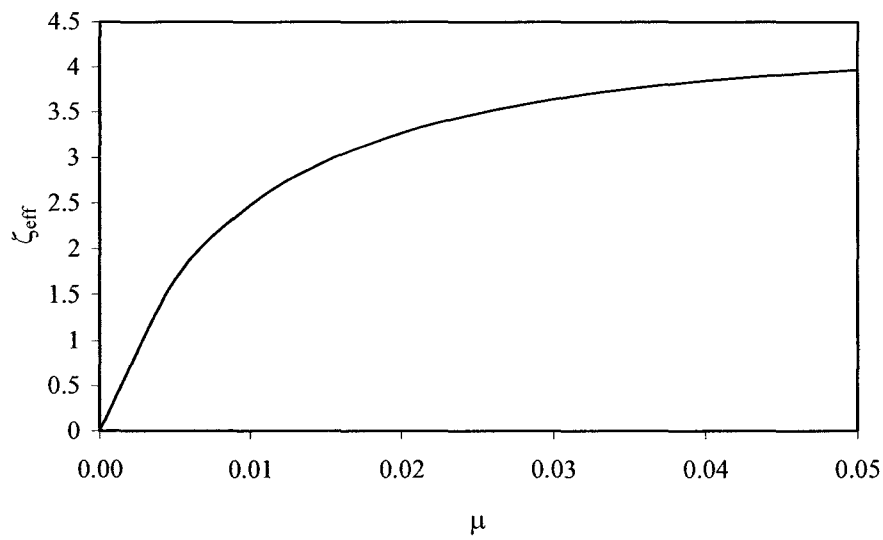

(a)

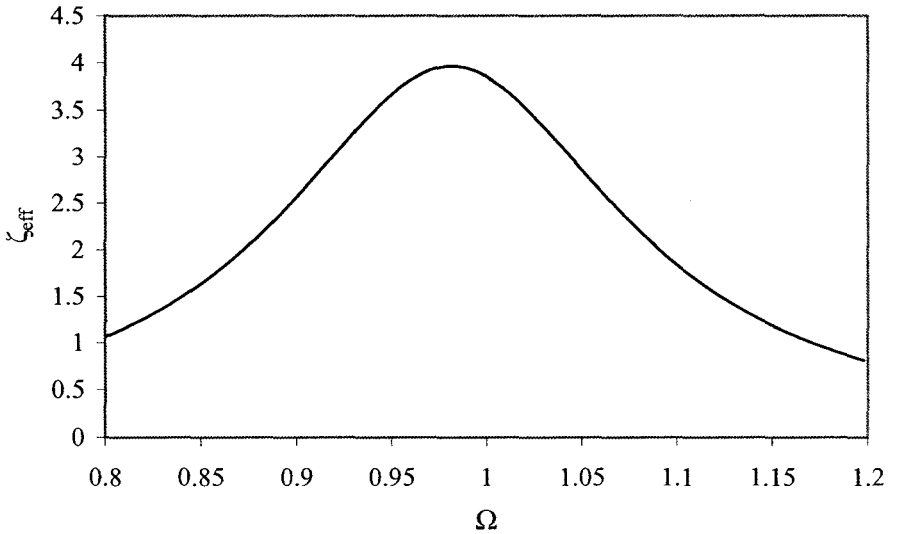

(b)

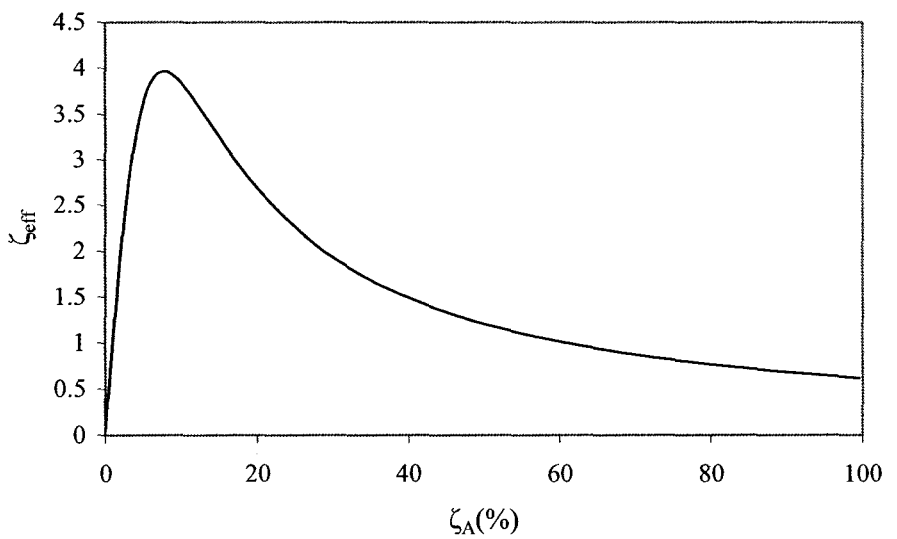

(c)

Figure 1.2 Influence of μ, Ω and ζ_A on ζ_{eff}

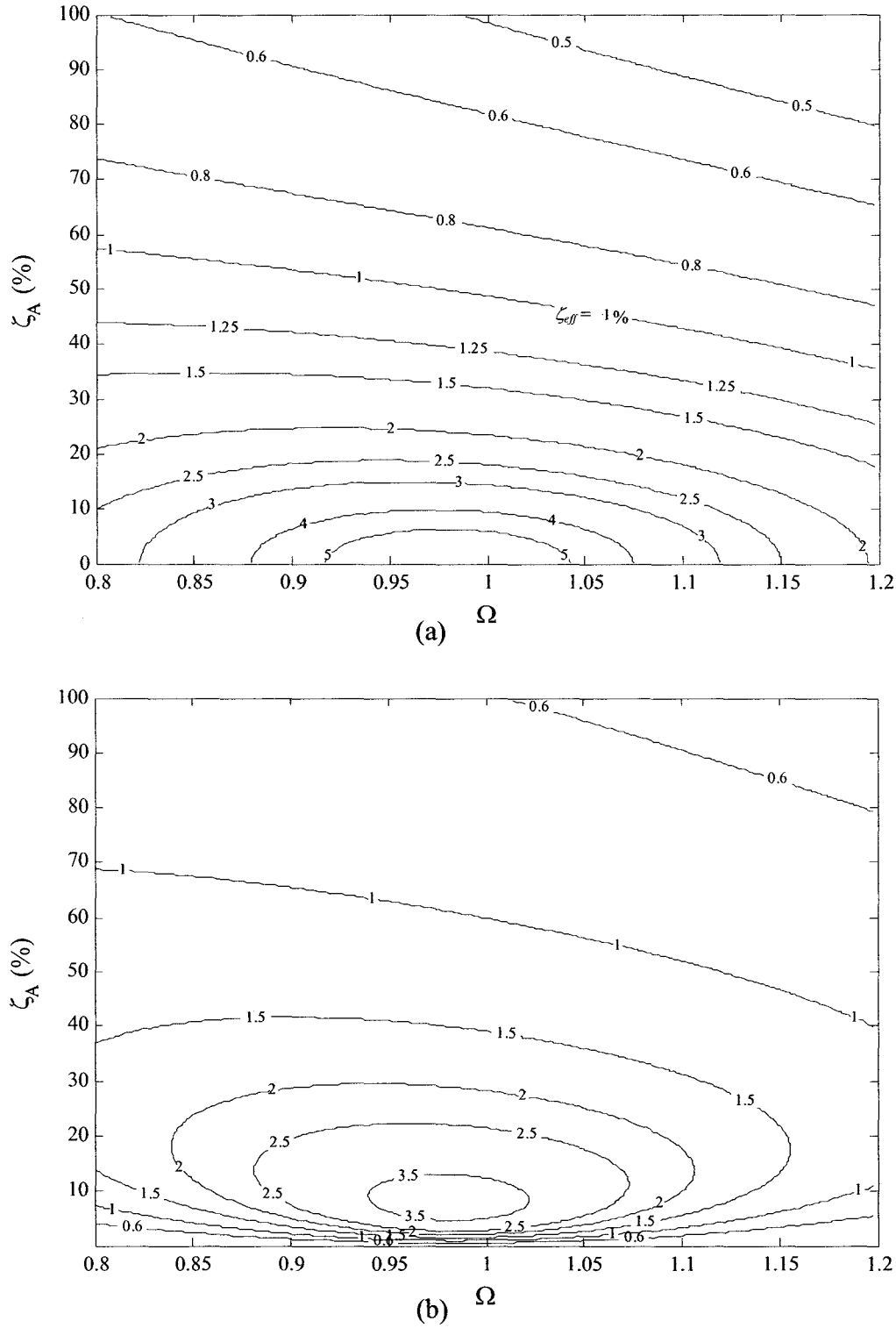

Figure 1.3 Performance Chart (a) ζ_{eff} (b) RMS Relative Motion Ratio (μ=0.025)

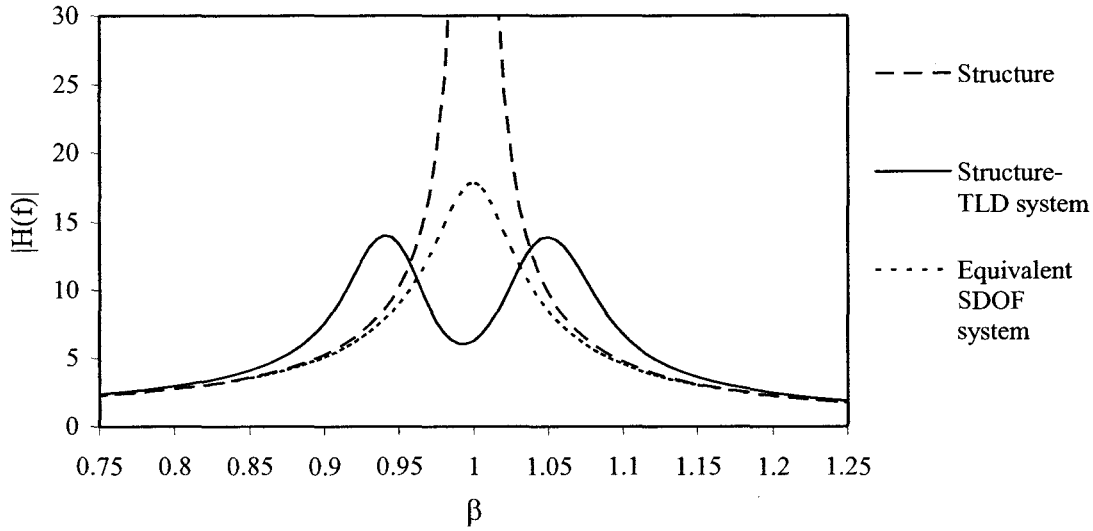

Figure 1.4 Mechanical Admittance Functions

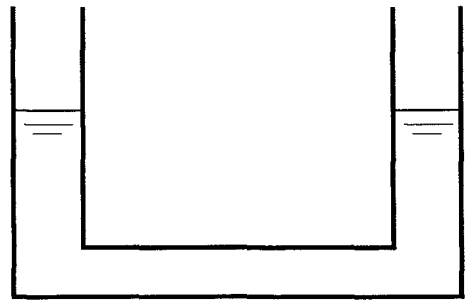

Figure 1.5 Tuned Liquid Column Damper

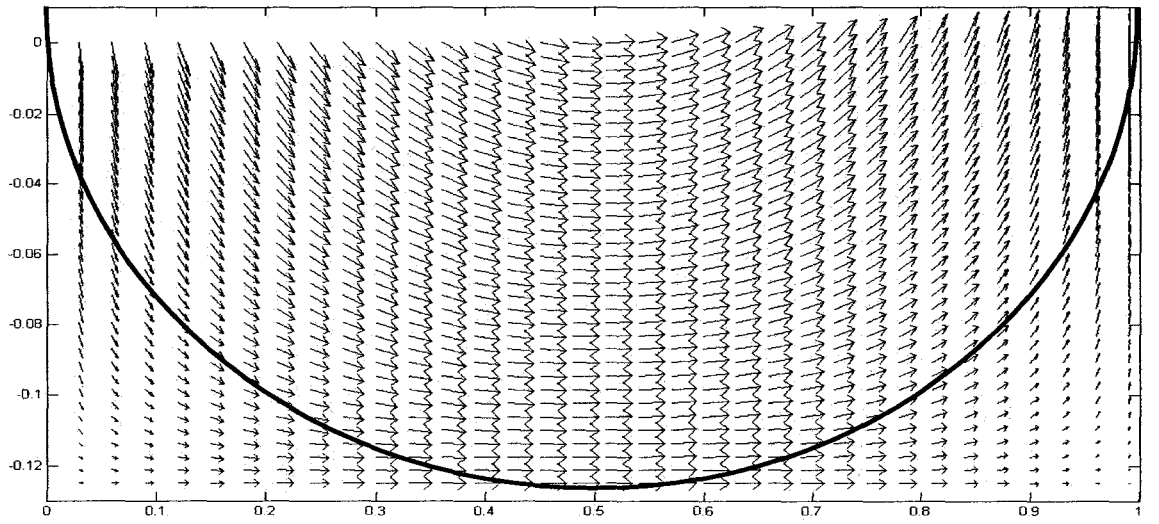

Figure 1.6 Velocity Profile of Sloshing Liquid in a Rectangular Tank

Chapter 2: Theoretical Modelling of TLDs with Different Tank Geometries Using Potential Flow Theory

This chapter focuses on the derivation of equivalent mechanical models for TLDs with different tank geometries. Potential flow theory, Lagrange's equations, and the virtual work method are employed to calculate the generalized properties of TLDs equipped with screens. The general procedure for the derivation of an equivalent mechanical model will be introduced first, followed by derivations for TLDs with different tank geometries. Specific parameters of the TLDs can be substituted into the equations shown in the general procedure, which leads to the properties of the mechanical model corresponding to the particular tank geometry of interest. Finally, comparisons of the equivalent mechanical properties of these TLDs are presented.

2.1 General Procedure of Derivation

Warnitchai and Pinkaew (1998) determined the generalized properties (mass, stiffness, damping and excitation factor) for a rectangular TLD, employing Lagrange's equations and Morison's formula. Tait (2007) derived an expression for the damping resulting from a number of energy dissipating devices (screens) inside a rectangular TLD, using the method of virtual work. In this section, the derivations will employ the above procedures and extend them to permit their application to TLDs with different tank geometries including horizontal-cylindrical and hyperboloid tanks.

As shown in Figure 2.1, a Cartesian coordinate system is established such that x denotes the transversal direction, y denotes the longitudinal direction (pointing out of

plane), and z denotes the vertical direction. In order to obtain the generalized properties, it is necessary to determine the velocity of sloshing liquid. In this study, this is accomplished by means of either potential flow theory or linear long wave theory. These theories are valid for different liquid depth ratio, h/L, and/or response amplitude ratio q_0/L, where h, L and q_0 denote liquid depth, free surface length and wave amplitude, respectively. It is noted that the free surface amplitude, η, can be expressed as $\eta(x,t) = q_0 f(x)g(t)$, where $f(x)$ and $g(t)$ are functions of space and time, respectively.

2.1.1 Generalized Properties: Mass, Stiffness and Natural Frequency

For a TLD subjected to base excitation, $X(t)$, applying the formulation for the velocity and Equations 2.1 and 2.2, given below, leads to the kinetic energy of the sloshing liquid.

$$d(KE) = \frac{1}{2}(dm)\left[(u+\dot{X})^2 + w^2\right] \tag{2.1}$$

$$KE = \int d(KE) \tag{2.2}$$

where $d(KE)$ is the kinetic energy due to the motion of the liquid particle of mass dm, KE is the kinetic energy due to the motion of the liquid inside the tank, $\dot{X}$ is horizontal velocity due to external excitation, and u and w are the horizontal and vertical fluid velocity components, respectively. In long wave theory, w is assumed to be much smaller than u such that it is neglected.

Next, the free surface amplitude, η, is assumed to be sufficiently small such that η can be computed by applying a linearized free surface boundary condition.

$$w = \left[\frac{\partial \phi}{\partial z}\right]_{z=\eta} = \frac{\partial \eta}{\partial t} \tag{2.3}$$

where ϕ is the velocity potential.

The potential energy of the sloshing liquid can be expressed as

$$d(PE) = (dm)g\bar{z} \tag{2.4}$$

$$PE = \int d(PE) \tag{2.5}$$

where $\bar{z}$ is the height measured from the bottom of the tank to the centre of gravity of the liquid mass and is a function of η.

The final step of the derivation for an undamped TLD is to apply the well-known Lagrange's equations to the kinetic energy equation and the potential energy equation

$$\frac{\partial}{\partial t}\left(\frac{\partial KE}{\partial \dot{q}}\right) - \frac{\partial KE}{\partial q} + \frac{\partial PE}{\partial q} = 0 \tag{2.6}$$

where q denotes the free surface sloshing amplitude at the end-walls; it is also a function of time, and dot denotes the time derivative. In addition, q is used as a set of generalized coordinates. The generalized properties (generalized mass m^*, generalized stiffness k^* and generalized excitation factor γ^*) are evaluated with reference to the generalized coordinate q. It is noted that all generalized properties are mode dependent, and only the first mode is considered in this study. Expanding the kinetic energy and potential energy in Equations 2.2 and 2.5 and substituting into Equation 2.6, the generalized mass m^* and generalized excitation factor γ^* can be found in the acceleration terms, and the generalized stiffness k^* in the displacement term.

$$\frac{\partial}{\partial t}\left(\frac{\partial KE}{\partial \dot{q}}\right) = m^* \ddot{q} - \gamma^* \ddot{X} \tag{2.7}$$

$$\frac{\partial PE}{\partial q} = k^* q \tag{2.8}$$

$$m^* \ddot{q} + k^* q = \gamma^* \ddot{X} \tag{2.9}$$

The generalized stiffness k^* can also be computed as

$$k^* = m^* \omega^2 \tag{2.10}$$

The natural frequency, ω, can be determined by applying the boundary condition. Details of this will be shown later for TLDs with different tank geometries. The effective mass, m_{eff}, of a TLD is the mass of liquid that participates in the sloshing motion. It is used as the mass for the equivalent mechanical model of a TLD and is expressed as

$$m_{eff} = \frac{\gamma^{*2}}{m^*} \tag{2.11}$$

2.1.2 Generalized Damping Due to Screens

The addition of damping due to the screens is attributed to the drag force, a flow-induced force in the horizontal direction of flow. Based on Morison's formula (Morison 1950), the drag force per unit area is as follows.

$$f_d(x,z,t) = \frac{1}{2}\rho C_L |u| u \tag{2.12}$$

where f_d is the drag force, C_L is the loss coefficient, and u is the horizontal component of the sloshing velocity. It can be assumed that this non-conservative force, f_d, acts upon the

liquid particles over a distance $\delta q(x,z,t)$, expressed in terms of the generalized coordinate $q(t)$, where $\delta q(x,z,t)$ is a virtual displacement. The virtual work done by the non-conservative damping force is expressed as

$$\delta W_{nc} = -\sum_{j=1}^{ns} \int_{b} \int_{-h}^{\eta} f_{dn} \delta q dz dy \tag{2.13}$$

Assuming small response amplitude, i.e. $\eta << h$,

$$\delta W_{nc} = -\sum_{j=1}^{ns} \int_{b} \int_{-h}^{0} f_{dn} \delta q dz dy \tag{2.14}$$

where ns denotes the number of screen(s) placed inside the tank, and b is the width of the tank.

Expressing u in term of $\dot{q}(t)$ and substituting Equation 2.12 into Equation 2.14, the virtual work can be rewritten as

$$\delta W_{nc} = Q \delta q \tag{2.15}$$

where

$$Q = -\frac{1}{2} \rho C_L \Delta \Xi |\dot{q}(t)| \dot{q}(t) \tag{2.16}$$

Q is defined here as the generalized non-conservative force corresponding to the generalized coordinate $q(t)$. The parameter Δ is a constant related to the tank geometry, and Ξ relates to number of screens and their location inside the tank. Applying Lagrange's equations of motion to the TLD system,

$$\frac{\partial}{\partial t}\left(\frac{\partial KE}{\partial \dot{q}}\right) - \frac{\partial KE}{\partial q} + \frac{\partial PE}{\partial q} = Q \tag{2.17}$$

The generalized damping c^* can be found in the velocity term of the equation of motion.

$$f_c^* = c^* \dot{q}(t) = \frac{1}{2} \rho C_L \Delta \Xi \mid \dot{q}(t) \mid \dot{q}(t) \tag{2.18}$$

where f_c^* is the generalized damping force.

2.1.3 Linearization of Generalized Damping

It can be seen from Equation 2.18 that the damping force, f_c^*, is proportional to $\mid \dot{q}(t) \mid \dot{q}(t)$. Determination of an equivalent linear viscous damping expression is a necessary step in the development of a mechanical model which permits the application of TMD theory to preliminary TLD design. The error between the nonlinear damping force $c^* \dot{q}$ and the equivalent generalized linear damping force $c_{eq}^* \dot{q}$ can be expressed as follows (Gao et al 1997)

$$\varepsilon = c^* \dot{q} - c_{eq}^* \dot{q} \tag{2.19}$$

To minimize the error, the following condition is applied

$$\frac{\partial E(\varepsilon^2)}{\partial c_{eq}^*} = 0 \tag{2.20}$$

where $E(\varepsilon^2)$ represents the expected value. Assuming a sinusoidal response, for instance, $q(t) = q_0 \cos(\omega t)$, Equation 2.20 yields

$$c_{eq}^* = \frac{4}{3} \frac{C_L \rho \Delta \Xi}{\pi} \omega q_0 \tag{2.21}$$

$$\zeta_{eq}^* = \frac{2}{3} \frac{C_L \rho \Delta \Xi}{\pi m^*} q_0 \tag{2.22}$$

where c_{eq}^* is the equivalent generalized viscous damping, and ζ_{eq}^* is the equivalent

damping ratio. Equation 2.22 is the general expression for the equivalent damping ratio for sinusoidal response.

An expression for the equivalent damping ratio for random excitation can be achieved by matching the energy dissipation rate of a linear device to that of a nonlinear device (Vickery et al. 2001). It is assumed that individual cycles are sinusoidal in form with slowly varying amplitude, $a(t)$; and the distribution of $a(t)$ follows the Rayleigh form associated with a narrow-band Gaussian process. The average dissipated energy per cycle for linear viscous and velocity squared damping are given as

$$\overline{E}(linear) = 2\pi c_{eq}^{*} \omega \sigma_{\eta}^{2} \tag{2.23}$$

$$\overline{E}(V^2) = 4\sqrt{2\pi} c^{*} \omega^2 \sigma_{\eta}^{3} \tag{2.24}$$

Equating Equations 2.23 and 2.24 yields

$$\zeta_{eq}^{*} = \sqrt{\frac{1}{2\pi}} \frac{C_L \rho \Delta \Xi}{m^{*}} \sigma_{\eta} \tag{2.25}$$

where σ_{η} is the RMS free surface motion at the tank end-wall.

The remaining steps required to determine the final value of the equivalent damping ratio are to compute the values of Δ and Ξ.

The general procedure for the derivation of equivalent mechanical parameters — mass, natural frequency and damping ratio — have been presented above. This allows a nonlinear TLD to be modelled as an amplitude dependent TMD using the derived equivalent parameters. This procedure can be applied to any tank geometry.

2.2 Potential Flow Theory

In this study, it is assumed that the nonlinear terms in the equations describing the boundary conditions are small and, therefore, can be neglected. The assumptions of incompressible and irrotational fluid lead to the Laplace equation.

$$\nabla^2\phi = 0 \tag{2.26}$$

or

$$\nabla^2\psi = 0 \tag{2.27}$$

where ϕ is the velocity potential and ψ is the stream function. These differential equations can be solved with the application of suitable boundary conditions. Since the liquid is assumed to be ideal and the tank is rigid and impermeable, the component of the velocity tangential to the boundary is nonzero whereas the component perpendicular to the boundary is zero, therefore,

$$\frac{\partial\phi}{\partial n} = 0 \tag{2.28}$$

on the container walls, where n is normal to the container walls.

For irrotational motion and inviscid fluid, the Bernoulli equation can be expressed as

$$\frac{1}{g}\frac{\partial\phi}{\partial t} + \frac{1}{2g}\left(\frac{\partial\phi}{\partial n}\right)^2 + \frac{p}{\rho g} + z = const. \tag{2.29}$$

where g, p and ρ denote the gravity acceleration, pressure and density of liquid, respectively. It is noted that $p = 0$ at the free surface. The assumption of small liquid

motion permits the nonlinear terms in the equation to be neglected. The linearized Bernoulli equation is given as

$$\eta = -\frac{1}{g}\left(\frac{\partial \phi}{\partial t}\right)\Big|_{z=F} \tag{2.30}$$

where F denotes the still liquid surface.

On the free surface, there is another kinematic boundary condition

$$\frac{\partial \phi}{\partial n} = \frac{\partial \eta}{\partial t}\Big|_{z=F} \tag{2.31}$$

Combining Equations 2.30 and 2.31 gives

$$\frac{\partial^2 \phi}{\partial t^2} + g\frac{\partial \phi}{\partial n} = 0\Big|_{z=F} \tag{2.32}$$

Equations 2.26, 2.28, 2.29, and 2.32 are the governing equations, which must be satisfied by the velocity potential. It is noted that potential flow theory is valid for any liquid depth ratio h/L, where h is the still liquid depth, L is half of wavelength for the first sloshing mode, and it is equal to the length of free surface (Le Méhauté 1976). Figure 2.1 shows the geometrical parameters and coordinates for an arbitrary tank with the free surface corresponding to the first sloshing mode.

The velocity potential functions of sloshing liquid in tanks with different geometries have been investigated theoretically. Bauer (1964 and 1984) provided the velocity potential for a rectangular and a vertical-cylindrical tank, respectively. Bartkowiak (1985) anticipated that the streamlines in a horizontal-cylindrical tank are circular, and posed a stream function for the streamlines. Budiansky (1960) calculated the

integration of the velocity component over a volume of liquid. Troesch (1960) formulated the natural frequency and velocity potential in a conical and hyperboloid tank, respectively. By following the procedure discussed in Section 2.1, the derivations of equivalent mechanical models for a rectangular, vertical-cylindrical, horizontal-cylindrical, conical and hyperboloid TLD are presented, respectively. Additionally, the equivalent viscous damping resulting from the screens will be determined. This has not previously been considered for several different tank geometries.

2.3 Derivation of Equivalent Mechanical Models of TLDs with Different Tank Geometries

2.3.1 Rectangular Tank

To express a two-dimensional wave, a local Cartesian coordinate (x-o-z) is introduced as shown in Figure 2.2. Here $z = 0$ represents the still liquid surface, h is the still liquid depth, L is the tank length, and $X(t)$ is the horizontal displacement of the tank due to external excitation.

2.3.1.1 Generalized Mass and Stiffness

The Laplace equation (Equation 2.26) can be written in the following form for a rectangular tank (Bauer 1984),

$$\frac{\partial^2 \phi}{\partial x^2} + \frac{\partial^2 \phi}{\partial z^2} = 0 \tag{2.33}$$

Equation (2.28) gives the kinematic boundary conditions at the end-walls ($x = 0, L$) and the bottom ($z = -h$),

$$u(x,z,t) = \frac{\partial \phi}{\partial x}\Big|_{x=0,x=L} = 0 \tag{2.34}$$

$$w(x,z,t) = \frac{\partial \phi}{\partial z}\Big|_{z=-h} = 0 \tag{2.35}$$

For a rectangular tank, the free surface condition (Equation 2.32) is given as,

$$\frac{\partial^2 \phi}{\partial t^2} + g\frac{\partial \phi}{\partial z} = 0\Big|_{z=0} \tag{2.36}$$

It is assumed that the velocity potential ϕ can be expressed in the form of

$$\phi(x,z,t) = X(x)Z(z)\cos\omega t \tag{2.37}$$

where ω is the natural frequency of the sloshing motion. Substituting Equation 2.37 into the Laplace equation (Equation 2.33), and applying the boundary conditions (Equations 2.34 and 2.35) to $X(x)$ and $Z(z)$, respectively, $X(x)$ and $Z(z)$ can be expressed in the following forms

$$X(x) = A\cos\frac{\pi}{L}x \tag{2.38}$$

$$Z(z) = B\frac{\cos\dfrac{\pi(z+h)}{L}}{\sinh\dfrac{\pi h}{L}} \tag{2.39}$$

where A and B are constants.

The velocity potential can therefore be expressed as

$$\phi(x,z,t) = AB\frac{\cosh(\frac{\pi(z+h)}{L})\cos(\frac{\pi x}{L})}{\sinh(\frac{\pi h}{L})}\cos(\omega t) \tag{2.40}$$

Substituting Equation 2.40 into Equation 2.36 leads to the natural frequency (Lamb, 1932)

$$\omega^2 = \frac{\pi g}{L}\tanh(\frac{\pi h}{L}) \tag{2.41}$$

The free surface amplitude η, can be expressed in terms of the generalized coordinate $q(t)$ and the mode shape,

$$\eta(x,t) = q(t)\cos(\frac{\pi x}{L}) \tag{2.42}$$

The generalized coordinate, $q(t)$, can be obtained by substituting Equation 2.40 into Equation 2.30, and equating the term $\eta(x,t)$ to that in Equation 2.42.

$$q(t) = AB\frac{\omega}{g}\frac{\cosh(\frac{\pi h}{L})}{\sinh(\frac{\pi h}{L})}\cos(\omega t) \tag{2.43}$$

Introducing $q(t)$ from Equation 2.43 and ω^2 from Equation 2.41 into Equation 2.40, the velocity potential can be expressed as

$$\phi(x,z,t) = \dot{q}(t)\frac{\cosh(\frac{\pi(z+h)}{L})\cos(\frac{\pi x}{L})}{(\frac{\pi}{L})\sinh(\frac{\pi h}{L})} \tag{2.44}$$

To obtain the kinetic energy, Equations 2.1 and 2.2 are employed.

$$\int KE = dm\frac{(\dot{X}+u)^2 + w^2}{2} = (\rho bdxdz)\frac{(\dot{X}+u)^2 + w^2}{2} \tag{4.45}$$

Substituting for the velocity terms, the kinetic energy is expressed as

$$KE = \frac{1}{2}\rho b \int_{-h}^{0}\int_{0}^{L}\left[\left(\dot{X} + \frac{\partial \phi}{\partial x}\right)^2 + \left(\frac{\partial \phi}{\partial z}\right)^2\right] dx dz \tag{2.46}$$

where

$$u = \frac{\partial \phi}{\partial x} = -\dot{q}(t)\frac{\cosh(\frac{\pi(z+h)}{L})\sin(\frac{\pi x}{L})}{\sinh(\frac{\pi h}{L})} \tag{2.47}$$

and

$$w = \frac{\partial \phi}{\partial z} = \dot{q}(t)\frac{\sinh(\frac{\pi(z+h)}{L})\cos(\frac{\pi x}{L})}{\sinh(\frac{\pi h}{L})} \tag{2.48}$$

Applying Lagrange's equations (Equation 2.6) to the kinetic energy (Equation 2.46) leads to the following expressions for the generalized mass m^* and the generalized excitation factor γ^*.

$$m^* = \frac{1}{2}\frac{\rho b L^2}{\pi \tanh(\frac{\pi h}{L})} \tag{2.49}$$

$$\gamma^* = \frac{2\rho b L^2}{\pi^2} \tag{2.50}$$

Substituting m^* and γ^* from Equations 2.49 and 2.50 into Equation 2.11, the effective mass, m_{eff}, is obtained (Graham and Rodriquez 1952).

$$m_r = \frac{8\tanh\left(\pi\frac{h}{L}\right)}{\pi^3\frac{h}{L}}m_w \tag{2.51}$$

where m_w denotes the mass of liquid in the tank, and m_r is used here to denote the effective mass, m_{eff}, of a rectangular TLD.

2.3.1.2 Additional Damping Due to Screens

A certain level of energy must be dissipated by a TLD in order for it to operate effectively as a dynamic vibration absorber. The required level of damping is often achieved by inserting screens into the TLD tank, as shown in Figure 2.2. Consider the case where a number of screens, *ns*, are placed at discrete locations, x_j, inside the tank. Based on the horizontal component of the velocity, u, in Equation 2.47, δq in Equation 2.15 becomes

$$\delta q(x_j, z, t) = \delta q(t)\frac{\cosh(\frac{\pi(z+h)}{L})\sin(\frac{\pi x_j}{L})}{\sinh(\frac{\pi h}{L})} \tag{2.52}$$

Substituting Equations 2.47, 2.52 and 2.12 into Equation 2.14 yields

$$\Xi = \sum_{j=1}^{ns}\left[\sin(\frac{\pi x_j}{L})\right]^3 \tag{2.53}$$

$$\Delta = \int_{b}\int_{-h}^{0}\left[\frac{\cosh(\frac{\pi(z+h)}{L})}{\sinh(\frac{\pi h}{L})}\right]^3 dzdx = \frac{bL}{\pi}\left[\frac{1}{3}+\frac{1}{\sinh^2\left(\frac{\pi h}{L}\right)}\right] \tag{2.54}$$

The damping ratio can be computed by substituting Δ and Ξ into Equations 2.22 and 2.25. For the case of sinusoidal excitation, the linearized damping ratio can be expressed as

$$\zeta_{eq}^{*} = \frac{2}{3}\frac{C_L \rho b L q_0}{\pi^2 m^*}\sum_{j=1}^{ns}\left[\sin(\frac{\pi x_j}{L})\right]^3\left[\frac{1}{3}+\frac{1}{\sinh^2\left(\frac{\pi h}{L}\right)}\right] \tag{2.55}$$

For the case of random excitation, the linearized damping ratio is found to be

$$\zeta_{eq}^{*} = \sqrt{\frac{1}{2\pi}}\frac{C_L \rho b L \sigma_\eta}{\pi^2 m^*}\sum_{j=1}^{ns}\left[\sin(\frac{\pi x_j}{L})\right]^3\left[\frac{1}{3}+\frac{1}{\sinh^2\left(\frac{\pi h}{L}\right)}\right] \tag{2.56}$$

It is evident that the equivalent damping ratio is dependent on the type of applied excitation, i.e. sinusoidal or random excitation.

2.3.2 Vertical-Cylindrical Tank

The geometry of a vertical-cylindrical tank is shown in Figure 2.3 together with the cylindrical coordinate system adopted in the following derivation. The still liquid surface is defined by $z = 0$, h is the still liquid depth, and a is the radius of the tank.

2.3.2.1 Generalized Mass and Stiffness

The Laplace equation (Equation 2.26) can be written in the following form for a vertical-cylindrical tank (Bauer 1964),

$$\frac{\partial^2\phi}{\partial r^2}+\frac{1}{r}\frac{\partial\phi}{\partial r}+\frac{1}{r^2}\frac{\partial^2\phi}{\partial\theta^2}+\frac{\partial^2\phi}{\partial z^2}=0 \tag{2.57}$$

Equation 2.28 gives the kinematic boundary conditions at the end-walls ($r = a$) and the bottom ($z = -h$) of the tank,

$$\frac{\partial\phi}{\partial r}\Big|_{r=a}=0 \tag{2.58}$$

$$\frac{\partial\phi}{\partial z}\Big|_{z=-h}=0 \tag{2.59}$$

For a vertical-cylindrical tank, the free surface condition (Equation 2.32) is given as,

$$\frac{\partial^2\phi}{\partial t^2}+g\frac{\partial\phi}{\partial z}=0\Big|_{z=0} \tag{2.60}$$

The velocity potential ϕ can be expressed in the form

$$\phi(r,z,\theta,t)=R(x)Z(z)\cos m\theta\cos\omega t \tag{2.61}$$

where ω is the natural frequency of the sloshing motion. When $m = 1$ in Equation 2.61, the sloshing mode results in a horizontal sloshing force (Abramson 1966), which is the mode of interest in this study. Substituting Equation 2.61 into the Laplace equation (Equation 2.57), and applying the appropriate boundary conditions (Equations 2.58 and 2.59) to $R(x)$ and $Z(x)$ respectively, they can be expressed in the following forms

$$R(r)=AJ_1(\lambda r) \tag{2.62}$$

$$Z(z) = B(\cosh \lambda z + \tanh \lambda h \sinh \lambda z) \tag{2.63}$$

where A and B are constants, $\lambda = \xi/a$, and $\xi = 1.841$ is obtained by applying the boundary condition at the container wall, which is given by Equation 2.58.

The velocity potential can, therefore, be expressed as

$$\phi(x,z,t) = ABJ_1(\lambda r)(\cosh \lambda z + \tanh \lambda h \sinh \lambda z)\cos(m\theta)\cos(\omega t) \tag{2.64}$$

Substituting Equation 2.64 into Equation 2.60 leads to the natural sloshing frequency for a vertical-cylindrical TLD (Bauer 1964)

$$\omega^2 = \lambda g \tanh(\lambda h) \tag{2.65}$$

The free surface amplitude, η, can be written in terms of generalized coordinate and shape function,

$$\eta(x,t) = q(t)\cos(m\theta)\frac{J_1(\xi \cdot r/a)}{J_1(\xi)} \tag{2.66}$$

Substituting $q(t)$ from Equation 2.66 and ω^2 from Equation 2.65 into Equation 2.64, the velocity potential can be expressed as

$$\phi(x,z,t) = \dot{q}(t)\frac{1}{(\xi/a)\sinh(\xi h/a)}\frac{J_1(\xi r/a)}{J_1(\xi)}\cosh \lambda(z+h)\cos m\theta \tag{2.67}$$

To obtain the kinetic energy, Equations 2.1 and 2.2 are employed. The kinetic energy of an infinitesimal volume of fluid can be expressed

$$\begin{aligned} dKE &= dm\frac{(\dot{X}\cos\theta + u_r)^2 + (\dot{X}\sin\theta + u_\theta)^2 + w^2}{2} \\ &= (\rho r dr d\theta dz)\frac{(\dot{X}\cos\theta + u_r)^2 + (\dot{X}\sin\theta + u_\theta)^2 + w^2}{2} \end{aligned} \tag{2.68}$$

where u_r, u_θ and w are radial, circumferential and axial velocity components, which are given by Equations 2.69, 2.70 and 2.71, respectively, below.

$$u_r = \frac{\partial \phi}{\partial r} = \dot{q}(t) \frac{\cosh \frac{\xi(z+h)}{a}}{\sinh(\frac{\xi h}{a}) J_1(\xi)} [J_0(\xi \cdot r/a) - a/(\xi \cdot r) J_1(\xi \cdot r/a)] \cos\theta \tag{2.69}$$

$$u_\theta = \frac{1}{r} \frac{\partial \phi}{\partial \theta} = \dot{q}(t) \frac{\cosh \frac{\xi(z+h)}{a}}{\sinh(\frac{\xi h}{a})} \frac{J_1(\xi \cdot r/a)}{J_1(\xi) \xi r/a} \sin\theta \tag{2.70}$$

$$w = \frac{\partial \phi}{\partial z} = \dot{q}(t) \frac{1}{\sinh(\frac{\xi h}{a}) J_1(\xi)} \frac{J_1(\xi \cdot r/a)}{J_1(\xi)} \sinh \frac{\xi(z+h)}{a} \cos\theta \tag{2.71}$$

Integrating Equation 2.68 over the volume of fluid yields

$$KE = \frac{1}{2} \rho \int_{-h}^{0} \int_{0}^{2\pi} \int_{0}^{a} \frac{(\dot{X} \cos\theta + u_r)^2 + (\dot{X} \sin\theta + u_\theta)^2 + w^2}{2} r dr d\theta dz \tag{2.72}$$

Applying Lagrange's equations (Equation 2.6) to the kinetic energy equation leads to the following expressions for generalized mass m^* and generalized excitation factor γ^*, respectively.

$$m^* = \frac{\xi^2 - 1}{2\xi^3} \rho \pi \cdot a^3 \coth \frac{\xi h}{a} \tag{2.73}$$

$$\gamma^* = \frac{1}{\xi^2} \pi \rho \cdot a^3 \tag{2.74}$$

Substituting m^* and γ^* into Equation 2.11, the effective mass is obtained as

$$m_{vc} = \frac{2}{\xi(\xi^2 - 1)} \frac{a}{h} \left(\tanh \frac{\xi h}{a} \right) m_w \tag{2.75}$$

where m_w denotes the mass of liquid in the tank, and m_{vc} denotes the effective mass of a vertical-cylindrical TLD. The effective mass of a vertical-cylindrical TLD derived using the method described above is the same as that obtained by integrating the hydrodynamic pressure acting on the tank walls (Bauer 1964).

2.3.2.2 Additional Damping Due to Screens

Consider the case where a number of screens are placed in parallel at discrete locations, x_j, inside the tank and the horizontal component of the velocity, u ($= u_r \cos\theta + u_\theta \sin\theta$), is normal to the screens (Figure 2.3). Based on the expressions of u_r and u_θ in Equations 2.69 and 2.70, δq in Equation 2.15 is expressed as

$$\begin{aligned} \delta q(x_j, z, t) = \delta q(t) & \frac{\cosh \frac{\xi(z+h)}{a}}{\sinh(\frac{\xi h}{a}) J_1(\xi)} \times \\ \{ \dot{q}(t) & \frac{\cosh \frac{\xi(z+h)}{a}}{J_1(\xi) \sinh(\frac{\xi h}{a})} \left[J_0(\xi \cdot r/a) - a/(\xi \cdot r) J_1(\xi \cdot r/a) \right] \cos^2\theta \\ - \dot{q}(t) & \frac{\cosh \frac{\xi(z+h)}{a}}{\frac{1}{a} \sinh(\frac{\xi h}{a})} \frac{J_1(\xi \cdot r/a)}{\xi J_1(\xi) r/a} \sin^2\theta \} \end{aligned} \tag{2.76}$$

Substituting u, Equations 2.76 and 2.12 in Equation 2.14 yields

$$\Xi = \sum_{j=1}^{ns} 2 \int_0^{\theta_j} \{ \frac{1}{J_1(\xi)} [J_0(\xi \cdot r/a) - a/(\xi \cdot r) J_1(\xi \cdot r/a)] \cos^2\theta - \frac{1}{J_1(\xi)} \frac{J_1(\xi \cdot r/a)}{\xi \cdot r/a} \sin^2\theta \}^3 a \cos\theta d\theta \tag{2.77}$$

$$\Delta = \int_{-h}^{0} \left[\frac{\cosh(\frac{\xi(z+h)}{a})}{\sinh(\frac{\xi h}{a})} \right]^3 dz = \frac{a}{\xi} \left[\frac{1}{3} + \frac{1}{\sinh^2(\frac{\xi \cdot h}{a})} \right] \tag{2.78}$$

The damping ratio can be computed by substituting Δ and Ξ into Equations 2.22 and 2.25. This procedure could also be used to compute the equivalent damping for the case of radial screens inserted in a vertical-cylindrical tank.

2.3.3 Horizontal-Cylindrical Tank

2.3.3.1 Natural Frequency and Effective Mass

Budiansky (1960) calculated the natural modes and frequencies of liquid sloshing in a horizontal-cylindrical tank having an arbitrary liquid depth using an integral-equation approach. Based on this work, the effective mass of sloshing motion can be computed. The geometry of a horizontal-cylindrical tank is shown in Figure 2.4a. The still liquid surface is given by $z = 0$, the still liquid depth is expressed in terms of eR, where e is ranged from -1 to 1 and R is the radius of the tank.

Assuming the velocity potential

$$\phi(x, y, z, t) = \phi(x, y, z) \cos\omega t \tag{2.79}$$

the vertical velocity at the free surface w can be expressed in terms of sloshing frequency ω and velocity potential. Substituting Equation 2.79 into Equation 2.32 the vertical velocity at the free surface can be expressed as

$$w = \frac{1}{g}\omega^2\phi \tag{2.80}$$

After the introduction of the dimensionless coordinate I–J (see Figure 2.4b), the relationship between vertical velocity and the velocity potential indicated in Equation 2.80 becomes

$$v(I,\bar{I}) = \lambda_n a \int_0^1 \phi(I,\bar{I})v(\bar{I})d\bar{I} \tag{2.81}$$

where $I = x/aR$, $J = z/aR$, $\bar{I}$ is a certain location on the I axis, $\lambda_n = \omega_n^2 R/g$; v is the vertical velocity along the I axis ($J = 0$) and the integration is the velocity potential for the internal flow along the I axis. By employing conformal mapping, Equation 2.81 can be solved numerically. The solution of Equation 2.81 provides the natural sloshing frequency of the liquid corresponding to the n^{th} mode

$$f_{hc} = \frac{1}{2\pi}\sqrt{\frac{\lambda_n g}{R}} \tag{2.82}$$

where λ_n is a function of e for the n^{th} sloshing mode. Based on the numerical results for λ_n from Budiansky (for $h \leq R$), a least square fit is conducted as shown in Figure 2.5a and a fitted equation for λ_n can be expressed as

$$\lambda_1 = \left(\frac{h}{2R}\right)^{3.129} + 1.542^{\left(\frac{h}{2R}\right)} \tag{2.83}$$

The theoretical results from Equation 2.82 are found to be in good agreement with the experimental results (McCarty and Stephens 1960). Applying Lagrange's equations, Budiansky (1960) also formulated the sloshing forces of the liquid in a horizontal-cylindrical tank. Based on this formulation, the effective mass can be evaluated as follows. Let χ be the displacement potential,

$$\chi = \sum a_n(t)\phi_n(x,y,z) \tag{2.84}$$

where $a_n(t)$ is a set of generalized coordinates. The displacement potential is associated with the fluid displacement relative to the tank. For instance, the free surface amplitude can be expressed as $\partial\chi/\partial z$. The potential energy and kinetic energy can subsequently be calculated based on the formulations above

$$PE = \frac{1}{2}\int_F \rho g(\partial\chi/\partial z)^2 dF \tag{2.85}$$

$$KE = (\rho/2)\int_V \{[\dot{X} + \sum \dot{a}_n(\partial\phi_n/\partial x)]^2 + [\sum \dot{a}_n(\partial\phi_n/\partial y)]^2 + [\sum \dot{a}_n(\partial\phi_n/\partial z)]^2\} dV \tag{2.86}$$

where F denotes the free surface and V is the volume of the liquid.

Substituting Equations 2.79 and 2.84 into Equation 2.85, and substituting Equations 2.79, 2.80 and the surface condition into Equation 2.86 leads to

$$PE = (\rho/2g)\sum \alpha_n a_n^2 \omega_n^4 \tag{2.87}$$

$$KE = (1/2)m\dot{X}^2 + (\rho/2g)\sum \alpha_n \omega_n{}^2 \dot{a}_n{}^2 + \rho\dot{X}\sum \beta_n \dot{a}_n \tag{2.88}$$

where

$$\alpha_n = \int_F \phi_n{}^2 dF \tag{2.89}$$

$$\beta_n = \int_V \left(\frac{\partial \phi_n}{\partial x} \right) dV \tag{2.90}$$

ρ is the liquid mass density, g is the acceleration of the gravity, and m_w is the mass of liquid. By applying Lagrange's equations to the potential energy and kinetic energy, a differential equation and the expression for sloshing force are obtained as follows

$$\ddot{a}_n + \omega_n{}^2 a_n = -(g/\omega_n{}^2)(\beta_n/\alpha_n)\ddot{X} \tag{2.91}$$

$$F_s = -m\ddot{X} - \rho \sum \beta_n \ddot{a}_n \tag{2.92}$$

In $I-J$ coordinates, Equations 2.91 and 2.92 become

$$\ddot{\tau}_n + \omega_n{}^2 \tau_n = (-\lambda_n a)(B_n/A_n)\ddot{X} \tag{2.93}$$

$$F_s = -m\ddot{X} - 2\rho(aR)^2 \sum B_n \ddot{\tau}_n \tag{2.94}$$

where

$$A_n = \int_0^1 [\nu_n(I)]^2 dI \tag{2.95}$$

$$B_n = \int_0^1 \xi \nu_n(I) dI \tag{2.96}$$

τ is the free surface amplitude in I-J coordinates, X is the displacement amplitude of the tank in x direction and A_n and B_n can be evaluated numerically. A least squares fit was applied to the numerically obtained values of A_n and B_n, for $n = 1$ as shown in Figure 2.5b. The following equations are obtained for $h/L = 0 \sim 0.6$.

$$A_1 = (1/3)(2.050)^{h/L} \tag{2.97}$$

$$B_1 = 0.339(1.392)^{h/L} \tag{2.98}$$

The generalized mass and generalized excitation factor, corresponding to the fundamental sloshing mode, can be obtained from Equations 2.93 and 2.94. The generalized mass is given by

$$m_n^* = \frac{2\rho(aR)^2 \sum B_1}{(\lambda_1 a)(B_1 / A_1)} \tag{2.99}$$

and the generalized excitation factor is expressed as

$$\gamma_n^* = 2\rho(aR)^2 \sum B_1 \tag{2.100}$$

For $n = 1$, the effective mass is given by

$$m_{hc} = \frac{2}{\pi}\rho(\lambda_1 a^3) B_1^2 / A_1 \tag{2.101}$$

A comparison of the effective mass calculated using values of A_1 and B_1 from Equations 2.95 and 2.96 to that based on the fitted A_1 and B_1 values is shown in Table 2.1. The error introduced when A_1 and B_1 calculated using the fitted values is found to be less than 3%. Therefore, for h/L values within the fitted range, the value of m_{hc} can be readily determined using the fitted values for A_1 and B_1.

2.3.3.2 Generalized Mass and Stiffness

Since the solution of the velocity potential is an integral, the previous method does not lend itself well to calculating the damping that results from inserting screens into the tank. In this section, a closed-form solution of a velocity potential is presented. A

Cartesian coordinate (*x-o-z*) is attached to the top of the cylinder as shown in Figure 2.6a. Bartkowiak (1985) postulated that the streamlines in a horizontal-cylindrical tank are circular, and posed a stream function to satisfy the Laplace equation (Equation 2.27). The stream function is given as

$$\psi(x,z,t) = -\frac{M}{2\pi}\frac{z}{x^2+z^2}\sin\omega t \tag{2.102}$$

This function corresponds to a doublet of strength M located at the origin of the coordinate system. A doublet is an equal strength source-sink pair with infinitesimal distance between them (White 1999). Based on this stream function and using the relationship between ψ and ϕ, a velocity potential function can be expressed as

$$\phi(x,z,t) = c_c\frac{x}{x^2+(z-R)^2}\sin\omega t \tag{2.103}$$

from the relationship

$$\frac{\partial\phi}{\partial x} = \frac{\partial\psi}{\partial z} \tag{2.104}$$

where c_c is an unknown constant. For simplicity of integration, the Cartesian coordinate is moved from the top of the circle to its origin as shown in Figure 2.6b. Since the stream function is circular, the velocity normal to the container wall is zero, i.e. the boundary condition given by Equation 2.28 is satisfied. Applying the linearized Bernoulli equation (Equation 2.30) to the velocity potential function (Equation 2.103) yields

$$\eta(x,t) = q(t)\frac{2R(R-H)}{\sqrt{R^2-H^2}}\frac{x}{x^2+(H-R)^2} = q(t)\varphi(x) \tag{2.105}$$

The response amplitude is expressed as

$$q(t) = q_0 \cos \omega t \tag{2.106}$$

where q_0 is the wave amplitude at point A as shown in Figure 2.6b, and $\varphi(x)$ is the mode shape (see Appendix B for detailed derivation).

Expressing $\phi(x, z, t)$ in terms of the generalized coordinate $q(t)$

$$\phi(x,z,t) = \dot{q}(t)\frac{g}{\omega^2}\frac{2R(R-H)}{\sqrt{R^2-H^2}}\frac{x}{x^2+(z-R)^2} \tag{2.107}$$

the velocity components, u and w, thus become

$$u(x,z,t) = \frac{\partial \phi}{\partial x} = \dot{q}(t)\frac{g}{\omega^2}\frac{2R(R-H)}{\sqrt{R^2-H^2}}\frac{(z-R)^2-x^2}{[x^2+(z-R)^2]^2} \tag{2.108}$$

$$w(x,z,t) = \frac{\partial \phi}{\partial z} = \dot{q}(t)\frac{g}{\omega^2}\frac{2R(R-H)}{\sqrt{R^2-H^2}}\frac{2x(z-R)}{[x^2+(z-R)^2]^2} \tag{2.109}$$

Unlike the rectangular and vertical-cylindrical tank cases, derived previously, the natural frequency of the sloshing motion in a horizontal-cylindrical tank cannot be obtained by utilizing the free surface boundary condition due to the nature of the posed stream function. However, the natural frequency can be determined by using either the mass-stiffness relationship (Equation.2.10) or Equation 2.82 derived by Budiansky (1960).

The kinetic energy of liquid sloshing can therefore be expressed in terms of u and w as follows

$$\int KE = dm\frac{(\dot{X}+u)^2+w^2}{2} = (\rho b dx dz)\frac{(\dot{X}+u)^2+w^2}{2} \tag{2.110}$$

$$KE = \frac{1}{2}\rho b \int_{-R}^{H} \int_{-\sqrt{R^2-z^2}}^{\sqrt{R^2-z^2}} [(\dot{X}+u)^2 + w^2] dx dz \tag{2.111}$$

No explicit solution for this integral was found. However, this equation can be evaluated numerically for given values of H and R. In this study, H is the liquid depth measured from the origin of the circular cross-section, and R is the radius of the tank (Figure 2.6b). Applying Lagrange's equations (Equation 2.6) to the kinetic energy (Equation 2.111) and using Equation 2.11, the effective mass for the horizontal-cylindrical tank can be calculated. Values of normalized effective mass, m_{eff}/m_w, calculated using this procedure are listed in Table 2.1. The m_{eff}/m_w values can also be obtained using Equation 2.101, formulated by Budiansky (1960). The effective mass values determined using the velocity potential based on the stream function are in good agreement with those based on Budiansky's work, however, as the depth ratio increases, greater discrepancy is observed. The effective mass values calculated using the two different methods are found to be within 3% when $h/L<0.4$ and is within 7% at $h/L = 0.5$. Therefore, for $h/L < 0.5$, the equation of the stream function given by Equation 2.102 is considered suitable for determining the effective mass.

2.3.3.3 Additional Damping due Screens

Using the velocity potential, based on the assumed stream function, given by Equation 2.107, the damping provided by screens can be calculated. Consider a number of screens placed at discrete locations, x_j, inside the tank, based on the horizontal

component of the velocity u in Equation 2.108, the virtual displacement δq in Equation 2.15 becomes

$$\delta q(x_j, z, t) = \delta q(t) \frac{g}{\omega^2} \frac{2R(R-H)}{\sqrt{R^2 - H^2}} \frac{(z-R)^2 - x^2}{[x^2 + (z-R)^2]^2} \tag{2.112}$$

Substituting Equations 2.107, 2.112 and 2.12 into Equation 2.14 yields

$$\Delta = \left[\frac{g}{\omega^2} \frac{2R(R-H)}{\sqrt{R^2 - H^2}} \right]^3 \tag{2.113}$$

$$\Xi = \sum_{j=1}^{ns} \int_b \int_{-\sqrt{R^2 - x^2}}^{-H} \left(\frac{(z-R)^2 - x_j^{\,2}}{[x_j^{\,2} + (z-R)^2]^2} \right)^3 dz dy \tag{2.114}$$

The damping ratio can be computed by substituting Δ and Ξ into Equations 2.22 and 2.25.

2.3.4 Conical and Hyperboloid Tank

2.3.4.1 Natural Frequency and Effective Mass

Troesch (1960) solved the Laplace equation (Equation 2.26) for conical and hyperboloid tanks, and found the natural frequency of the sloshing motion. The geometry of a conical and hyperboloid tanks are shown in Figure 2.7 together with the cylindrical coordinate system.

A velocity potential function, which satisfies the Laplace equation, is introduced

$$\phi = (r + \lambda r z) \cos\theta \cos\omega t \tag{2.115}$$

Substituting Equation 2.115 into Equation 2.32, the free surface boundary condition, yields

$$\lambda = \frac{\omega^2}{g} \tag{2.116}$$

The kinematic boundary condition at the tank walls (Equation 2.28) can be rewritten in the following form in the cylindrical coordinate system for the conical and hyperboloid TLDs,

$$\frac{\partial \phi}{\partial z} dr - \frac{\partial \phi}{\partial r} dz = 0 \tag{2.117}$$

Substituting the velocity potential in Equation 2.115 into Equation 2.117 and integrating gives

$$r^2 = (z + \frac{1}{\lambda})^2 - C \tag{2.118}$$

When the constant C is chosen to be zero, the container represent a 45-degree cone with a depth of $h = 1/\lambda$ and a radius at the free surface of $R = 1/\lambda$. The natural frequency of the free surface oscillation with one nodal diameter can be obtained from Equation 2.117 as

$$\omega = \sqrt{\frac{g}{h}} \tag{2.119}$$

When the constant C in Equation 2.118 is a positive number, the shape of the tank is a hyperboloid asymptotic to a 45-degreee half-angle cone, and the natural frequency is

$$\omega = \sqrt{\frac{2hg}{R^2 + h^2}} \tag{2.120}$$

The natural frequency of a 45-degree conical tank, given by Equation 2.119, agrees with the theoretical results found by Moiseev and Petrov (1968).

Substituting the velocity potential (Equation 2.115) into Equation 2.30 yields the wave height

$$\eta(r,t) = \frac{r}{R}\cos\theta(\frac{\omega R}{g}\sin\omega t) = \frac{r}{R}\cos\theta q(t) \tag{2.121}$$

where

$$q(t) = \frac{\omega R}{g}\sin\omega t = q_0 \sin\omega t \tag{2.122}$$

Here $q(t)$ represents the wave height when θ equals -1 or 1 in free oscillation. The velocity potential can be rewritten in term of $\dot{q}(t)$, and the velocity components are given as

$$u = \frac{\partial\phi}{\partial x} = \left(\frac{1}{\lambda} + z\right)\frac{1}{R}\dot{q}(t) \tag{2.123}$$

$$w = \frac{\partial\phi}{\partial z} = \frac{r}{R}\cos(\theta)\dot{q}(t) \tag{2.124}$$

To obtain the kinetic energy, Equations 2.1 and 2.2 are employed.

$$\int KE = dm\frac{(\dot{X}+u)^2 + w^2}{2} = (\rho\frac{1}{2}r^2 d\theta dz)\frac{(\dot{X}+u)^2 + w^2}{2} \tag{2.125}$$

$$KE = \frac{1}{2}\rho\int_{-h}^{0}\int_{0}^{2\pi}[(\dot{X}+u)^2 + w^2]\cdot r^2 d\theta dz \tag{2.126}$$

Applying Lagrange's equations (Equation 2.6) to the kinetic energy equation leads to the following expressions for generalized mass m^*

$$m^* = \frac{1}{120}\rho\pi\frac{15R^6 + 25R^4h^2 - 5R^2h^4 + h^6}{R^2 h} \tag{2.127}$$

and generalized excitation factor γ^*

$$\gamma^* = \frac{1}{4}\rho\pi R^3 \tag{2.128}$$

Substituting m^* and γ^* from Equations 2.127 and 2.128 into Equation 2.11, the effective mass m_{eff} is obtained as

$$m_h = 45\{(64(h/L)^6 - 80(h/L)^4 + 100(h/L)^2 + 15][3 - 4(h/L)^2]\}^{-1} m_w \tag{2.129}$$

where m_w denotes the mass of liquid in the tank, and m_h denotes the effective mass of a hyperboloid and conical TLD.

2.3.4.3 Additional Damping Due to Screens

Based on the horizontal component of the velocity u in Equation 2.123, the virtual displacement δq in Equation 2.15 becomes

$$\delta q(z,t) = \delta q(t)\left(\frac{1}{\lambda} + z\right)\frac{1}{R} \tag{2.130}$$

Substituting Equations 2.123, 2.130 and 2.12 into Equation 2.14 yields

$$\Delta = 1 \tag{2.131}$$

$$\Xi = \sum_{j=1}^{ns}\left\{\frac{\begin{array}{l}[(-3 + a^2\lambda^2 + 2a^4\lambda^4)\sqrt{1/\lambda^2 - a^2} + (3h_j{}^4\lambda^4 + 18h_j{}^2\lambda^2 - h_j{}^2\lambda^4 a^2 \\ -12h_j{}^3\lambda^3 - 12h_j\lambda + 2h_j\lambda^3 a^2 - a^2\lambda^2 - 2a^4\lambda^4 + 3)\sqrt{(h_j - 1/\lambda)^2 - a^2}]\end{array}}{(-15\lambda^4 R^3)}\right\} \tag{2.132}$$

The parameters λ, a, and h_j are given as

$$\lambda = \frac{2h}{R^2 + h^2} \tag{2.133}$$

$$a = \sqrt{\left(\frac{1}{\lambda}\right)^2 - R^2} \tag{2.134}$$

$$h_j = \sqrt{a^2 - r^2} - 1/\lambda \tag{2.135}$$

where h is the liquid depth at the centre of the tank, and h_j is the liquid depth at the location of the screen. The damping ratio can be computed by substituting Δ and Ξ into Equations 2.22 and 2.25.

With the natural frequency, effective mass and amplitude-dependent damping ratio, a mechanical model of a TLD, for the tank geometries considered, can be constructed. All equations for the parameters corresponding to the equivalent mechanical model of TLDs derived in this chapter are summarized in Appendix A.

2.4 Comparison of Properties between Equivalent Mechanical Models

The key properties of TLDs, which significantly affect the dynamic response of a structure-TLD system, include the natural frequency, effective mass and damping ratio. They will be discussed in this section and comparison of the TLD properties for different tank geometries will be presented.

2.4.1 Natural Frequency

The formulas for calculating natural frequency have been derived in the previous sections. From Equations 2.41, 2.65, 2.82 and 2.120, the fundamental sloshing frequency

of a rectangular, vertical-cylindrical, horizontal-cylindrical and hyperboloid TLD can be expressed as

$$f_r = \frac{1}{2}\sqrt{\frac{g}{\pi L}\tanh\frac{\pi h}{L}} \qquad \text{Rectangular}$$

$$f_{vc} = \frac{1}{2\pi}\sqrt{\frac{1.841g}{R}\tanh\frac{1.841h}{R}} = \frac{1}{2\pi}\sqrt{\frac{3.682g}{L}\tanh\frac{3.682h}{L}} \qquad \text{Vertical-Cylindrical}$$

$$f_{hc} = \frac{1}{2\pi}\sqrt{\frac{\lambda_n g}{R}} = \frac{1}{2\pi}\sqrt{\frac{2\lambda_n g}{L}} \qquad \text{Horizontal-Cylindrical}$$

$$f_h = \frac{1}{2\pi}\sqrt{\frac{2hg}{R^2+h^2}} = \frac{1}{\pi}\sqrt{\frac{2g}{L}\frac{h/L}{1+4(h/L)^2}} \qquad \text{Hyperboloid/Conical}$$

The free surface length and depth ratio influence the natural sloshing frequency of the various TLDs, as shown in Figures 2.8 to 2.11. For all tank geometries considered, the natural frequency is found to increase as the liquid depth ratio *h/L* increases, or as the tank length, *L*, is decreased. The rate of increase in the natural frequencies of the TLDs is found to be the largest when the liquid depth ratio is small. For a horizontal-cylindrical tank, it is found from geometry that $L = \sqrt{(Rh/2 - h^2/4)}$. Therefore, unlike other TLDs, when computing the natural frequency of a horizontal-cylindrical TLD, in order to hold the free surface length *L* at a certain constant value with adjustment of *h/L*, the radius *R* must be varied (Figure 2.10a). It is more practical to study the natural frequency by defining the liquid depth ratio as *h/2R*, although *2R* is not half the wavelength corresponding to the fundamental sloshing mode. Figure 2.10b is the natural frequency of a horizontal-cylindrical TLD with the newly defined liquid depth ratio. The natural frequencies for all TLDs considered here are normalized by f_r and shown in Figure 2.12.

In most of the studied *h/L* range, the following trend is found: $f_{hc} > f_{vc} > f_r > f_h$. This is a result of the difference in equivalent tank length between the different geometries considered in this study.

2.4.2 Effective Mass

Observing Equations 2.51, 2.75, 2.101 and 2.129 given below, the effective mass of a TLD formulated based on potential flow theory depends upon the liquid depth ratio, *h/L*.

$$m_r = \frac{8\tanh(\pi\frac{h}{L})}{\pi^3\frac{h}{L}}m$$ Rectangular

$$m_{vc} = \frac{2}{\xi(\xi^2-1)}\frac{a}{h}\left(\tanh\frac{\xi h}{a}\right)m$$ Vertical-Cylindrical

$$m_{hc} = \frac{2}{\pi}\rho(\lambda_1 a^3)B_1^{\,2}/A_1$$ Horizontal-Cylindrical

$$m_h = 45\{(64(h/L)^6 - 80(h/L)^4 + 100(h/L)^2 + 15][3 - 4(h/L)^2]\}^{-1}m$$ Hyperboloid/Conical

It is evident from Figure 2.13 that the normalized effective mass, m_{eff}/m_w, decreases as liquid depth ratio, *h/L*, is increased for all tank geometries considered. In other words, a smaller liquid depth ratio value results in a greater percentage of liquid participating in the sloshing motion. Usually rectangular TLDs are examined in the region where the effective mass is approximately 70 to 80 % of the total liquid mass. This corresponds to an *h/L* value ranging from 0.1 to 0.3. For most *h/L* ratio values, $m_{hc} > m_h > m_r \approx m_{vc}$. The

inactive liquid at the end-walls of a rectangular and vertical-cylindrical TLD is eliminated by using a horizontal-cylindrical or hyperboloid tank. This results in nearly 100% of the fluid participating in the sloshing motion for horizontal-cylindrical and hyperboloid tanks at small h/L values. However, for the rectangular and vertical-cylindrical cylindrical tanks the maximum m_{eff}/m_w values are approximately 80%. The dotted lines in Figure 2.13 indicate commonly employed h/L values for rectangular and vertical-cylindrical tanks. A horizontal-cylindrical tank is found to have m_{eff} values approximately 15% greater that rectangular or vertical-cylindrical tank values for corresponding h/L values. This is a significant increase and results in a larger mass ratio value, given the same total liquid mass m_w, as that of a rectangular or vertical-cylindrical tank.

2.4.3 Damping

Given the dimensions of a TLD, the four factors that influence the damping ratio are the liquid depth ratio h/L, number of screens ns, loss coefficient C_L and fluid response amplitude q_0. For simplicity, the case of one screen inserted at the centre of the tank for a TLD having the same length of free surface (L = 1m) is studied here. As shown in Figure 2.14, the normalized damping ratio, ζ/C_L, for a rectangular tank is found to decrease as the liquid depth ratio, h/L, is increased, which is attributed to the decrease in Δ and Ξ. In addition, the effects of liquid depth ratio, h/L, and normalized free surface response amplitude, η/L, on the normalized damping ratio, ζ/C_L, are shown in Figures 2.15 to 2.18 for the TLDs considered in Section 2.3. The increase in ζ/C_L with η/L is linear for all TLDs as a result of the velocity squared damping. This is expected as the damping ratio is amplitude dependent (see Equations 2.22 and 2.25). Large response amplitude and

shallow liquid depth result in high fluid velocity causing increased drag force. The drag force is proportional to the fluid velocity squared and is directly related to the energy dissipated by the screen. As a result, increased damping is attributed to large response amplitude and shallow liquid depth. For a h/L = 0.1, 0.15 and 0.2, the following trend is found, respectively: $\zeta_r/C_L > \zeta_{vc}/C_L > \zeta_{hc}/C_L > \zeta_h/C_L$, $\zeta_r/C_L > \zeta_{vc}/C_L \approx \zeta_{hc}/C_L > \zeta_h/C_L$ and $\zeta_r/C_L > \zeta_{hc}/C_L > \zeta_{vc}/C_L > \zeta_h/C_L$. According to Equations 2.22 and 2.25, the above findings are similar for both sinusoidal and random excitation.

2.5 Summary

The parameters of an equivalent mechanical model, which are the effective mass, damping ratio and natural frequency, are derived for TLDs with different tank geometries by applying Lagrange's equations, Morison's formula and the method of virtual work. The effective mass of rectangular and vertical-cylindrical TLDs, derived using the method described in Section 2.1, are the same as those obtained using an analytical mechanical system approach (Graham and Rodriguez 1952) or by integrating the hydrodynamic pressure acting on the tank wall (Bauer 1964). The derived effective mass for a horizontal-cylindrical TLD is in good agreement with results based on Budiansky's work (1960). The damping ratio, which is modelled as an amplitude-dependent parameter, is found to increase with fluid response amplitude due to the velocity squared damping resulting from the screens. Additionally, for all TLDs, as the liquid depth ratio increases, the effective mass of the TLD decreases, and the natural frequency of the TLD increases. Furthermore, comparisons are made among each parameter for TLDs with different tank geometries. From the results obtained using linear potential flow theory, the equivalent

mechanical model parameters for the TLDs considered have the following relationship. In the common design and operational range of h/L values, the following trends are found for the sloshing frequency values, $f_{hc} > f_{vc} > f_r > f_h$; for the effective mass values, $m_{hc} > m_h > m_r \approx m_{vc}$, and for the normalized equivalent viscous damping values, $\zeta_r/C_L > \zeta_{vc}/C_L \approx \zeta_{hc}/C_L > \zeta_h/C_L$, i.e. the horizontal-cylindrical TLD possess the properties of high natural frequency and effective mass but the lowest normalized damping value. The effective mass of a horizontal-cylindrical tank is approximately 15% larger than those of a rectangular or vertical-cylindrical tank. This increase in effective mass results in a larger mass ratio value.

This model is limited to small wave amplitude such that linear potential theory is valid, and that the effective mass and natural frequency are regarded as amplitude-independent parameters. This model is valid for TLD response amplitudes associated with wind-induced building motions. However, large free surface response amplitudes, which may occur, for example, during an earthquake event, are expected to exceed the valid response amplitude range of this model.

A velocity potential function of fluid flow is not always available for certain tank geometries. However, linear long wave theory can be applied to evaluate the fluid velocity in complex tank geometries. Thus, equivalent mechanical models for TLDs with more complex geometries can be constructed, which will be presented in the next chapter.

Table 2.1 Comparison of Calculated Effective Mass Values

	Budiansky (1960) actual A_1, B_1	Budiansky fitted A_1, B_1	% different between $(m_{hc}/m_w)_a$ &$(m_{hc}/m_w)_f$	Velocity Potential Theory	% different between $(m_{hc}/m_w)_a$ &$(m_{hc}/m_w)_v$
h/2R	$(m_{hc}/m_w)_a$	$(m_{hc}/m_w)_f$		$(m_{hc}/m_w)_v$	
0.1	92%	94%	2%	92%	0%
0.2	84%	86%	2%	83%	-1%
0.3	75%	77%	3%	74%	-1%
0.4	66%	67%	2%	64%	-3%
0.5	57%	58%	2%	53%	-7%

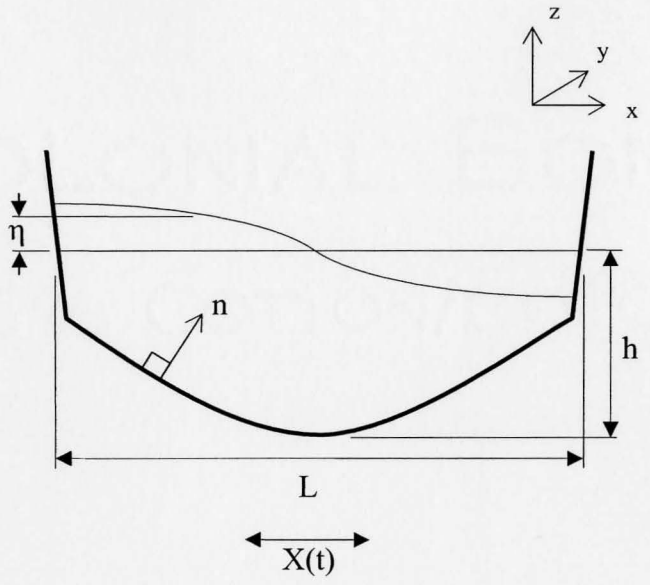

Figure 2.1 A Cartesian Coordinate Attached to an Arbitrary Tank Geometry

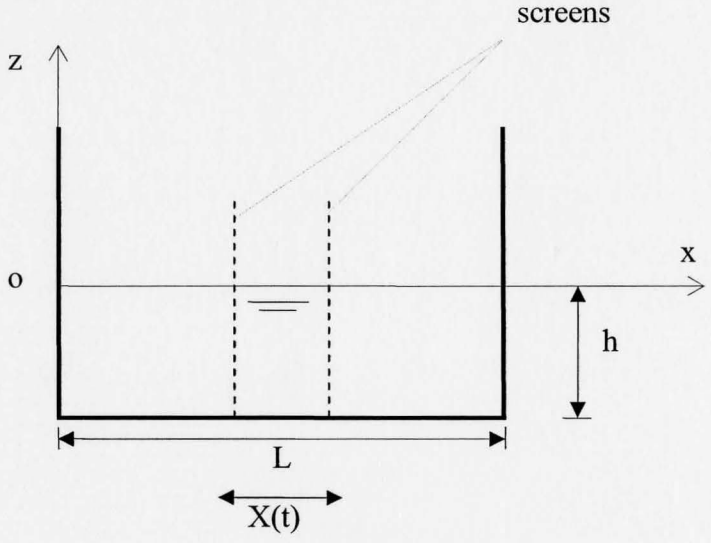

Figure 2.2 Definition Sketch for Liquid Sloshing in a Rectangular Tank

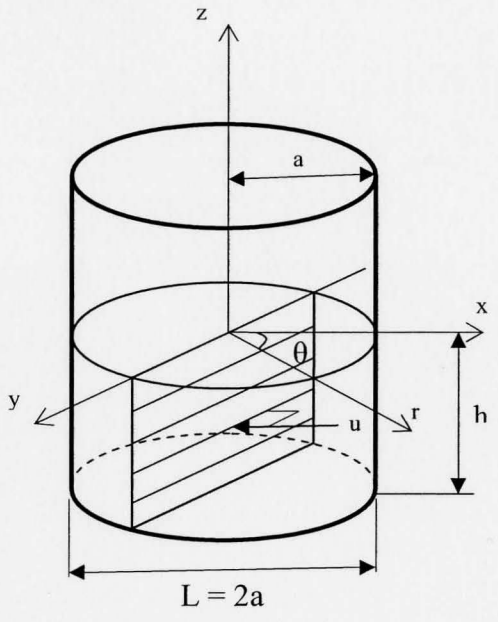

Figure 2.3 Definition Sketch for Liquid Sloshing in a Vertical-Cylindrical Tank

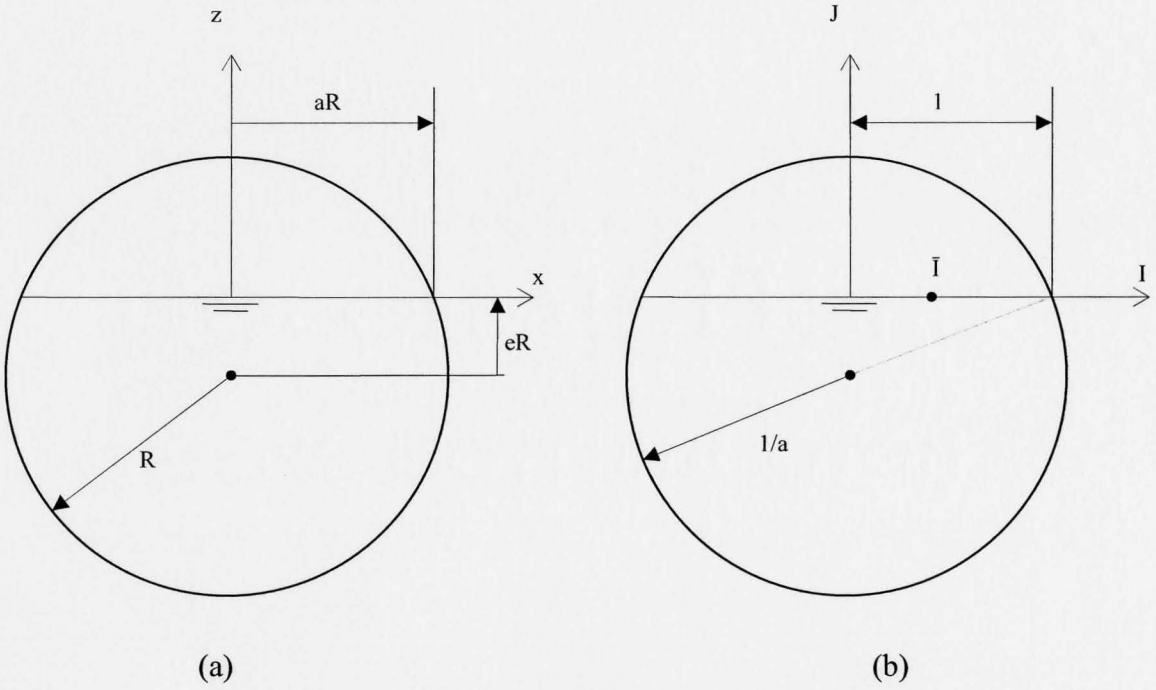

Figure 2.4 (a) Definition Sketch for Liquid Sloshing in a Horizontal-Cylinder Tank (b) Normalized Coordinate

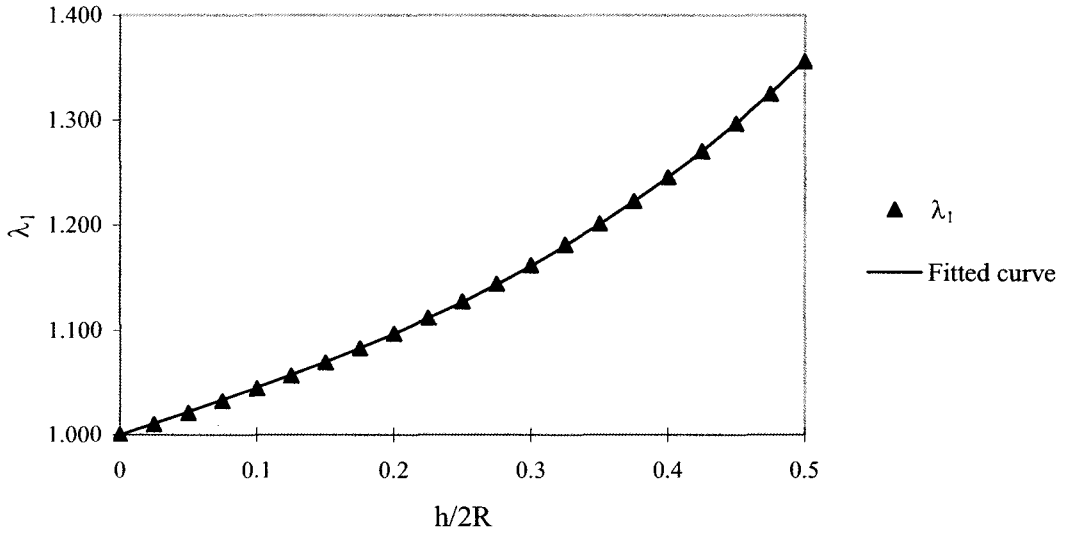

(a)

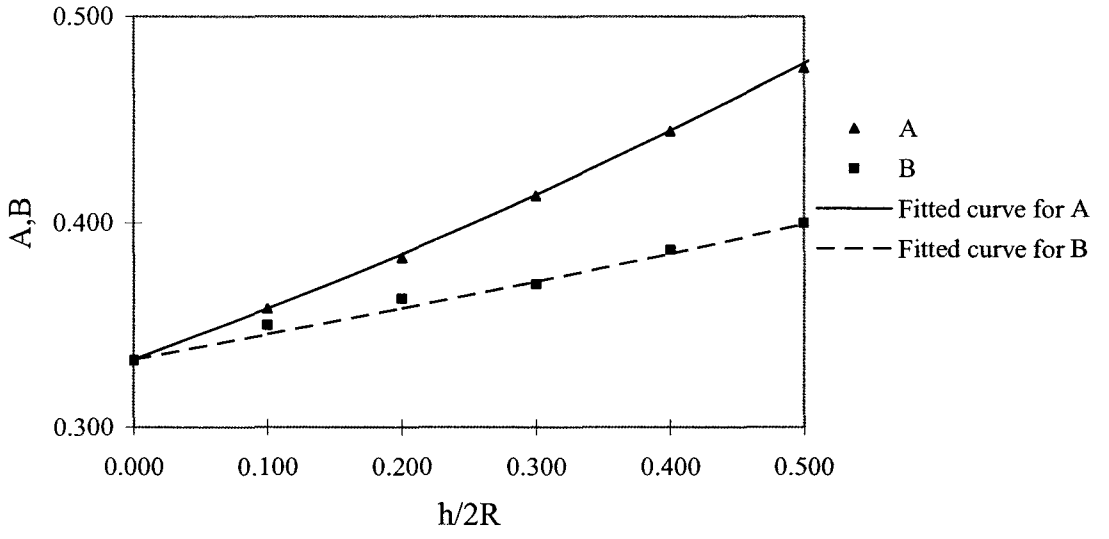

(b)

Figure 2.5 (a) Calculated and Fitted λ_1 (b) Calculated and Fitted A and B Parameters

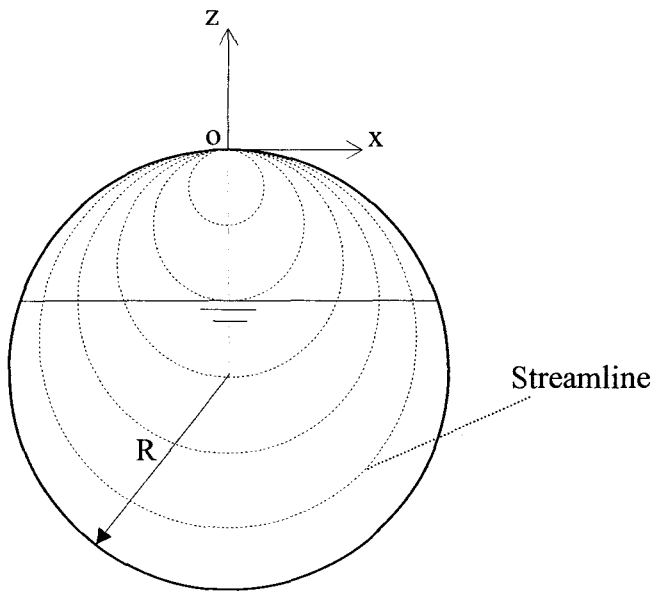

(a)

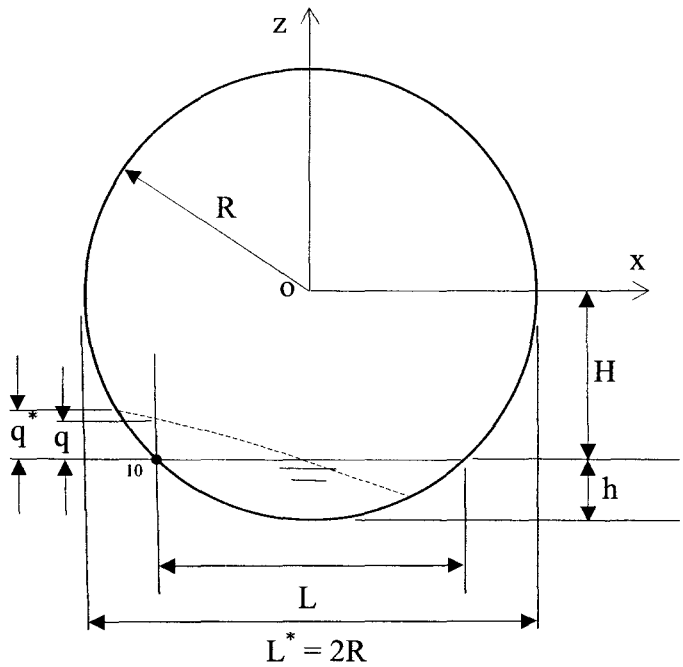

(b)

Figure 2.6 (a) Definition Sketch for Liquid Sloshing in a Horizontal-Cylindrical Tank with Streamlines (b) Coordinate Transformation

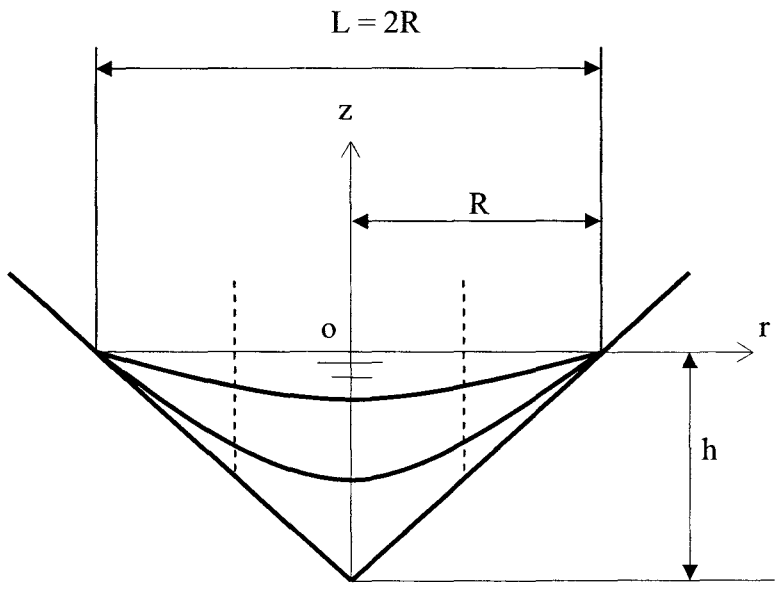

Figure 2.7 Definition Sketch for Liquid Sloshing in a 45° Conical and Hyperboloid Tanks

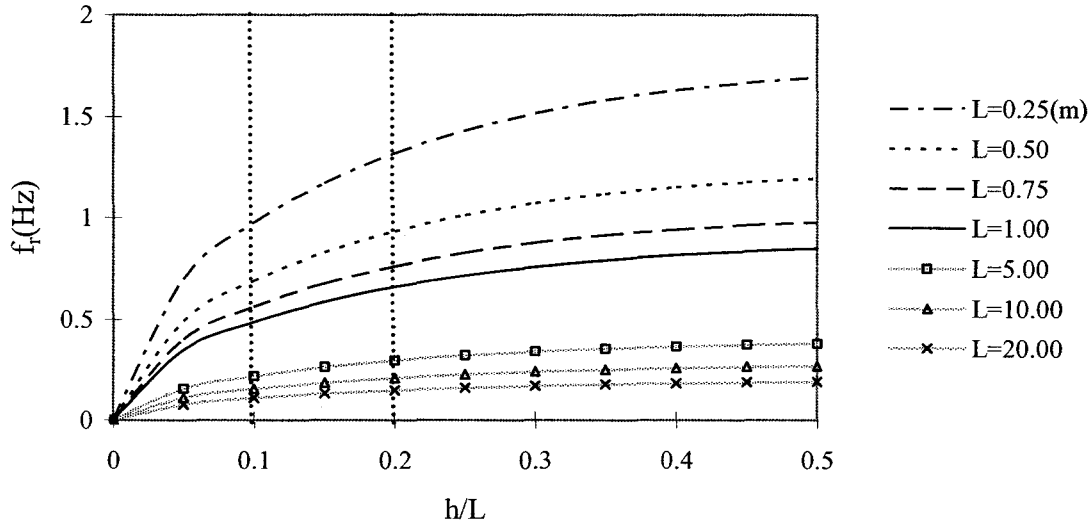

Figure 2.8 Natural Frequency for a Rectangular Tank

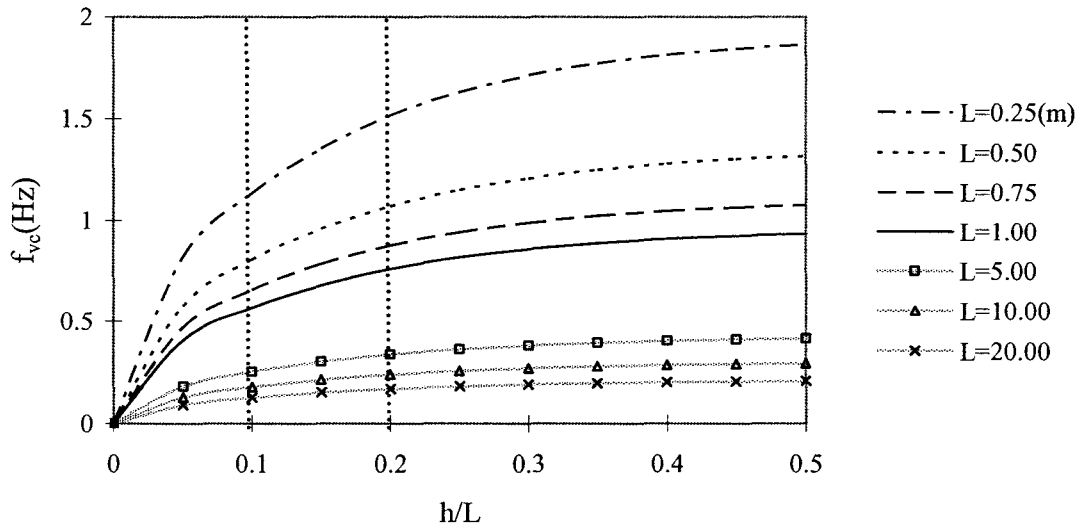

Figure 2.9 Natural Frequency for a Cylindrical Tank

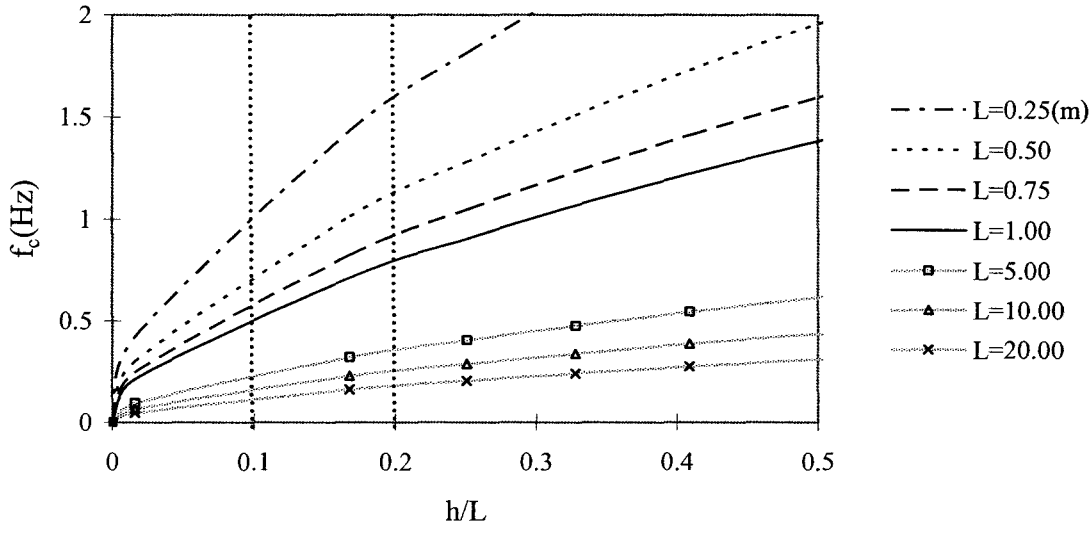

(a)

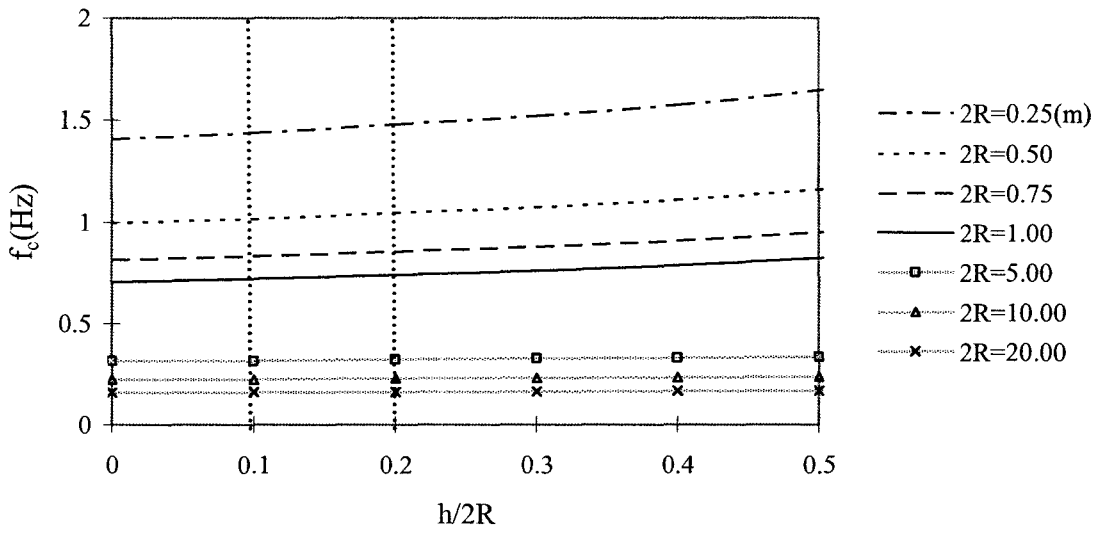

(b)

Figure 2.10 Natural Frequency for a Horizontal-Cylindrical Tank (a) Radius Changes with Liquid Depth Ratio; (b) Liquid Depth Ratio Defined as h/2R

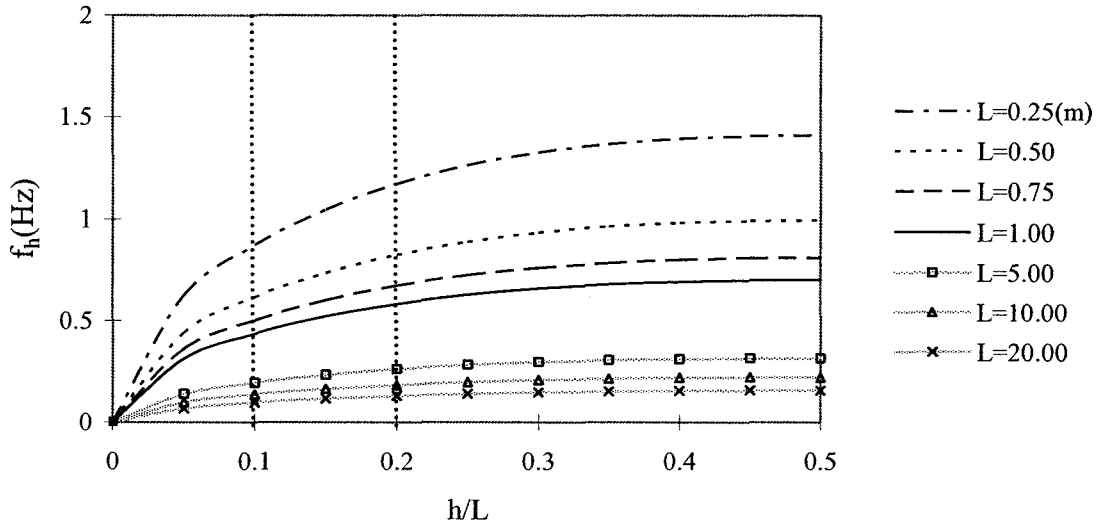

Figure 2.11 Natural Frequency for a Hyperboloid Tank

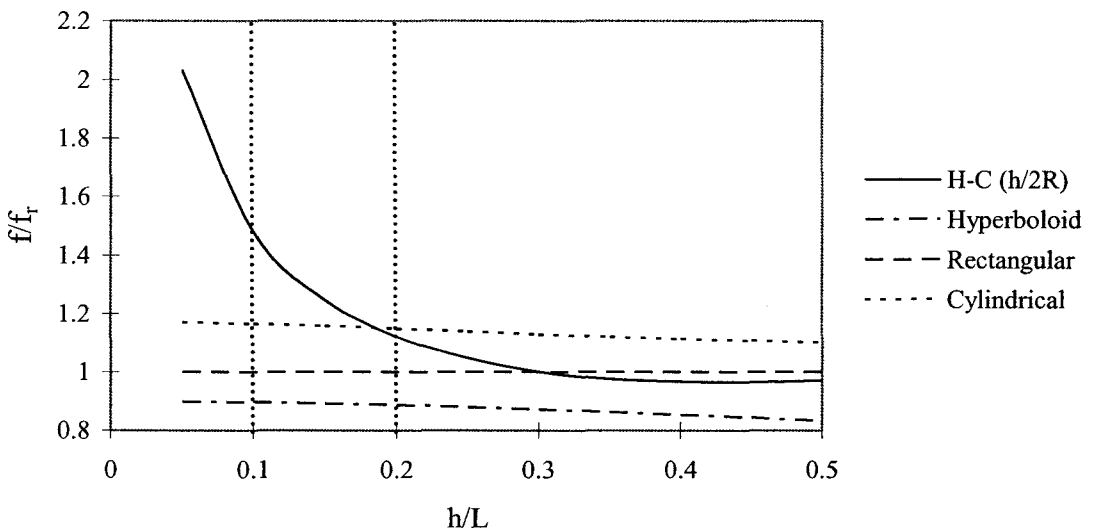

Figure 2.12 Comparison of Normailzied Natural Frequency for Different Tank Geometries

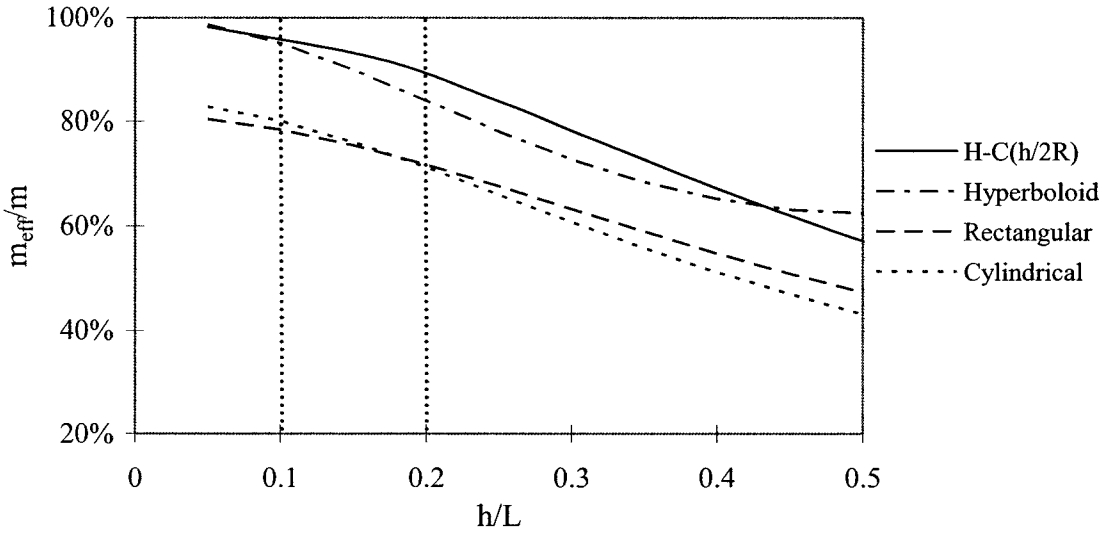

Figure 2.13 Comparison of Normalized Effective Mass for Different Tank Geometries

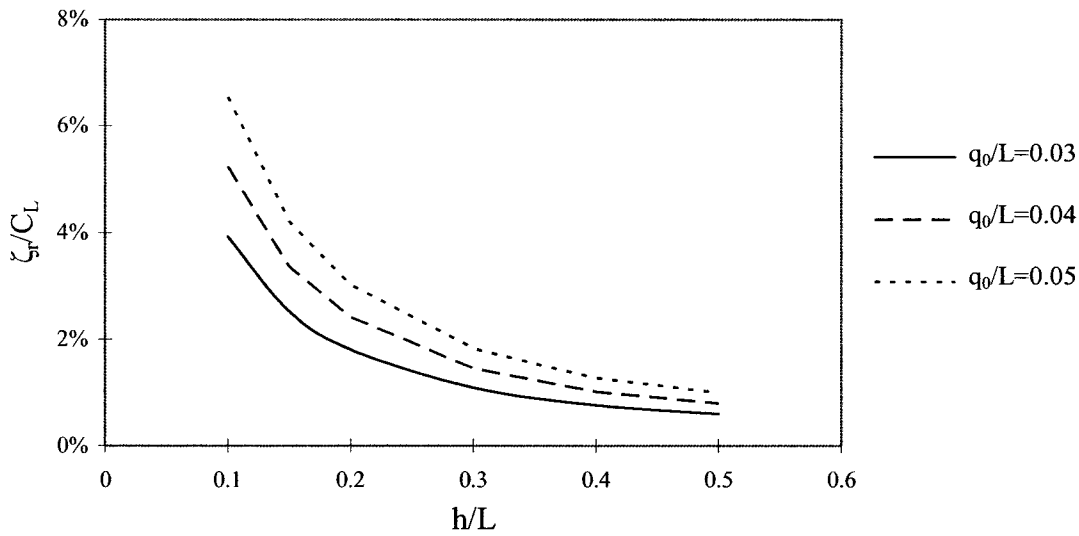

Figure 2. 14 Depth Ratio and Normalized Damping Ratio for a Rectangular Tank

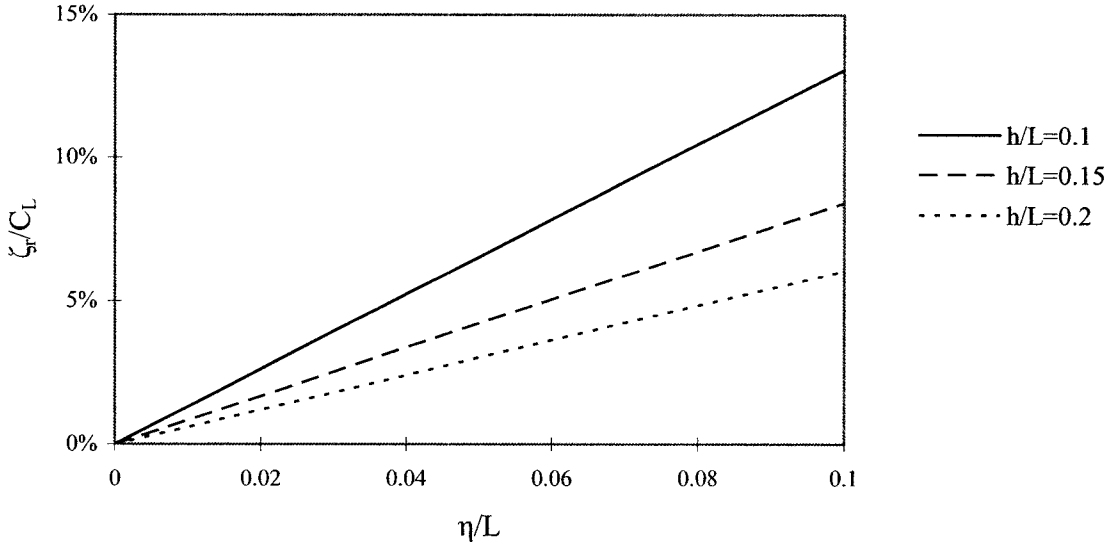

Figure 2.15 Variation of Normalized Damping Ratio with Liquid Depth and Normalized Response Amplitude for a Rectangular Tank

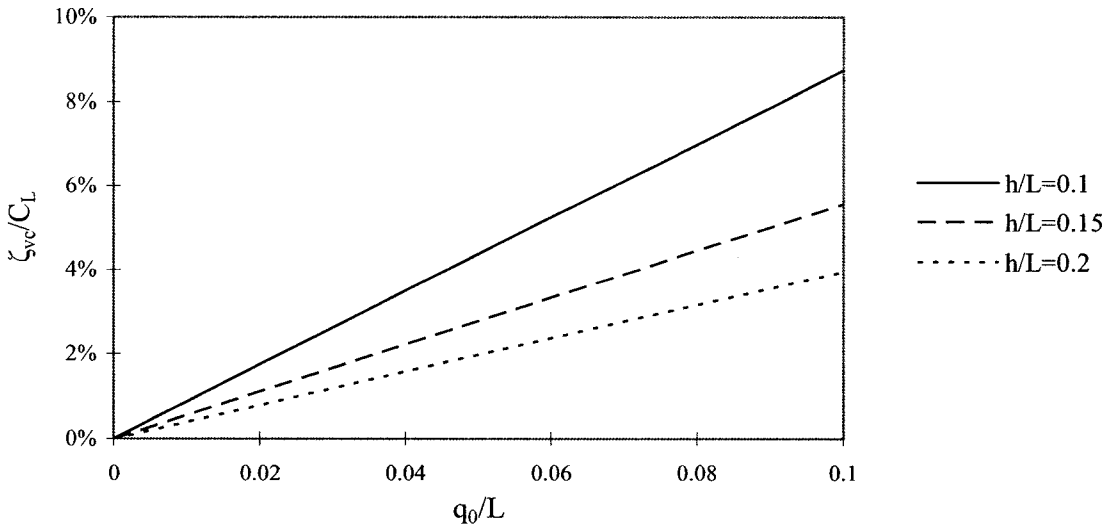

Figure 2.16 Variation of Normalized Damping Ratio with Liquid Depth and Normalized Response Amplitude for a Vertical-Cylindrical Tank

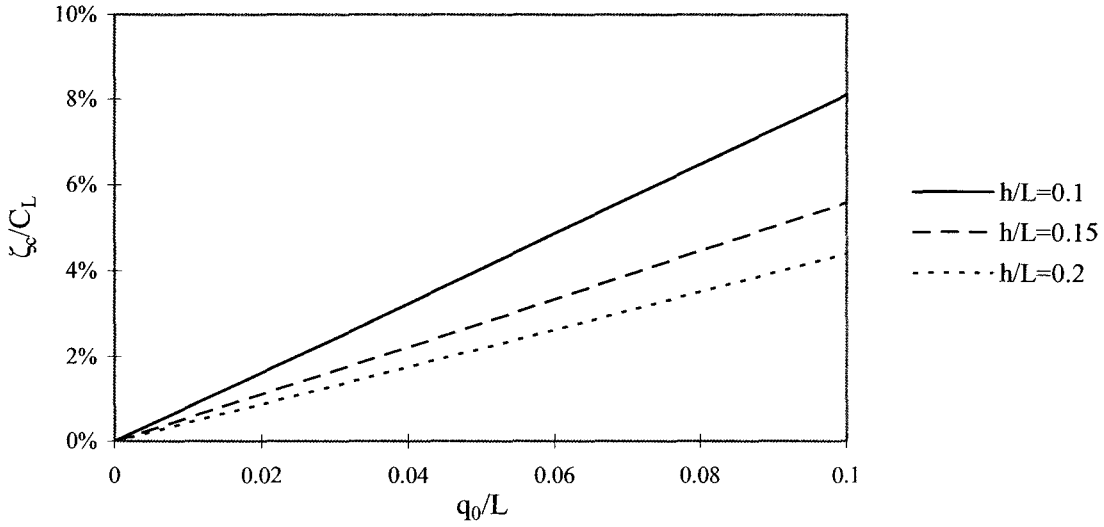

Figure 2. 17 Variation of Normalized Damping Ratio with Liquid Depth and Normalized Response Amplitude for a Horizontal-Cylinder Tank

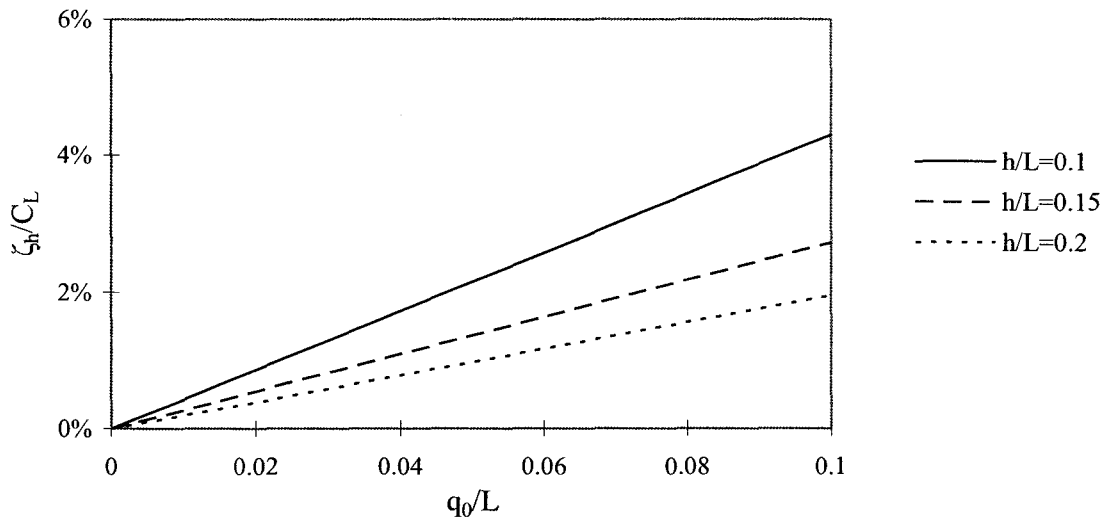

Figure 2. 18 Variation of Normalized Damping Ratio with Liquid Depth and Normalized Response Amplitude for a Hyperboloid Tank

Chapter 3 Theoretical Modelling of TLDs with Different Tank Geometries Using Linear Long Wave Theory

The dynamic properties required to construct an equivalent mechanical model of a TLD were derived in the previous chapter using potential flow theory. It is valid for any liquid depth ratio, h/L, whereas linear long wave theory can be utilized when $h/L < 0.1$. Additionally, linear long wave theory is limited to small free surface amplitude, that is, $\eta << h$ and $\eta /(16L^4/h^3) << 1$ (Le Méhauté 1976). Derivation of the dynamic properties of TLDs will be presented in this chapter using linear long wave theory, following the procedure outlined in Section 2.1. The following section provides a brief introduction to linear long wave theory.

3.1 Linear Long Wave Theory

The governing equations of linear long wave theory are the one-dimension linear continuity (Equation 3.1) and momentum equations (Equation 3.2), in which the convective inertia, friction terms and the nonlinear terms are neglected, respectively

$$\frac{\partial(uhb)}{\partial x} = -b\frac{\partial \eta}{\partial t} \tag{3.1}$$

$$b\frac{\partial u}{\partial t} = -gb\frac{\partial \eta}{\partial x} \tag{3.2}$$

where b is the tank width and η is the free surface amplitude. The wavelength for the first sloshing mode is denoted by $2L$ and it is equal to twice the length of the free surface. The horizontal velocity component is assumed to be constant through the liquid depth due to

the small liquid depth ratio. Differentiating Equation 3.1 with respect to time, and eliminating $b(\partial u/\partial t)$, using Equation 3.2, leads to

$$\frac{\partial^2 \eta}{\partial t^2} = \frac{g}{b}\frac{\partial}{\partial x}(hb\frac{\partial \eta}{\partial x}) \tag{3.3}$$

For the case of a constant tank width b, and the assumption of simple harmonic motion, the wave height at any location along the tank length can be expressed as

$$\eta(x,t) = f(x)q_0 \cos \omega t \tag{3.4}$$

where $f(x)$ is an arbitrary function of x and q_0 is the wave amplitude at the end-wall. Substituting Equation 3.4 into Equation 3.3, the following differential equation for the free surface response is obtained (Lamb 1932, Le Méhauté 1976)

$$g\frac{\partial}{\partial x}(h\frac{\partial \eta}{\partial x}) + \omega^2 \eta = 0 \tag{3.5}$$

The horizontal velocity component and wave height of the sloshing liquid in different tank geometries have previously been investigated using linear long wave theory. Lamb (1932) formulated the wave height and natural frequency for rectangular, triangular and parabolic tanks. Zelt (1986) extended the formulas of wave height and natural frequency for a sloped-bottom tank. Bauer (1981) approximated the velocity potential and natural frequency of sloshing liquid in a sloped-bottom tank using potential flow theory. However, these approximations yield acceptable results only when the sloping angle of the tank is large. The derivations of equivalent mechanical models for triangular, sloped-bottom, parabolic, and rectangular TLD are provided in the following sections.

3.2 Derivation of Equivalent Mechanical Models of TLDs with Different Tank Geometries Using Linear Long Wave Theory

3.2.1 Triangular Tank

3.2.1.1 Generalized Mass and Natural Frequency

A local Cartesian coordinate (x-o-z) is introduced as shown in Figure 3.1. The still liquid surface is defined by $z = 0$, h is the still liquid depth at the centre, and s is the length of the sloping region. The liquid depth, $h(x)$, increases linearly from either end to the centre of the tank.

Setting

$$h(x) = hx / s \tag{3.6}$$

and substituting Equation 3.6 into Equation 3.5 and subsequently solving the differential equation yields (Lamb 1932)

$$\eta(x) = AJ_0(2\sqrt{\kappa x}) \tag{3.7}$$

where

$$\kappa = \omega^2 s / gh \tag{3.8}$$

The constant A can be determined by equating the term η in Equation 3.7 to that given by Equation 3.4. The solution to Equation 3.5 is found to be in the following form

$$\eta(x) = q_0 J_0(2\sqrt{\kappa x}) \tag{3.9}$$

Restoring the time factor yields

$$\eta(x,t) = q_0 J_0(2\sqrt{\kappa x})\cos\omega t \tag{3.10}$$

or

$$\eta(x,t) = J_0(2\sqrt{\kappa x})q(t) \tag{3.11}$$

where

$$q(t) = q_0 \cos \omega t \tag{3.12}$$

For the lowest sloshing mode, the wave height, η, is zero at the centre of the tank ($x = s$), and the natural frequency can be determined by solving the following equation,

$$\eta(s) = q_0 J_0(2\sqrt{\kappa s}) = 0 \tag{3.13}$$

or

$$J_0(2\sqrt{\kappa s}) = 0 \tag{3.14}$$

The solution to Equation 3.14 is $2\sqrt{\kappa s} = 2.405$. From Equation 3.8, it is found that

$$\omega^2 = 5.784\frac{gh}{L^2} \tag{3.15}$$

The horizontal velocity component can be obtained by integrating the momentum equation (Equation 3.2) over time

$$u = -g\int\frac{\partial \eta(x,t)}{\partial x}dt \tag{3.16}$$

Substituting Equations 3.8 and 3.11 into Equation 3.16 yields (see Appendix C)

$$u = \frac{s}{\kappa h}\sqrt{\frac{\kappa}{x}}J_1(2\sqrt{\kappa x})\dot{q}(t) \tag{3.17}$$

In long wave theory, it is assumed that the vertical velocity component is much smaller than the horizontal velocity component. Therefore, the vertical velocity

component can be neglected with negligible loss of accuracy when the kinetic energy is calculated (Dean and Dalrymple 1984). The mass of a liquid particle can be expressed as

$$dm = \rho \frac{h}{s} x dx \tag{3.18}$$

Using Equation 2.2, the kinetic energy of the sloshing liquid in a triangular tank can be expressed as

$$KE = 2\int_0^s \frac{1}{2}(u + \dot{X})^2 \rho \frac{h}{s} x dx \tag{3.19}$$

Applying Lagrange's equations (Equation 2.6) to the kinetic energy equation above leads to the generalized mass, m^*, generalized excitation factor, γ^*, and effective mass, m_t, respectively, of a triangular tank,

$$m^* = \frac{\rho}{h}\left(\frac{s}{\kappa}\right)^{3/2} [cJ_0^2(c) - 2J_0(c)J_1(c) + cJ_1^2(c)] \tag{3.20}$$

$$\gamma^* = \rho \frac{s^{1/2}}{\kappa^{3/2}} [cJ_0(c) - 2J_1(c)] \tag{3.21}$$

$$m_t = \frac{8[cJ_0(c) - 2J_1(c)]^2}{c^3[cJ_0^2(c) - 2J_0(c)J_1(c) + cJ_1^2(c)]} m_w \tag{3.22}$$

where

$$c = 2\sqrt{ks}\,, \tag{3.23}$$

and m_w denotes the total mass of liquid in the tank. Substituting the solution of Equation 3.14 into Equation 3.22, an effective mass of $m_t = 95.7\%\ m_w$ is obtained.

3.2.1.2 Additional Damping Due to Screens

Based on the horizontal component of the velocity u in Equation 3.17, the virtual displacement δq in Equation 2.15 becomes

$$\delta q(x,t) = \delta q(t)\frac{s}{\kappa h}\sqrt{\frac{\kappa}{x}}J_1(2\sqrt{\kappa x}) \tag{3.24}$$

Substituting Equations 3.17, 3.24 and 2.12 into Equation 2.14, the parameters Δ and Ξ for a triangular tank can be expressed as

$$\Xi = \sum_{j=1}^{ns}\left[\sqrt{\frac{\kappa}{x}}J_1(2\sqrt{\kappa x})\right]^3\frac{h}{s}x_j \tag{3.25}$$

$$\Delta = \left[\frac{s}{\kappa h}\right]^3 \tag{3.26}$$

The damping ratio can be computed by substituting Δ and Ξ into Equations 2.22 and 2.25.

3.2.2 Sloped-Bottom Tank

3.2.2.1 Generalized Mass and Stiffness

The coordinate system used for a triangular TLD is also used for a sloped-bottom TLD (Figure 3.2). The liquid depth $h(x)$ is expressed as

$$h(x) = \begin{cases} hx/s & x < s \\ h & s \le x \le L_0 \end{cases} \tag{3.27}$$

where s is the length of the sloping region, and L_0 is equal to half of the free surface length. Substituting Equation 3.27 into Equation 3.5 and solving the differential equation yields

$$\eta = J_0(2\sqrt{\kappa x})q(t) \qquad \text{for } (x < s) \qquad (3.28)$$

$$\frac{\partial \eta}{\partial x} = -\sqrt{\frac{\kappa}{x}} J_1(2\sqrt{\kappa x})q(t) \qquad \text{for } (x < s) \qquad (3.29)$$

$$\eta = \left(a_1 \cos\sqrt{\frac{\kappa}{s}}x + a_2 \sin\sqrt{\frac{\kappa}{s}}x \right) q(t) \qquad \text{for } (s < x < L_0) \qquad (3.30)$$

$$\frac{\partial \eta}{\partial x} = \left(-a_1\sqrt{\frac{\kappa}{s}} \sin\sqrt{\frac{\kappa}{s}}x + a_2\sqrt{\frac{\kappa}{s}} \cos\sqrt{\frac{\kappa}{s}}x \right) q(t) \qquad \text{for } (s < x < L_0) \qquad (3.31)$$

In order to obtain the constants a_1 and a_2 in Equations 3.30 and 3.31, the conditions of equal head loss and velocity at $x = s$ are applied. That is to force η and $\partial\eta/\partial x$ to be continuous at $x = s$, where the sloping region and the uniform-depth region meet. Complete expressions for Equations 3.30 and 3.31 are given by Zelt (1986).

$$\eta = \left[J_0(c)\cos\sqrt{\frac{\kappa}{s}}(x-s) - J_1(c)\sin\sqrt{\frac{\kappa}{s}}(x-s) \right] q(t) \qquad \text{for } (s < x < L_0) \qquad (3.32)$$

$$\frac{\partial \eta}{\partial x} = -\sqrt{\frac{\kappa}{s}} \left[J_1(c)\cos\sqrt{\frac{\kappa}{s}}(x-s) + J_0(c)\sin\sqrt{\frac{\kappa}{s}}(x-s) \right] q(t) \qquad \text{for } (s < x < L_0) \qquad (3.33)$$

The horizontal velocity component of the sloshing motion can be determined using Equations 3.16, 3.29 and 3.33 and can be expressed as

$$u = \frac{s}{\kappa h}\sqrt{\frac{\kappa}{x}} J_1(2\sqrt{\kappa x})\dot{q}(t) \qquad \text{for } (x < s) \qquad (3.34)$$

$$u = \frac{s}{\kappa h} \left[J_1(c)\cos\sqrt{\frac{\kappa}{s}}(x-s) + J_0(c)\sin\sqrt{\frac{\kappa}{s}}(x-s) \right] \dot{q}(t) \qquad \text{for } (s < x < L_0) \qquad (3.35)$$

To obtain the natural frequency of oscillation, the condition of $\eta(L_0, t) = 0$ is applied to Equation 3.32, that is,

$$J_0(c)\cos\sqrt{\frac{\kappa}{s}}(L_0 - s) - J_1(c)\sin\sqrt{\frac{\kappa}{s}}(L_0 - s) = 0 \qquad \text{for } (s < x < 1) \qquad (3.36)$$

The final solution to the above equation, which yields values of κ, is computed using MathCAD, as a closed-form solution was not found.

Equations 2.1 and 2.2 are used to calculate the kinetic energy with

$$dm = \rho\frac{h}{s}xdx \qquad \text{for } (x < s) \qquad (3.37)$$

$$dm = \rho h dx \qquad \text{for } (s < x < L_0) \qquad (3.38)$$

The kinetic energy of sloshing liquid in a sloped-bottom tank can be expressed as

$$KE = 2\left[\int_0^s \frac{1}{2}(u + \dot{X})^2 \rho\frac{h}{s}xdx + \int_s^{L_0}\frac{1}{2}(u + \dot{X})^2 \rho h dx\right] \qquad (3.39)$$

Applying Lagrange's equations to the kinetic energy equation leads to the generalized mass and the generalized excitation factor.

$$m^* = 2\rho\left(\frac{s}{ch}\right)^2\begin{bmatrix} cJ_0^{\,2}(c) - 2J_0(c)J_1(c) + cJ_1^{\,2}(c) + cL_0J_1^{\,2}(c)/2s \\ -2J_0(c)J_1(c)\cos c(1-1/s) - J_1^{\,2}(c)\sin c(1-1/s) \\ +J_0^{\,2}(c)\sin c(1-1/s) + cL_0J_0^{\,2}(c)/s \end{bmatrix} \qquad (3.40)$$

$$\gamma^* = \frac{8\rho s^2}{c^3}\left[-2J_1(c) + cJ_1(c)\sin c(1-1/s) + cJ_0(c)\cos c(1-1/s)\right] \qquad (3.41)$$

The effective mass can be found by substituting Equations 3.40 and 3.41 into Equation 2.11

$$m_s = \frac{32\rho s^2 h^2 \left[-2J_1(c)+cJ_1(c)\sin c(1-1/s)+cJ_0(c)\cos c(1-1/s)\right]^2}{c^4\left[\begin{array}{l} cJ_0{}^2(c)-2J_0(c)J_1(c)+cJ_1{}^2(c)+cL_0J_1{}^2(c)/2s \\ -2J_0(c)J_1(c)\cos c(1-1/s)-J_1{}^2(c)\sin c(1-1/s) \\ +J_0{}^2(c)\sin c(1-1/s)+cL_0J_0{}^2(c)/s \end{array}\right]} \tag{3.42}$$

3.2.2.2 Additional Damping Due to Screens

Equations 3.34 and 3.35, which describe the horizontal component of the velocity u, are employed to compute the virtual displacement δq of the liquid particles in Equation 2.15, which can be expressed as,

$$\delta q(x,t) = \delta q(t)\frac{s}{\kappa h}\sqrt{\frac{\kappa}{x}}J_1(2\sqrt{\kappa x}) \qquad \text{for } (x < s) \tag{3.43}$$

$$\delta q(x,t) = \delta q(t)\frac{s}{\kappa h}\sqrt{\frac{\kappa}{x}}J_1(2\sqrt{\kappa x}) \qquad \text{for } (s < x < L_0) \tag{3.44}$$

Substituting Equations 3.34 and 3.35 for u, Equations 3.43, 3.44 and 2.12 into Equations 2.14 yields

- for the case of $x_j < s$, Ξ and Δ are the same as the expressions found for a triangular tank given by Equations 3.25 and 3.26.
- for the case of $s < x_j < L_0$, Δ is the same as Equation 3.26, and

$$\Xi = \sum_{j=1}^{ns}\sqrt{\frac{\kappa}{s}}\left[J_1(c)\cos\sqrt{\frac{\kappa}{s}}(x-s)+J_0(c)\sin\sqrt{\frac{\kappa}{s}}(x-s)\right]h \tag{3.45}$$

3.2.3 Parabolic Tank

3.2.3.1 Generalized Mass and Natural Frequency

The geometry of a parabolic TLD is shown in Figure 3.3 with a Cartesian coordinate system, where L_0 represents half of the free surface length.

$$h(x) = h(1 - \frac{x^2}{L_0^2}) \tag{3.46}$$

Substituting Equation 3.46 into Equation 3.5 and solving the differential equation gives (Lamb 1932)

$$\eta = q_0 \frac{x}{L_0} \tag{3.47}$$

for the first sloshing mode ($n = 1$) and

$$\omega^2 = n(n+1)\frac{gh}{L_0^2} \tag{3.48}$$

Substituting Equation 3.47 into the momentum equation (Equation 3.2) and integrating over time yields

$$u(x,t) = \frac{L_0}{2h}\dot{q}(t) \tag{3.49}$$

To obtain the kinetic energy, Equations 2.1 and 2.2 are employed

$$dm = \rho h(1 - \frac{x^2}{L_0^2})bdx \tag{3.50}$$

$$KE = \int_0^s \frac{1}{2}(u + \dot{X})^2 \rho h(1 - \frac{x^2}{L_0^2})bdx \tag{3.51}$$

Applying Lagrange's equations to the kinetic energy leads to generalized mass, m^*, generalized excitation factor, γ^*, and effective mass, m_p, respectively, for a parabolic tank,

$$m^* = \frac{1}{3}\frac{L_0{}^3 b}{h} \tag{3.52}$$

$$\gamma^* = \frac{2}{3} L_0{}^2 b \tag{3.53}$$

$$m_p = m_w \tag{3.54}$$

All liquid is found to participate in the sloshing motion. It is noted that in the linear long wave theory the velocity is assumed to be constant through the liquid the depth.

3.2.3.2. Additional Damping Due to Screens

Based on the horizontal component of the velocity u in Equation 3.49, δq in Equation 2.15 becomes

$$\delta q(x,t) = -\delta q(t)\frac{L_0}{2h} \tag{3.55}$$

Substituting Equations 3.49, 3.55 and 2.12 into Equation 2.14, the parameters Δ and Ξ are found to be

$$\Xi = \sum_{j=0}^{ns} h(x_j) \tag{3.56}$$

$$\Delta = \left[\frac{L_0}{2h}\right]^3 \tag{3.57}$$

3.2.4 Rectangular Tank

3.2.4.1 Generalized Mass and Natural Frequency

The geometry of a rectangular TLD is shown in Figure 3.4 with a Cartesian coordinate system. The still liquid depth $h(x)$ is constant in this case, therefore,

$$h(x) = h \tag{3.58}$$

Substituting Equation 3.58 into Equation 3.5 and solving the differential equation yields

$$\eta(x,t) = q(t)\cos(\frac{\omega}{\sqrt{gh}}x) \tag{3.59}$$

where

$$q(t) = q_0 \cos\omega t\,|_{x=0} \tag{3.60}$$

For the lowest sloshing mode, the free surface elevation η is zero at the centre of the tank ($x = L/2$), and the natural frequency can be determined by solving the following equation (Lamb 1932),

$$\cos(\frac{\omega}{\sqrt{gh}}x) = 0 \tag{3.61}$$

and is found to be

$$\omega^2 = g\pi\frac{h}{L} \tag{3.62}$$

Integrating the momentum equation (Equation 3.2) over time yields

$$u(x,t) = -\frac{L}{\pi h}\sin(\frac{\pi}{L}x)\dot{q}(t) \tag{3.63}$$

Additionally, the mass of a liquid particle can be expressed as

$$dm = \rho h x dx \tag{3.64}$$

Applying Equation 2.2, the kinetic energy of sloshing liquid in a rectangular tank can be expressed as

$$KE = \int_0^s \frac{1}{2}(u + \dot{X})^2 \rho h dx \tag{3.65}$$

Applying Lagrange's equations to the kinetic energy equation leads to generalized mass, m^*, generalized excitation factor, γ^*, and effective mass, m_{rl}, respectively,

$$m^* = \frac{1}{2}\frac{\rho L^3}{\pi^2 h} \tag{3.66}$$

$$\gamma^* = 2\rho\left(\frac{L}{\pi}\right)^2 \tag{3.67}$$

$$m_{rl} = \frac{8}{\pi^2} m_w \tag{3.68}$$

where m_{rl} denotes the effective mass of a rectangular TLD based on linear long wave theory. Note that Equation 3.68 can be considered as a special case of Equation 2.51 with $h/L \leq 0.1$ and

$$\frac{\tanh\left(\frac{\pi h}{L}\right)}{\frac{\pi h}{L}} \approx 1 \tag{3.69}$$

3.2.4.2. Additional Damping Due to Screens

Based on the horizontal component of the velocity u in Equation 3.63, the virtual displacement δq in Equation 2.15 becomes

$$\delta q(x,t) = -\frac{L}{\pi h}\sin(\frac{\pi}{L}x)\delta q(t) \tag{3.70}$$

Substituting Equations 3.63, 3.70 and 2.12 into Equation 2.14 yields

$$\Xi = \sum_{j=1}^{ns}\left[\sin\left(\frac{\pi}{L}x_j\right)\right]^3 \tag{3.71}$$

$$\Delta = h\left[\frac{L}{\pi h}\right]^3 \tag{3.72}$$

For comparative purposes, equations for the equivalent mechanical model properties for all tank geometries investigated in this chapter are summarized in Appendix A.

3.3 Comparison of Equivalent Mechanical Model Properties

Linear long wave theory can be considered as a special case of small amplitude wave theory when *h/L* approaches zero (Le Méhauté 1976). Linear long wave is valid when *h/L* is less than 0.1. If *h/L* exceeds the limit of 0.1, the natural frequency, effective mass and damping ratio will be overestimated, as this theory assumes the horizontal velocity is uniform through the liquid depth.

3.3.1 Natural Frequency

The formulas for calculating the natural frequency for four different tank geometries have been derived. From Equations 3.15, 3.36, 3.48, and 3.62, the fundamental sloshing frequency of triangular, parabolic, sloped-bottom, and rectangular tanks, respectively, can expressed as

$$f_t = \frac{1.023}{\pi L}\sqrt{gh} \tag{3.73}$$

$$f_p = \frac{1}{\pi L}\sqrt{gh} \tag{3.74}$$

$$f_s = \frac{\varepsilon}{2L}\sqrt{gh} \tag{3.75}$$

where

$$\varepsilon = \frac{f_s}{f_{rl}} \tag{3.76}$$

$$f_{rl} = \frac{1}{2L}\sqrt{gh} \tag{3.77}$$

The ratio of the natural frequency of a sloped-bottom TLD to that of a rectangular TLD is denoted by ε, which is a function of s/L as shown in Figure 3.5 (Gardarsson et al 2001).

It is shown in Figures 3.5 to 3.9 that tank length and liquid depth ratio affect the natural frequencies of these TLDs. The natural frequency is found to increase as the depth ratio h/L increases, or as the tank length L decreases. The rate of increase in the natural frequencies of the TLDs is large when depth ratio is small. For a sloped-bottom TLD, the ratio of the length of sloping region to free surface length s/L_0 also affects the natural frequency as shown in Figure 3.5. The natural frequency decreases with an increase in s/L_0. Triangular and rectangular tanks correspond to s/L_0 values of unity and zero, respectively (Gardarsson et al. 2001). The error between the theoretical results and the experimental results is found to be less than 4% (Gardarsson 1997).

The formulations of natural frequency based on linear long wave theory are valid when the liquid depth ratio is less than 0.1. Thus, Equation 3.73 to Equation 3.77 for triangular, sloped-bottom, parabolic and rectangular TLD cannot be used to accurately evaluate the natural frequency when the depth ratio is larger than 0.1.

Lamb (1932) developed a solution for a triangular tank with 45° sloping angle (corresponding to $h/L = 0.5$) using potential flow theory. In Figure 3.6, the lines present the natural frequency calculated using linear long wave theory, and the makers at $h/L = 0.5$ are the natural frequency values which have been determined using Lamb's solution. It is shown that the natural frequency, derived using linear long wave theory, is overestimated when h/L exceeds 0.1. This overestimation of the natural frequency is also shown in Figure 3.9 for a rectangular tank (where the markers represent the results based on potential flow theory, note that good agreement is found for $h/L < 0.15$). Figure 3.6 can be used to approximate the natural frequency of a triangular tank with any sloping angle in the range of 0 to 45° by assuming the natural frequency increases linearly between the linear long wave theory results at $h/L = 0.1$ and the potential flow theory results at $h/L = 0.5$. Bauer (1981) approximated the natural frequency of a triangular and sloped-bottom tank with a large sloping angle using potential flow theory. It is postulated that the method described above to estimate the natural sloshing frequency for h/L values greater than 0.1 can be applied to sloped-bottom tanks as well. The natural frequency of triangular and sloped-bottom tanks in this range of h/L values has not been determined theoretically. For all h/L values, the trend is found, $f_{rl} > f_s > f_t > f_p$, as shown in Figure 3.10.

3.3.2 Effective Mass

The effective mass of a TLD derived from linear long wave theory is independent of the depth ratio h/L. The effective mass for a parabolic, triangular and rectangular TLD has been found to be 100, 95.7 and 81.1 % of the total liquid mass, respectively. For a sloped-bottom TLD, the effective mass depends upon the length of free surface L and the length of the sloping region s. By holding L_0 constant, and changing the value of s, it is found that a maximum effective mass of $99.4\%m_w$ occurs at $s/L_0 = 0.6$ or sloping angle of 18° (Figure 3.11), i.e. this configuration of a sloped-bottom TLD is the most effective in eliminating the inactive liquid at the end-walls of a rectangular tank. Also, when keeping s constant, and varying the value of L_0, the maximum effective mass occurs at $L_0/s = 1.8$ (Figure 3.12) i.e. $s/L_0 = 0.6$. The effect of the sloping region on the properties of the TLDs is reduced, as L_0 increases. As a result, the sloped-bottom TLD possesses similar properties to those of a rectangular TLD. For instance, the effective mass of a sloped-bottom TLD will reach 81% as L_0/s approaches infinity as shown in Figure 3.12. For $s/L_0 = 0.6$, the following trend is found: $m_p > m_s > m_t > m_{rl}$. The effective mass values of parabolic and sloped-bottom tanks are large, therefore, valid mechanical models for these tanks for larger h/L values are of interest.

3.3.3 Additional Damping Due to Screens

Given the dimensions of a TLD, the four factors which affect the damping ratio are liquid depth ratio, number of screens, drag coefficient and free surface response amplitude. Variations of the normalized damping ratio, ζ/C_L, with liquid depth ratio, h/L, and normalized response amplitude, η/L, are plotted in Figures 3.13 to 3.17 for the TLDs

considered in this chapter. For simplicity, the case of one screen inserted at the centre of the tank is studied here. The same variations of ζ/C_L with h/L and η/L, as those observed in Chapter 2, are found. The damping ratio is found to increase linearly with the normalized excitation amplitude for all the tanks considered in this chapter due to velocity squared damping (see Equation 2.22). Additionally, the increase in damping ratio with a reduction in liquid depth ratio is attributed to an increase in the horizontal velocity. The relationship between the normalized damping ratio for the different tanks considered is as follows, $\zeta_{rl}/C_L > \zeta_p/C_L \approx \zeta_s/C_L > \zeta_t/C_L$.

3.4 Summary

In this chapter, linear long wave theory was used to calculate the horizontal velocity component of the sloshing liquid, which is assumed to be constant through the liquid depth. Also, it is assumed that the vertical velocity component is negligible. These assumptions are reasonable when $\eta << h$ and $h/L < 0.1$. The parameters for an equivalent mechanical model for triangular, sloped-bottom, parabolic and rectangular TLDs have been derived using linear long wave theory in conjunction with the method described in Section 2.1. Subsequently, the natural frequency, effective mass and damping ratio for the tanks with different tank geometries are compared, respectively. Relationships between the derived parameters for the studied tanks are as follows. For the sloshing frequency values, which were computed for a range of h/L values, the following trend was observed, $f_{rl} > f_s > f_t > f_p$. Furthermore, the following pattern was determined for effective mass values, $m_p > m_s > m_t > m_{rl}$. Finally, the normalized equivalent viscous damping values, due to the screens, were determined and the normalized damping ratio values for different

tank were examined. It was found that $\zeta_{rl}/C_L > \zeta_p/C_L \approx \zeta_s/C_L > \zeta_t/C_L$. The effective mass for a parabolic tank and sloped-bottom tank, with a sloping angle of 18°, is 100%. This indicates that all the liquid mass is participating in the fluid sloshing motion. The derived models are valid for small fluid response amplitudes. For larger response amplitudes, which result in a hardening type behaviour, an equivalent mechanical system which is capable of simulating the amplitude dependent nonlinear natural frequency would be more suitable.

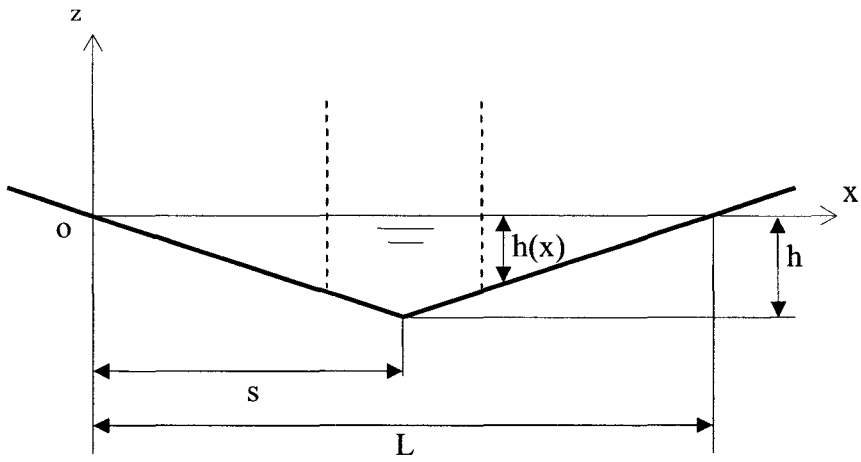

Figure 3.1 Definition Sketch for Liquid Sloshing in a Triangular Tank

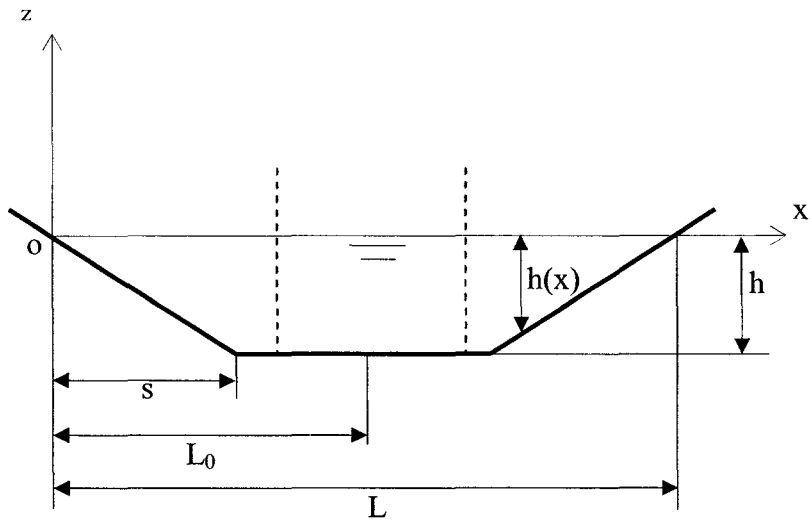

Figure 3.2 Definition Sketch for Liquid Sloshing in a Sloped-Bottom Tank

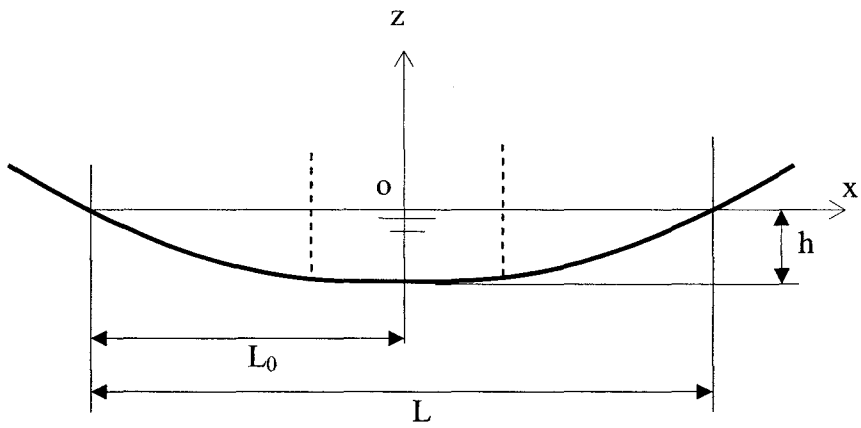

Figure 3.3 Definition Sketch for Liquid Sloshing in a Parabolic Tank

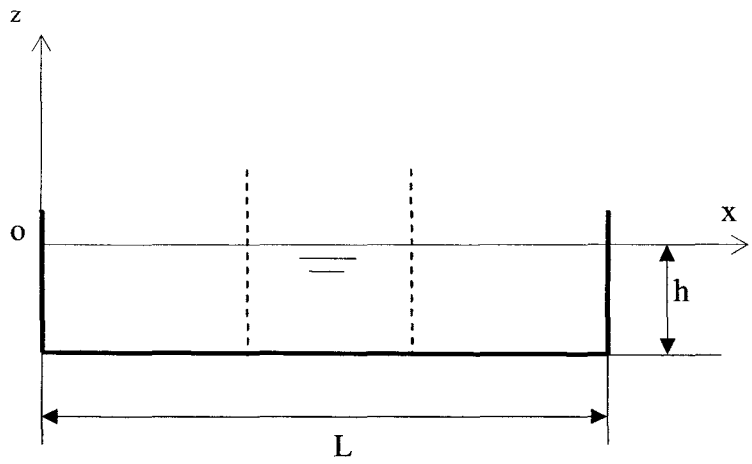

Figure 3.4 Definition Sketch for Liquid Sloshing in a Sloped-Bottom Tank

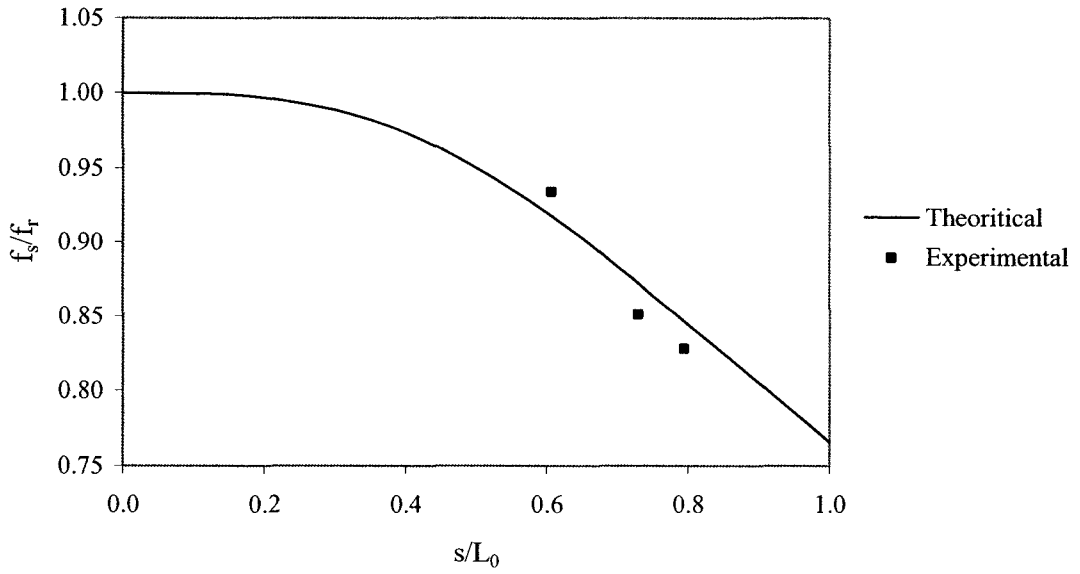

Figure 3.5 Relation between Natural Frequency for a Rectangular and Sloped-Bottom Tank

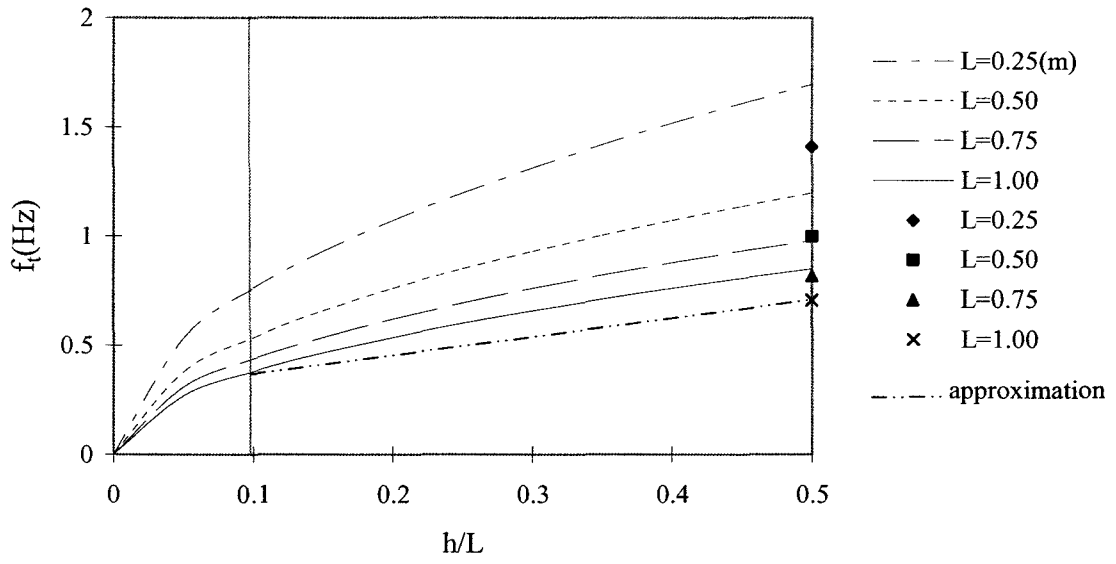

Figure 3.6 Natural Frequency for a Triangular Tank

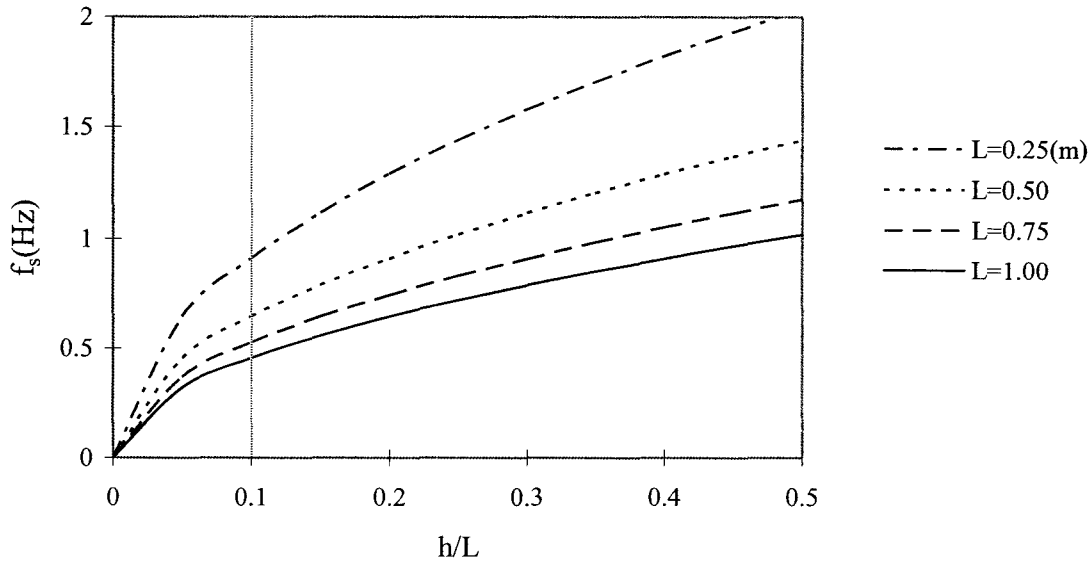

Figure 3.7 Natural Frequency for a Sloped-Bottom Tank with s/L = 0.6

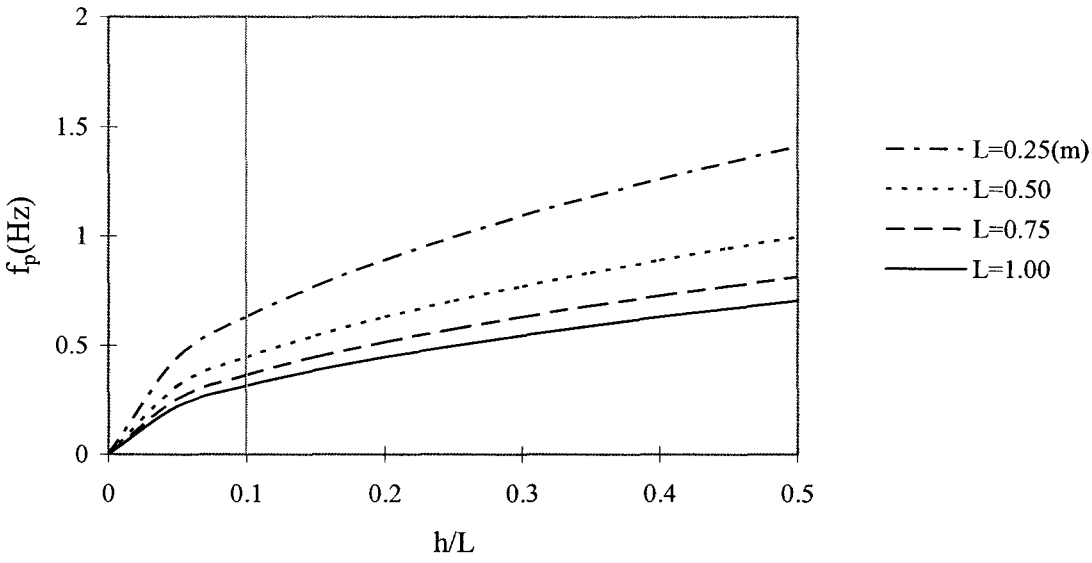

Figure 3.8 Natural Frequency for a Parabolic Tank

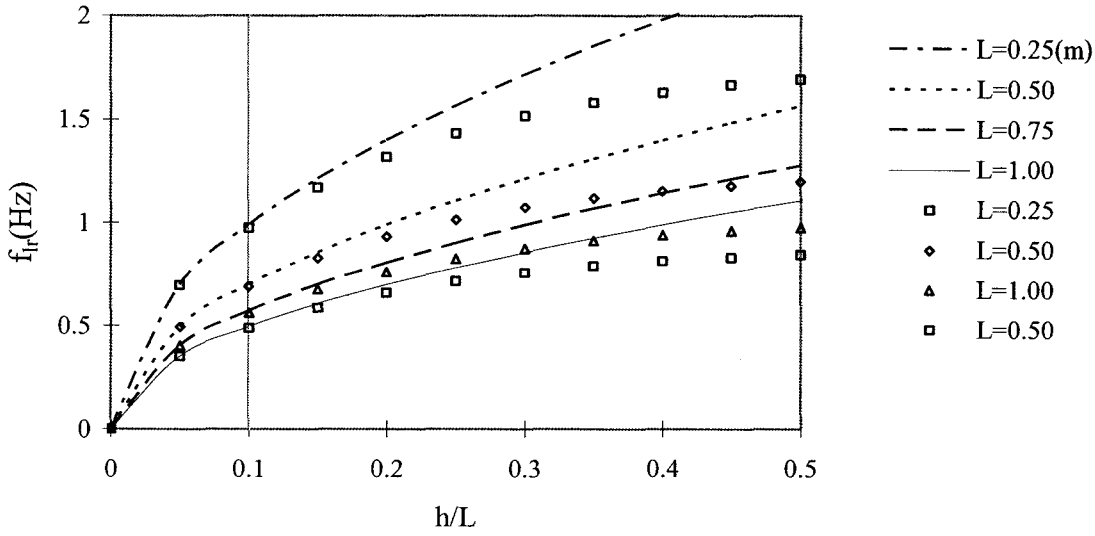

Figure 3.9 Natural Frequency for a Rectangular Tank

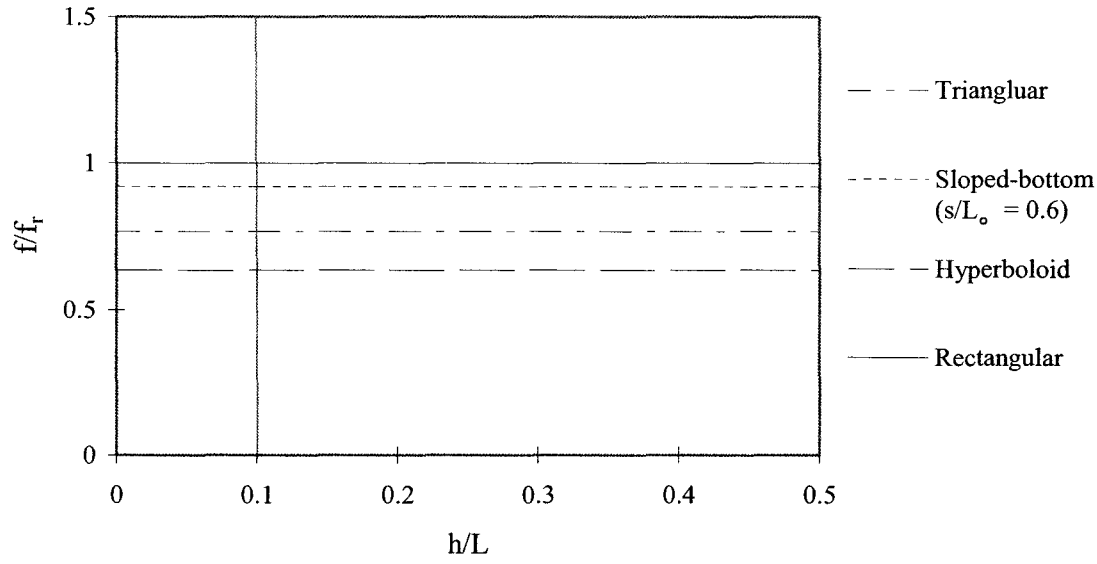

Figure 3.10 Comparison of Normalized Natural Frequency between Tanks

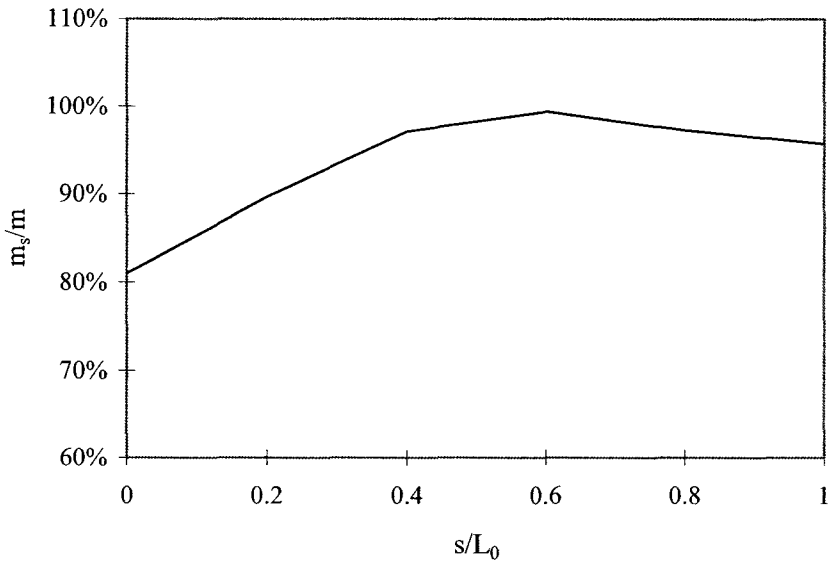

Figure 3.11 The Effect of Sloping Region on Effective Mass
h=0.1, slope angle = 90, 45, 27, 18, 14 and 11 deg. corresponds to s/L_0 =0, 0.2, 0.4, 0.6, 0.8 and 1.0 respectively

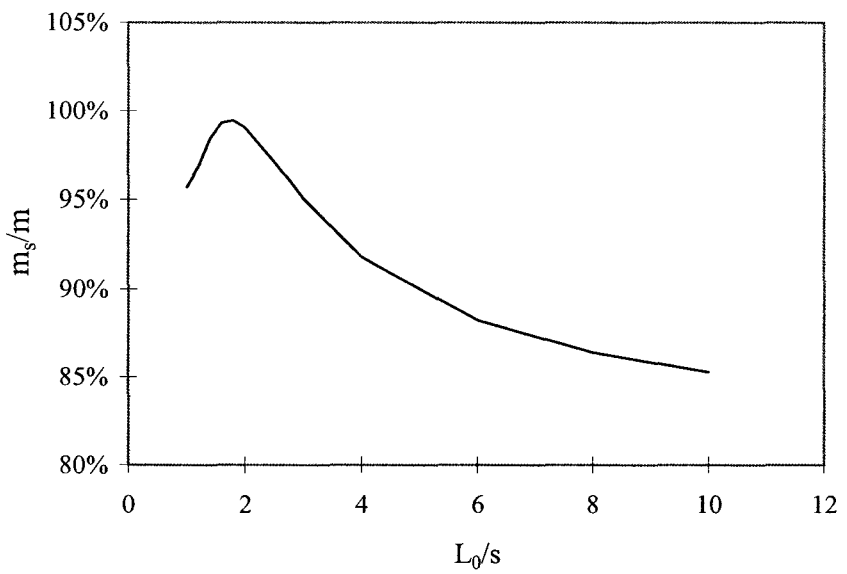

Figure 3.12 The Effect of L_0 on Effective Mass

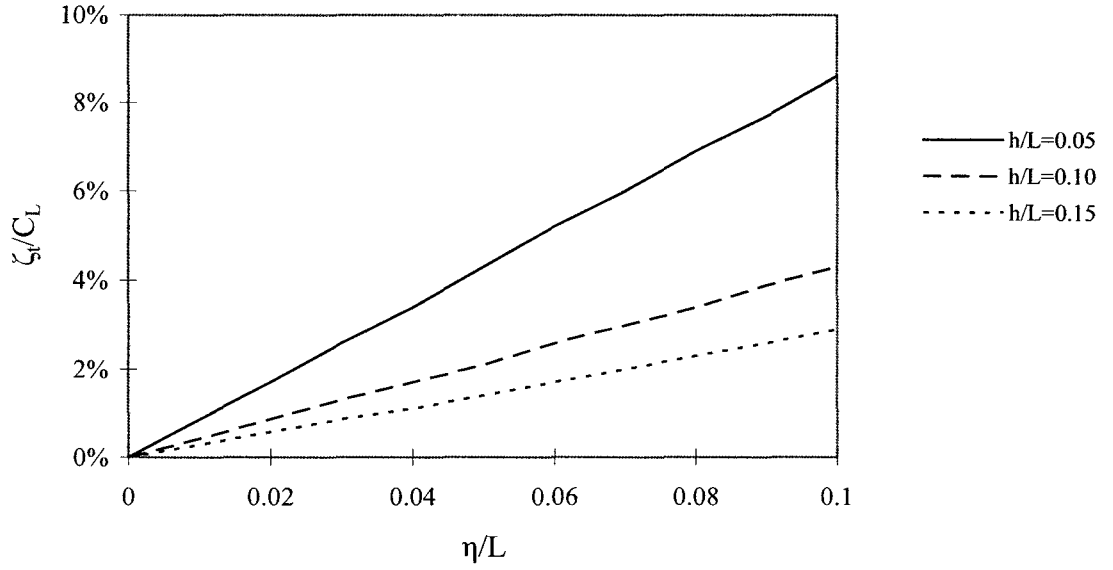

Figure 3.13 Variation of Normalized Damping Ratio with Liquid Depth and Normalized Response Amplitude for a Triangular Tank

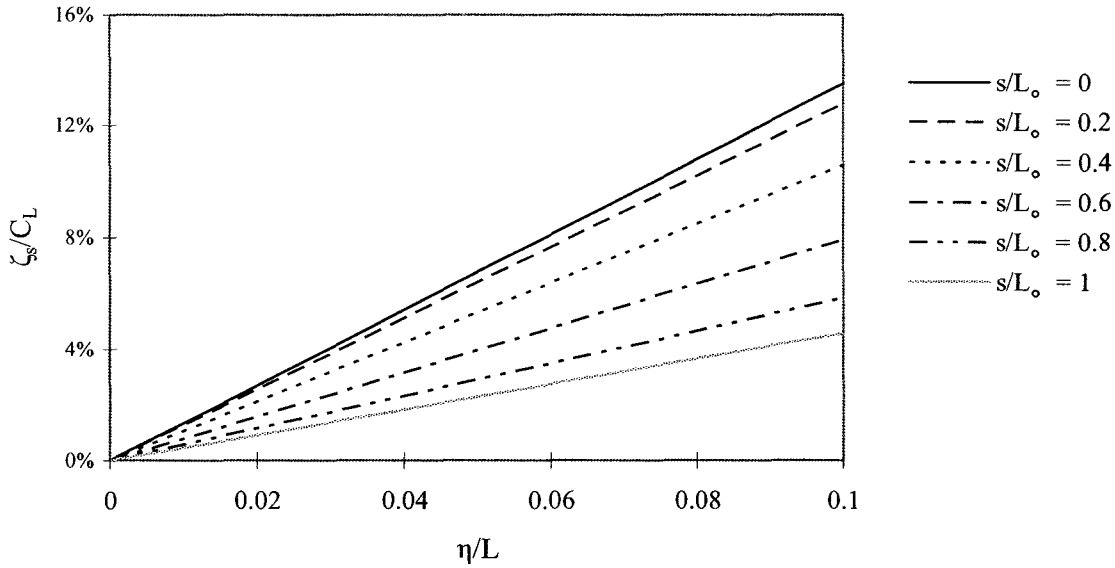

Figure 3.14 Variation of Normalized Damping Ratio with Liquid Depth and Normalized Response Amplitude for a Sloped-Bottom Tank (h/L = 0.1, L_0 = 0.5m)

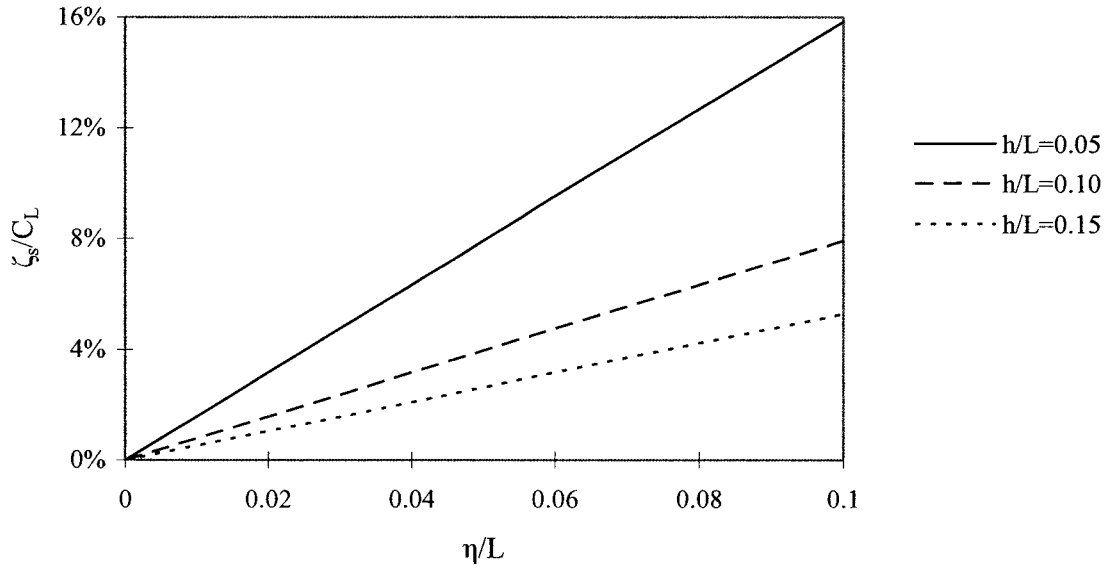

Figure 3.15 Variation of Normalized Damping Ratio with Liquid Depth and Normalized Response Amplitude for a Sloped-Bottom Tank (s = 0.3m, L_0 = 0.5m)

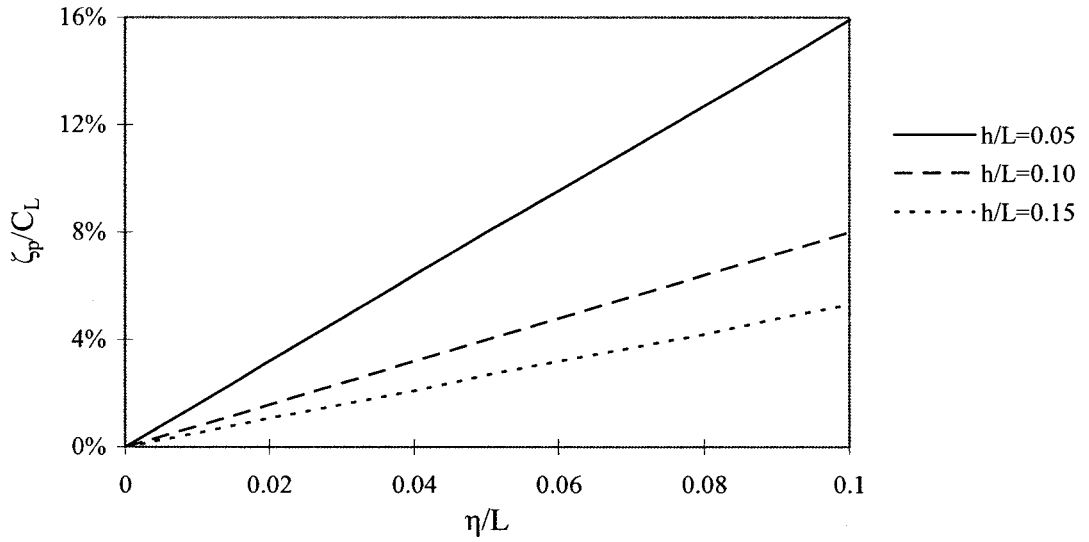

Figure 3.16 Variation of Normalized Damping Ratio with Liquid Depth and Normalized Response Amplitude for a Parabolic Tank

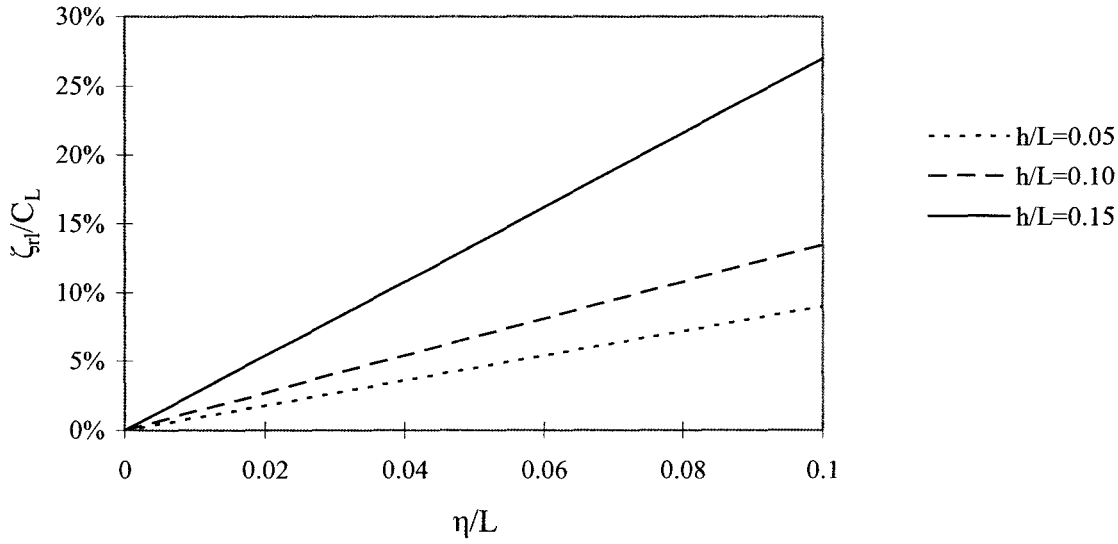

Figure 3.17 Variation of Normalized Damping Ratio with Liquid Depth for a Rectangular Tank

Chapter 4 Dynamic Response Characteristics of TLDs with Different Tank Geometries

This chapter examines and compares the dynamic response behaviour of TLDs with different tank geometries using an equivalent linear mechanical model. The properties for the equivalent single-degree-of-freedom (SDOF) linear mechanical models have been determined in Chapter 2. Since an increase in both the effective mass and natural frequency of a TLD are negligible for small excitation amplitudes, the effective mass and natural frequency are assumed to remain constant in the model (Warnitchai and Pinkaew 1998); whereas the damping is treated as an amplitude-dependent parameter. The model, which only takes the fundamental sloshing mode into account, can be used to predict the dynamic response characteristics of a SDOF system under sinusoidal or random excitation. The dynamic response of the free surface motion, sloshing force and energy dissipation of a TLD will be investigated first, followed by a comparison of the dynamic response behaviour of TLDs with different tank geometries.

4.1 Dynamic Characteristics of TLDs as a SDOF System

First, the equations used to compute the dynamic response of a TLD will be derived. Subsequently, the free surface response amplitude, sloshing force and energy dissipation of rectangular, vertical-cylindrical and horizontal-cylindrical TLDs with screen(s) inserted inside the tank will be investigated at several excitation amplitudes.

4.1.1 Formulation of Dynamic Characteristics

For a TLD is subjected to sinusoidal base excitation $X(t)$ with amplitude X_0 and excitation frequency ω_e (Figure. 1 (a)),

$$X(t) = X_0 \sin \omega_e t \tag{4.1}$$

the equation of motion, derived from Equation 2.17, becomes

$$m^* \ddot{q} + c_{eq}{}^* \dot{q} + k^* q = \gamma^* \ddot{X} \tag{4.2}$$

Dividing the above equation by the generalized mass leads to

$$\ddot{q} + 2\omega\zeta_{eq}{}^* \dot{q} + \omega^2 q = \Gamma \ddot{X} \tag{4.3}$$

Where

$$\Gamma = \frac{\gamma^*}{m^*} \tag{4.4}$$

and it is denoted as the modal participation factor.

The steady-state solution of $q(t)$ can be expressed as

$$q(t) = q_0 \sin(\omega_e t + \theta) \tag{4.5}$$

where θ is the phase angle. For a SDOF system having amplitude dependent damping, the response amplitude q_0 of the sloshing wave height is given as (Clough 1993)

$$q_0 = \frac{X_0 \Gamma \beta^2}{\sqrt{\left(1-\beta^2\right)^2 + \left(2\zeta_{eq}{}^* \beta\right)^2}} \tag{4.6}$$

where the forced frequency ratio, β, is defined as the ratio between the excitation frequency and the natural frequency of a TLD

$$\beta = \frac{\omega_e}{\omega_{TLD}} \tag{4.7}$$

and the equivalent viscous damping is expressed as

$$\zeta_{eq}^{*} = \zeta_0 q_0 \tag{4.8}$$

where ζ_0 was determined in Section 2.1.3 of Chapter 2.

The solution for $q_0(\omega_e)$ is the positive real root of Equation 4.6 and is found to be

$$q_0(\omega_e) = \sqrt{\frac{2X_0{}^2\Gamma^2\beta^4}{\left(1-\beta^2\right)^2 + \left[\left(1-\beta^2\right)^4 + \left(4\beta^3\zeta_0 X_0\Gamma\right)^2\right]^{1/2}}} \tag{4.9}$$

The phase angle, θ, can be written in terms of q_0

$$\theta = \tan^{-1}\left(\frac{2\zeta_0 q_0\beta}{1-\beta^2}\right) \tag{4.10}$$

For a liquid filled tank, where $m(x,y,z)$ is defined as the liquid mass per volume and $\varphi(x,y,z)$ is the corresponding mode shape for the horizontal sloshing motion, then at any location, the corresponding horizontal component of the generalized sloshing force can be expressed as

$$f(x,y,z,t) = \ddot{q}(t)\varphi(x,y,z)m(x,y,z) \tag{4.11}$$

The horizontal component of sloshing force, F_d, can be obtained by integrating the generalized force over the volume of fluid.

$$\begin{aligned} F_d &= \int_V f(x,y,z,t)dV = \int_V \ddot{q}(t)\varphi(x,y,z)m(x,y,z)dV \\ &= \ddot{q}(t)\int_V \varphi(x,y,z)m(x,y,z)dV = \ddot{q}(t)\gamma^* \end{aligned} \tag{4.12}$$

It can also be computed by integrating the fluid pressure at the end-walls of the tank.

$$F_d = \int_A p(x,t)dA = \int_A -\rho\frac{\partial\phi(x,t)}{\partial t}dA = \ddot{q}(t)\gamma^* \tag{4.13}$$

where $p(x, t)$ is the fluid pressure inside the tank at the end-walls, A is the area of the end-walls, and $\phi(x,t)$ denotes the velocity potential (Bauer 1964).

The sloshing force, F_d, is also equal to the product of the effective mass and its acceleration.

$$F_d = m_{eff}\ddot{x}(t) = \Gamma\ddot{x}(t)\gamma^* \tag{4.14}$$

Equating the expressions for F_d in Equations 4.12 and 4.14, a coordinate relationship is found,

$$\ddot{x}(t) = \ddot{q}(t)/\Gamma \tag{4.15}$$

and therefore,

$$x(t) = q(t)/\Gamma \tag{4.16}$$

To obtain the acceleration in an equivalent TMD system (Figure 4.1b), the co-ordinate relationship (Equation 4.16) can be utilized. Using either Equation 4.12 or Equation 4.14 and the co-ordinate relationship, the sloshing force can be expressed as

$$F_d(t) = \gamma^*\omega_e^{\,2}q(t) = F_{d0}\sin(\omega_e t + \theta) \tag{4.17}$$

where the amplitude is found to be

$$F_{d0} = \gamma^*\omega_e^{\,2}q_0 \tag{4.18}$$

The energy dissipated by the sloshing liquid motion per cycle, E_d, is defined as the work done by the sloshing force over one period of base excitation.

$$E_d = \int_T F_d dX_e \tag{4.19}$$

Substituting Equations 4.1 and 4.17 into Equation 4.19 leads to

$$E_d = \gamma^*\omega_e^{\,2}q_0X_0\pi\sin\theta \tag{4.20}$$

4.1.2 The Influence of Viscous Damping Due to Boundaries

The viscous damping due to boundaries is assumed to be zero in the formulation of the dynamic characteristics in Section 4.1.1. This damping is due to energy dissipation from the boundary layers due to shear stress exerted on the bottom of the tank, the sides of the tank and the free surface dynamics. The equation of motion accounting for the viscous damping due to the boundaries is expressed as (Warnichai and Pinkaew 1998),

$$\ddot{q} + 2\omega(\zeta_w^* + \zeta_{eq}^*)\dot{q} + \omega^2 q = \Gamma\ddot{X} \tag{4.21}$$

where ζ_{eq}^* is the equivalent viscous damping ratio determined in Chapter 2, and ζ_w^* is the equivalent viscous damping computed using linearized boundary layer theory (Fujino et al. 1990)

$$\zeta_w^* = \frac{(1+h/b)}{2h}\sqrt{\frac{2\nu}{\omega}} \tag{4.22}$$

where ν is the kinematic viscosity of the liquid.

From Equation 4.21, the response amplitude q_0 of the sloshing wave height can be expressed as

$$q_0 = \frac{X_0\Gamma\beta^2}{\sqrt{(1-\beta^2)^2 + [2(\zeta_w^* + \zeta_0 q_0)\beta]^2}} \tag{4.23}$$

The solution for q_0 is significantly more complicated than that given by Equation 4.9. A study is conducted to investigate the affect of ζ_w^* on q_0. Findings will be used to determine if ζ_w^* can be neglected in order to simplify the analysis.

In order to validate the assumption of neglecting ζ_w^*, the loss coefficient required to achieve a certain fluid response amplitude is computed for two different cases. Case 1,

corresponding to Equation 4.3, neglects the contribution of ζ_w^*. Case 2, corresponding to Equation 4.21, includes the contribution of ζ_w^*. An iterative procedure is employed to obtain a loss coefficient C_L for a particular base excitation amplitude, by matching the normalized free surface response amplitude q_0/L corresponding to a total damping ratio of 5% for the two cases considered. Loss coefficients are computed with f = 0.15, 0.5 and 1.5 Hz and h/L = 0.1, 0.15, 0.2, 0.25 and 0.3. Five base excitation amplitude are selected such that the normalized response amplitudes q_0/L are in the range of 0.01 - 0.1, i.e., the free surface response amplitude is in the small amplitude wave range.

Table 4.1 shows the affect of viscous damping due to boundaries in terms of C_L for different natural frequency and liquid depth ratio values. In the table, C_{L1} is normalized by C_{L2}, where C_{L1} denotes the loss coefficient computed ignoring the viscous damping (Case 1) and C_{L2} is the loss coefficient computed taking the viscous damping into account (Case 2). Except for the case of f = 1.5 Hz, the viscous damping due to boundaries can be neglected with negligible influence on the estimated value of C_L. The results for Case 2 approach the Case 1 values, as liquid depth ratio increases and as the natural frequency of the TLD deceases, i.e. the dimensions of the tank increase. It is observed from Equation 4.22 that as the dimensions of a tank become large, and considering liquid depth ratio values in the range of 0.1 to 0.5, the viscous damping due to the boundaries is found to be significantly less than the velocity squared damping resulting from the screens. As a result, the viscous damping due to the boundaries can be neglected for large tank dimensions allowing Equation 4.21 to be replaced by Equation 4.3. For wind applications, the natural sloshing frequency is expected to be less than 0.5

Hz and the design value of h/L is typically in the range of 0.1 to 0.25. As indicated from Table 4.1, the assumption of neglecting the viscous damping due to boundaries can be considered acceptable permitting the use of Equation 4.9.

4.1.3 Dynamic characteristics of TLDs

This section reports on the dynamic characteristics of rectangular, vertical-cylindrical and horizontal-cylindrical TLDs based on the equations derived in Section 4.1.1. Normalized parameters will be used to present the results, which are defined below (Fujino et al. 1992).

- Normalized wave amplitude η':

$$\eta' = \frac{q_0}{h} \tag{4.24}$$

where q_0 is the wave amplitude at the tank end-wall and h is the still liquid depth.

- Normalized sloshing force F':

$$F' = \frac{F_d}{m\omega_e^2 X_0} \tag{4.25}$$

where F_d is the sloshing force, m_w is the mass of the liquid, ω_e is the excitation frequency, and X_0 is the excitation amplitude. The product $m\omega_e^2 X_0$, in the denominator, is the maximum inertia force of the liquid mass if treated as a solid mass.

- Normalized energy dissipation per cycle E':

$$E' = \frac{E_d}{\frac{1}{2}m(\omega_e X_0)^2} \tag{4.26}$$

where the denominator is the maximum kinetic energy of the liquid mass if treated as a solid mass.

Theoretical and experimental results for a rectangular TLD with inserted screens are compared to validate the proposed model. The experimental data is provided by Hamelin (2007) for shaking table experiments to determine the dynamic characteristics of a rectangular TLD. The dimensions of the tank are L = 0.966 m, h = 0.119 m, and b = 0.360 m. Two screens with a solidity ratio of S = 0.426 are inserted at locations of $0.4L$ and $0.6L$ inside the tank as shown in Figure 2.2. The dynamic response characteristics are investigated for three excitation amplitudes X_0 = 2.5, 5.0 and 10.0 mm, respectively. Results are shown in Figures 4.2 to 4.4 for the normalized free surface response amplitude, sloshing force and energy dissipation, respectively. The experimental data for the free surface response amplitude is digitally filtered; therefore, the response amplitude corresponding only to the fundamental sloshing mode is presented. The free surface response amplitude is found to increase with increased excitation amplitude. Both the normalized sloshing force and energy dissipation decrease with an increase in excitation amplitude (Figures 4.3 and 4.4), which indicates the amplitude-dependency of the TLD and is a direct result of the amplitude dependent damping. Since the model only takes the fundamental mode into account, it is unable to simulate the "hardening" phenomenon and predict the multi-peaked values in the frequency response of the TLD.

The nonlinear response of the TLD tested is found to exhibit a hardening type behaviour, characterized by an increase in the sloshing resonant frequency value with increased excitation amplitude. This has been observed in experimental tests on TLDs

both with (Tait 2004) and without screens (Yu 1999). A characteristic of this type of nonlinear dynamic system is that higher harmonics, referred to as superharmonics, are present in the sloshing fluid response (Chester 1968). The presence of higher harmonics results in the excitation of higher sloshing modes. The higher sloshing modes are excited at frequencies that are integer multiple values less than the corresponding calculated natural sloshing frequency values (Shimizu and Hayama 1987). This results in the multi-peaked response observed in experimental test results.

The free surface response amplitude was measured at a distance of 0.05L from the end-wall of the tank. Figure 4.2 shows the experimentally measured free surface response amplitude corresponding to the fundamental sloshing mode along with predicted values from the equivalent mechanical model. Greater discrepancy between the measured and predicted response values is observed as the excitation amplitude is increased. This is a result of the nonlinear response behaviour of the sloshing fluid. At the 2.5 mm, 5 mm and 10 mm excitation amplitudes, the maximum predicted free surface response amplitude was within 3%, 10% and 8% of the measured values, respectively.

Sloshing forces develop as a direct result of the fluid motion. Frequency response curves for the experimentally measured normalized sloshing forces are presented and compared with calculated values from the equivalent mechanical model in Figure 4.3. Good agreement is found for all three excitation amplitudes considered. These results indicate that the proposed model can predict the TLD sloshing forces corresponding to expected wind-induced excitation amplitudes. This confirms that the velocity squared

losses due to the screens can be modelled using an equivalent linearized viscous damping ratio.

Figure 4.4 shows experimental and calculated nondimensional energy dissipation frequency response curves. The model can accurately predict the peak nondimensional energy dissipated by the TLD for all three excitation amplitudes considered. This indicates that the model correctly predicts the sloshing force and the phase angle between the base excitation motion and the TLD sloshing forces.

Overall comparisons between the model prediction and the experimental results for η', F' and E' for two screen case show reasonably good agreement. However, the model cannot capture the nonlinear response behaviour of the TLD.

Figures 4.5 to 4.7 show results for the case of one screen at the centre of the tank. The calculated results show greater discrepancy compared to the case of two screens, which is attributed to a reduction in the TLD damping as only a single screen is present ($\zeta_{eq} < 5\%$) resulting in a larger response wave amplitude. It should be noted that the two screen case is more representative of the amount of equivalent viscous damping that would be required for a TLD ($\zeta_{eq} \approx 5\%$). In order to achieve the required level of damping, the solidity of the single screen at the centre of the tank simply needs to be increased, resulting in an increased value of C_L.

4.2 Comparison of Dynamic Response Characteristics of TLDs as SDOF Systems

The following section reports on a study conducted to compare the dynamic characteristics and response behaviour between rectangular, vertical cylindrical and horizontal-cylindrical TLDs, respectively, in terms of the free surface response amplitude,

sloshing force, energy dissipation, liquid mass and required space for TLD installation. For the TLDs considered in this particular study, one screen is inserted at the centre of the tank. It is evident from the findings in Chapter 2 that TLDs with different tank geometries possess different equivalent mechanical model properties, which are the natural frequency, effective mass and damping. As a result, it is assumed that an optimal tank geometry among these different TLDs in terms of dynamic characteristics exists. The first part of this study is conducted to investigate the dynamic response characteristics of the different TLDs. The matching parameters used here are the natural frequency, damping ratio, liquid mass and liquid depth ratio; while the tank width and loss coefficient are adjusted to hold both the liquid mass and damping ratio equal for all three different TLDs, respectively (f = 0.15 Hz, ζ_{TLD} = 5%, h/L = 0.1, $m_w = 2.31\times10^5$ kg). A damping ratio of 5% corresponds to the level of damping obtained for the two screen case considered in the previous section. Since a vertical-cylindrical tank does not possess the dimension b, the properties of the vertical-cylindrical tank are computed first, and subsequently, b and C_L of the other two tanks are adjusted to match m_w and ζ_{TLD}.

From Figures 4.8, 4.9 and 4.10, it is evident that the free surface response, base shear force and energy dissipated are the largest for the horizontal-cylindrical TLD followed by the rectangular TLD. The vertical-cylindrical TLD is found to have the smallest response parameter values. These results are attributed to the different effective mass values corresponding to the different tank geometries.

Part 2 of this study is conducted to identify the TLD that requires the least amount of liquid to achieve a certain sloshing force value. The matching parameters used are the

damping ratio and sloshing force; while the varying parameters are the loss coefficient and tank width. The findings for the case of f = 0.15 Hz, ζ = 5% and X_0 = 0.1 m are summarized in Tables 4.2a-4.2c. It is found that the required liquid mass and the loss coefficient are the largest for a vertical-cylindrical TLD. The required liquid mass is less for a horizontal-cylindrical TLD than for vertical-cylindrical or rectangular TLDs. These results are attributed to the differences in effective mass and damping properties of the TLDs as discussed in Chapter 2. For the h/L = 0.1 and 0.2 cases at f = 0.15 Hz, a larger loss coefficient is required for a horizontal-cylindrical TLD than for a rectangular TLD; for h/L = 0.3, a larger loss coefficient is required for a rectangular tank. Nevertheless, in order to maintain a damping ratio of 5%, the required loss coefficient can easily be obtained by selecting a suitable screen solidity ratio.

The floor area, A, and the volume, V, for the installation of the TLDs are computed as bL (or πa^2 for a vertical-cylindrical tank) and Ach, respectively, where L is the length at height, ch, and c equals 1.0, 1.5 or 2.0, such that the space under the curve and available freeboard of a horizontal-cylindrical tank are taken into consideration. Figure 4.11 is a definition sketch of floor area and volume requirements for the installation of rectangular and horizontal-cylindrical TLDs. Tables 4.3a-4.3d show the percent difference of the required liquid mass, area and volume for installation, between the three TLDs, respectively. The floor areas for installation of a vertical-cylindrical, rectangular and horizontal-cylindrical TLD are denoted by A_{vc}, A_r and A_{hc}, respectively. In addition, V_{vc}, V_r and V_{hc} represent the volume for installation of a vertical-cylindrical, rectangular and horizontal-cylindrical TLD, respectively. From the tables, the following

trends are observed: $A_{vc} < A_r < A_{hc}$ and, $V_r < V_{vc} < V_{hc}$. However, the required mass of liquid for a horizontal-cylindrical TLD, m_{whc}, is at least 16% and 17% less than that of a rectangular and vertical-cylindrical TLD, respectively, as shown in Table 4.4d. The difference between m_{whc} and m_{wr} is found to increase with the liquid depth ratio, since the effective mass of a rectangular TLD decreases faster than that of a horizontal-cylindrical TLD. As a result, the differences between V_{hc} and V_r and between A_{hc} and A_r decrease as h/L increases. Similar results of required liquid mass, loss coefficient, area and space for the installation of the three TLDs are found in the case of $f = 0.5$ Hz as shown in Tables 4.2d-4.2f and Tables 4.3e-4.3h.

4.3 Summary

The dynamic behaviour of rectangular, vertical-cylindrical and horizontal-cylindrical TLDs has been investigated using an equivalent linear mechanical model. Results show that the viscous damping due to boundaries in the model can be neglected without loss of accuracy. Both the normalized sloshing force and energy dissipation are found to decrease with an increase in excitation amplitude as a result of the amplitude-dependent damping of the TLD. The dynamic characteristics of a rectangular TLD obtained from an experimental study are compared to results determined using the equivalent mechanical model. It is found that the model is in good agreement with experimental results for small response amplitudes. Furthermore, the dynamic characteristics of rectangular, vertical-cylindrical and horizontal-cylindrical TLDs are compared in a two-part study. In the first part of this study, natural frequency, damping ratio, liquid mass and liquid depth ratio values are matched in order to investigate the

dynamic characteristics of the TLDs. The sloshing liquid in a horizontal-cylindrical TLD is found to dissipate the largest amount of energy given the same liquid mass as that of a rectangular TLD or a vertical-cylindrical TLD. Part two of the study is conducted to identify a TLD with the least amount of liquid required to achieve the same amount of sloshing force. Required area and volume for installation of the different TLDs is also investigated. The results are as follows: for the required liquid mass, $m_{whc} < m_{wr} < m_{wvc}$, for the required floor area, $A_{vc} < A_r < A_{hc}$, for the required volume, $V_r < V_{vc} < V_{hc}$.

Table 4.1 Values of C_{L1}/ C_{L2} for a Rectangular TLD

h/L / f	0.1	0.15	0.2	0.25	0.3
0.15	1.02	1.02	1.02	1.01	1.01
0.5	1.15	1.08	1.04	1.04	1.03
1.5	3.59	1.56	1.21	1.20	1.12

Table 4.2 Mass of Liquid Required and Loss Coefficient for TLDs with Different Tank Geometries

(a) Matching properties: F = 161072 N, h/L = 0.1, f = 0.15 Hz

	h (m)	L (m)	b (m)	C_L	m_w (kg)
Ver-Cyl	1.433	14.331	-	1.508	231147
Rect.	1.056	10.555	20.409	1.041	227480
Hor-Cyl	0.888	8.878	36.100	1.440	191260

(b) Matching properties: F = 731782 N, h/L = 0.2, f = 0.15 Hz

	h (m)	L (m)	b (m)	C_L	m_w (kg)
Ver-Cyl	1.433	14.331	-	1.508	231147
Rect.	1.056	10.555	20.409	1.041	227480
Hor-Cyl	0.888	8.878	36.100	1.440	191260

(c) Matching properties: F = 1961093 N, h/L = 0.3, f = 0.15 Hz

	h (m)	L (m)	b (m)	C_L	m_w (kg)
Ver-Cyl	9.786	32.618	-	5.514	8177000
Rect.	7.665	25.549	40.085	3.700	7849969
Hor-Cyl	6.812	22.705	58.601	3.500	6463092

(d) Matching properties: F = 161072 N, h/L = 0.1, f = 0.5 Hz

	h (m)	L (m)	b (m)	C_L	m_w (kg)
Ver-Cyl	0.129	1.290	-	1.360	169
Rect.	0.095	0.950	1.907	1.936	172
Hor-Cyl	0.080	0.799	3.333	1.261	143

(e) Matching properties: F = 731782 N, h/L = 0.2, f = 0.5 Hz

	h (m)	L (m)	b (m)	C_L	m_w (kg)
Ver-Cyl	0.459	2.294	-	3.002	1897
Rect.	0.348	1.739	3.111	2.029	1883
Hor-Cyl	0.301	1.507	5.069	2.440	1,580

(f) Matching properties: F = 1961093 N, h/L = 0.3, f = 0.5 Hz

	h (m)	L (m)	b (m)	C_L	m_w (kg)
Ver-Cyl	0.881	2.1006	-	4.965	5965
Rect.	0.690	2.299	3.608	3.331	5723
Hor-Cyl	0.613	2.043	5.339	3.220	4765

Table 4.3 Comparisons of m_w, A and V between Horizontal-Cylindrical, Vertical-Cylindrical and Rectangular TLDs

(a) L at 2h, f = 0.15 Hz

h/L	$(A_{hc}-A_{vc})/A_{vc}$	$(V_{hc}-V_{vc})/V_{vc}$	$(A_{hc}-A_r)/A_r$	$(V_{hc}-V_r)/V_r$
0.1	175%	71%	106%	73%
0.2	152%	57%	92%	58%
0.3	80%	26%	47%	31%

(b) L at 1.5h, f = 0.15 Hz

h/L	$(A_{hc}-A_{vc})/A_{vc}$	$(V_{hc}-V_{vc})/V_{vc}$	$(A_{hc}-A_r)/A_r$	$(V_{hc}-V_r)/V_r$
0.1	141%	49%	80%	52%
0.2	128%	42%	74%	43%
0.3	77%	23%	44%	28%

(c) L at h, f = 0.15 Hz

h/L	$(A_{hc}-A_{vc})/A_{vc}$	$(V_{hc}-V_{vc})/V_{vc}$	$(A_{hc}-A_r)/A_r$	$(V_{hc}-V_r)/V_r$
0.1	99%	23%	49%	25%
0.2	93%	21%	48%	22%
0.3	59%	11%	30%	16%

(d) f = 0.15 Hz

h/L	$(m_{whc}-m_{wr})/m_{wr}$	$(m_{whc}-m_{wr})/m_{wr}$
0.1	-16%	-17%
0.2	-17%	-17%
0.3	-18%	-21%

(e) L at 2h, f = 0.5 Hz

h/L	$(A_{hc}-A_{vc})/A_{vc}$	$(V_{hc}-V_{vc})/V_{vc}$	$(A_{hc}-A_r)/A_r$	$(V_{hc}-V_r)/V_r$
0.1	182%	75%	104%	72%
0.2	139%	57%	83%	58%
0.3	82%	27%	49%	32%

(f) L at 1.5h, f = 0.5 Hz

h/L	$(A_{hc}-A_{vc})/A_{vc}$	$(V_{hc}-V_{vc})/V_{vc}$	$(A_{hc}-A_r)/A_r$	$(V_{hc}-V_r)/V_r$
0.1	147%	53%	78%	50%
0.2	117%	42%	66%	43%
0.3	79%	24%	46%	30%

(g) L at h, f = 0.5 Hz

h/L	$(A_{hc}-A_{vc})/A_{vc}$	$(V_{hc}-V_{vc})/V_{vc}$	$(A_{hc}-A_r)/A_r$	$(V_{hc}-V_r)/V_r$
0.1	104%	26%	47%	24%
0.2	85%	21%	41%	22%
0.3	61%	12%	32%	17%

(h) f = 0.5 Hz

h/L	$(m_{whc}-m_{wr})/m_{wr}$	$(m_{whc}-m_{wr})/m_{wr}$
0.1	-17%	-15%
0.2	-16%	-17%
0.3	-17%	-2%

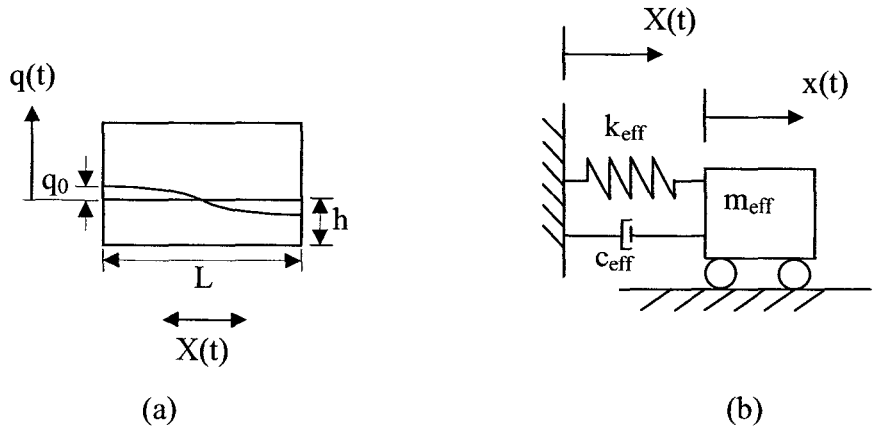

Figure 4.1 (a) TLD; (b) Equivalent Mechanical Model of a TLD

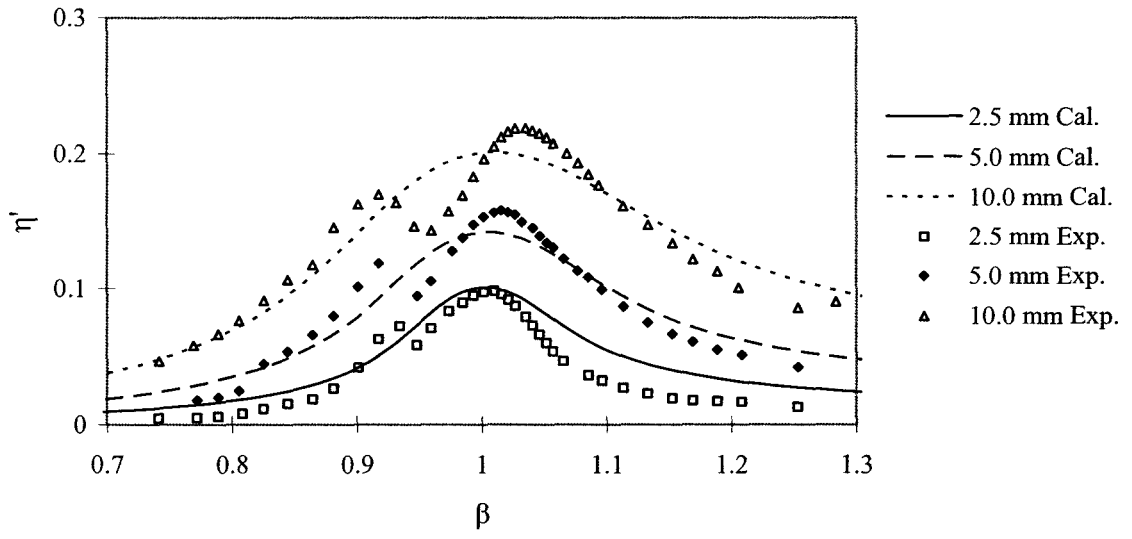

Figure 4.2 Comparison of Normalized Free Surface Response Amplitudes (Two Screens)

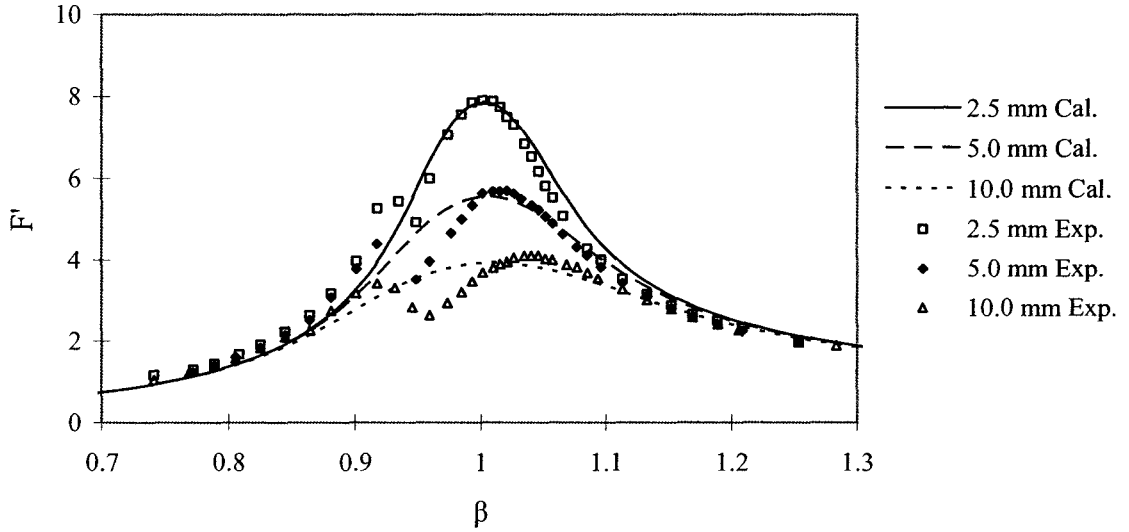

Figure 4.3 Comparison of Normalized Sloshing Force (Two Screens)

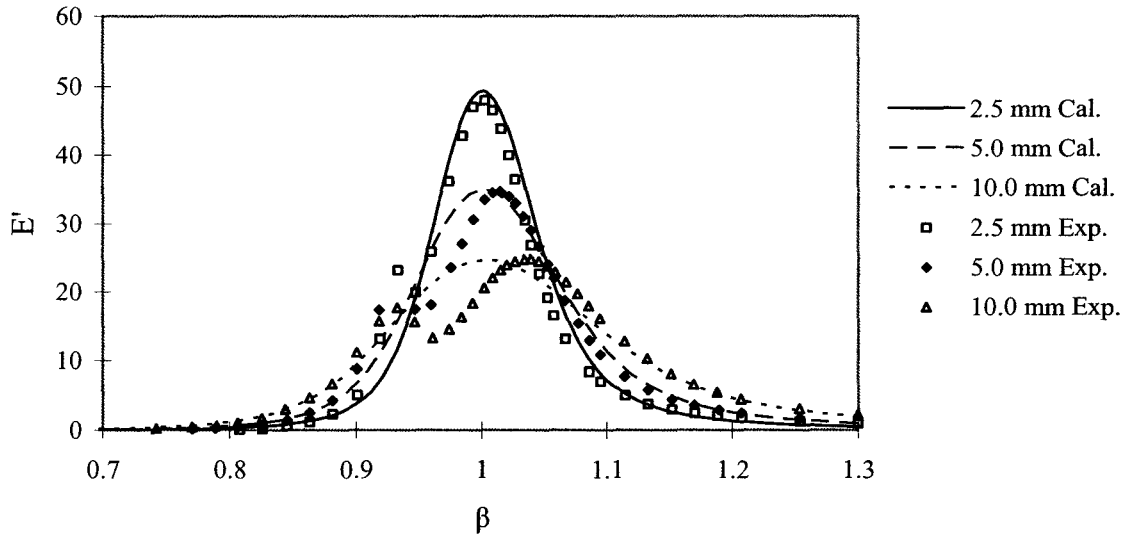

Figure 4.4 Comparison of Normalized Energy Dissipation (Two Screens)

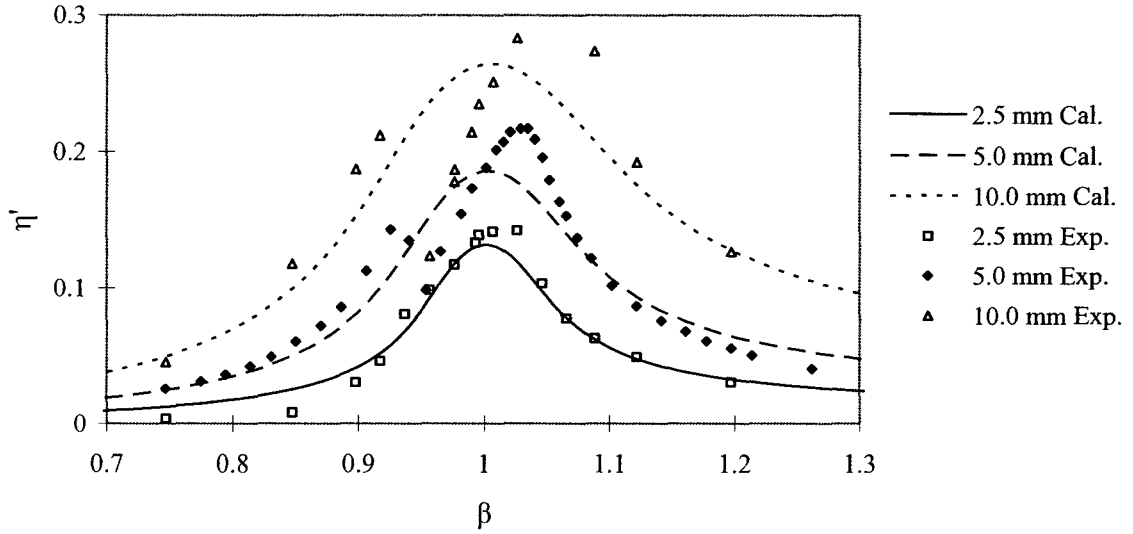

Figure 4.5 Comparison of Normalized Response Free Surface Amplitude (One Screen)

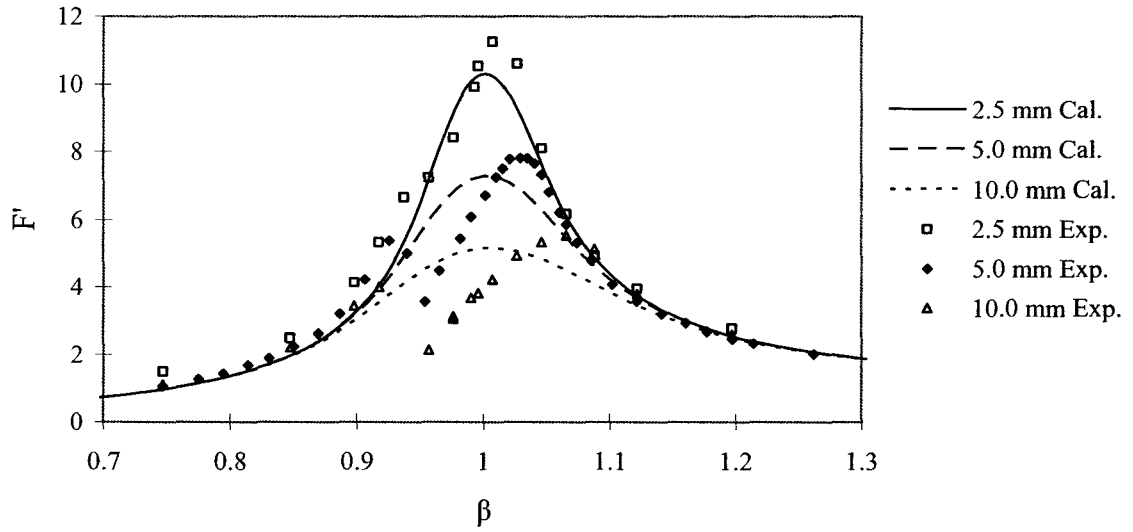

Figure 4.6 Comparison of Normalized Sloshing Force (One Screen)

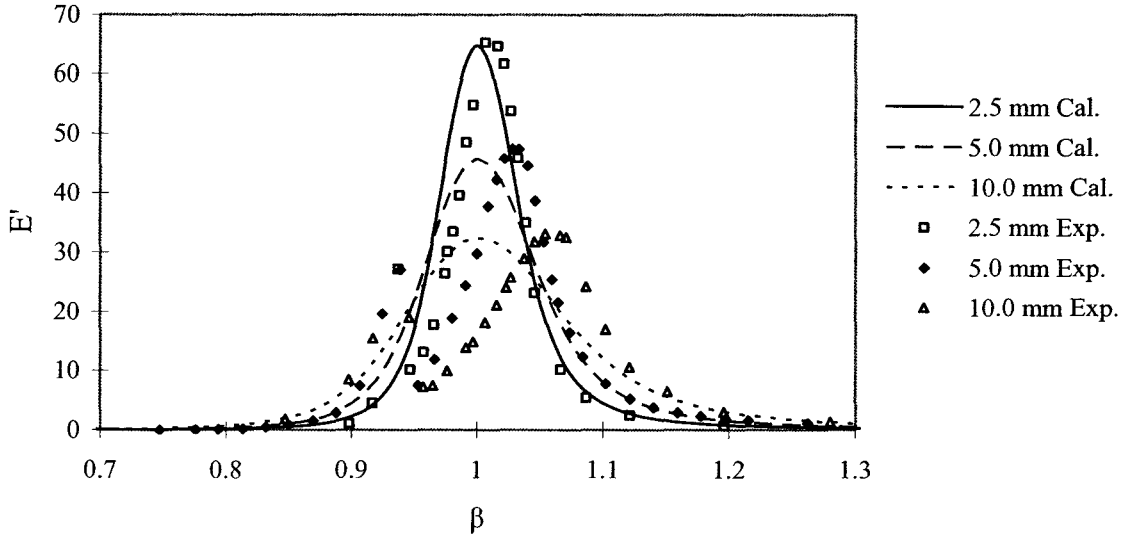

Figure 4.7 Comparison of Normalized Energy Dissipation (One Screen)

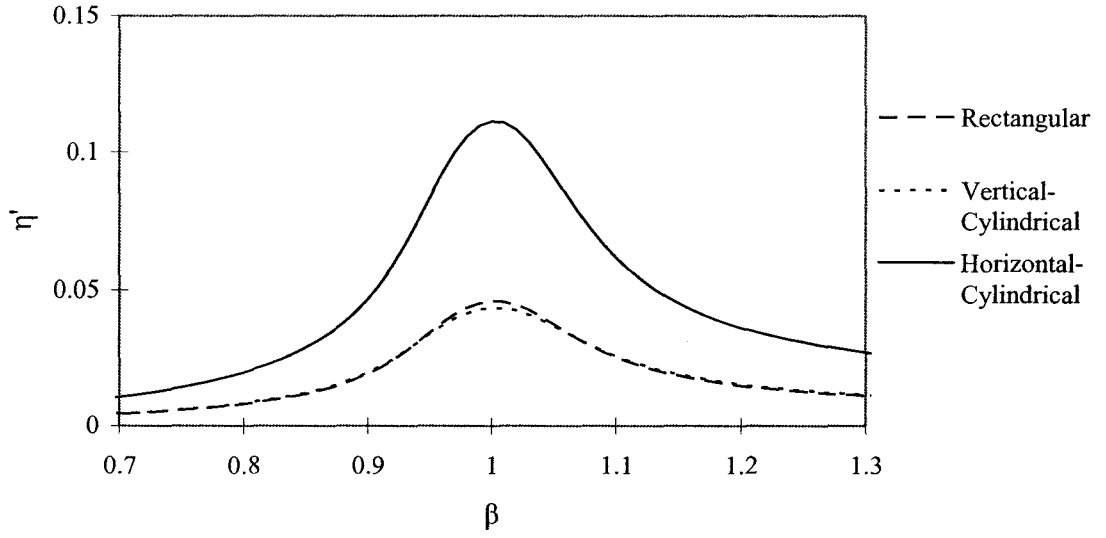

Figure 4.8 Comparison of Normalized Free Surface Response Amplitude for Different TLDs

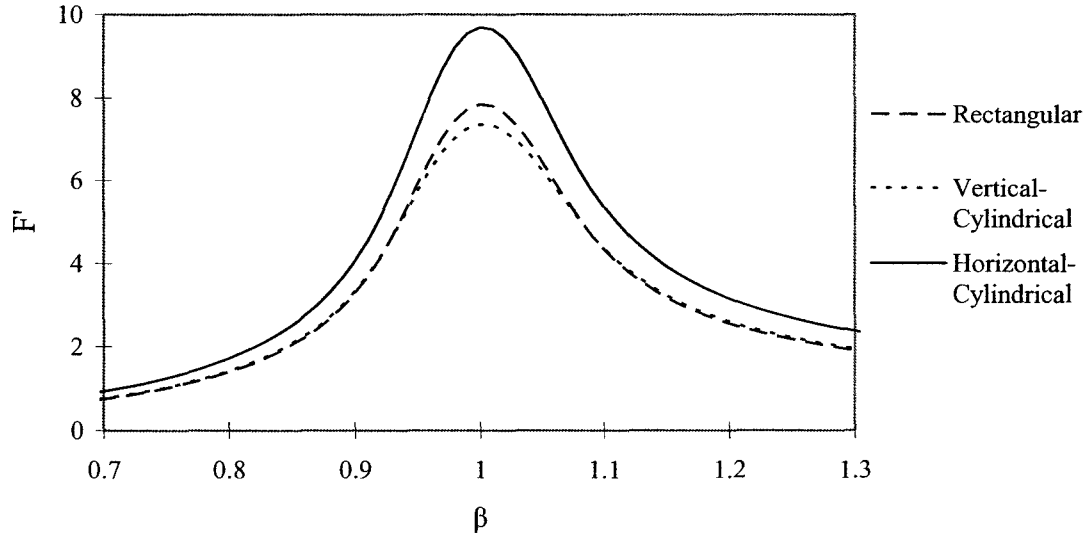

Figure 4.9 Comparison of Normalized Sloshing Force for Different TLDs

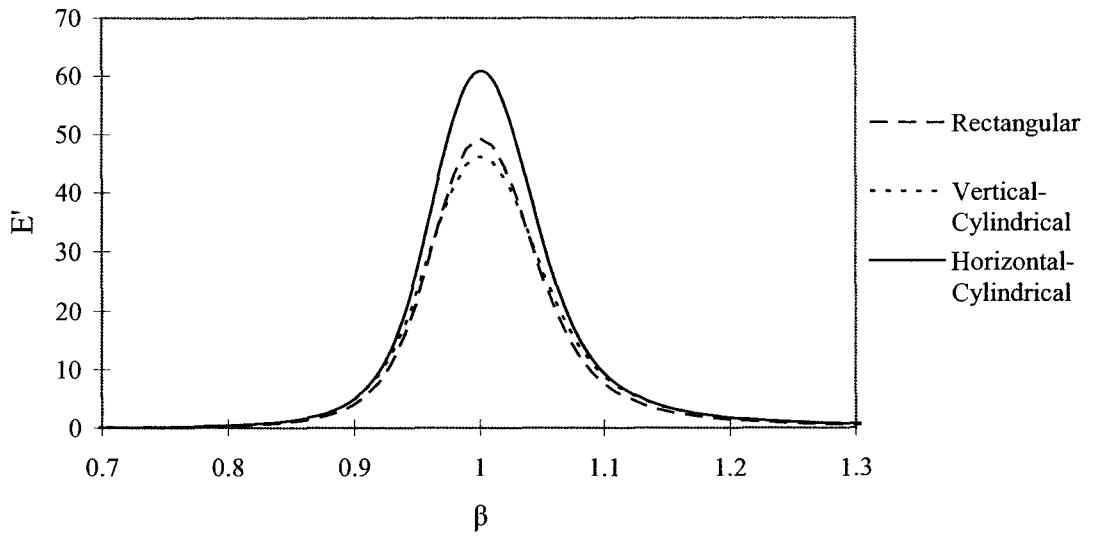

Figure 4.10 Comparison of Normalized Energy Dissipation for Different TLDs

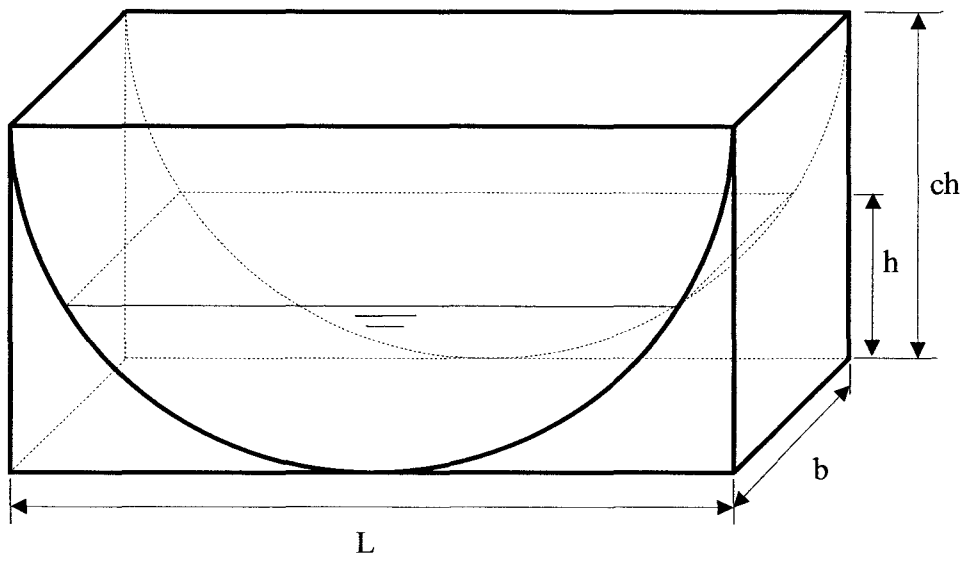

Figure 4.11 Definition Sketch of Floor Area and Volume Required for the Installation of a TLD

Chapter 5 Performance of Structure-TLD Systems

The nonlinear dynamic characteristics of a TLD increase the complexities of design and analysis. Nevertheless, an equivalent mechanical model of a TLD equipped with screen(s) has been constructed (see Chapter 2) to simplify the dynamic characteristics of a TLD and its response behaviour was studied as a SDOF system in Chapter 4. In this model, the damping of the TLD is expressed in terms of an amplitude dependent equivalent viscous damping, while the natural frequency and the mass of the SDOF system are assumed to be constant for small response amplitudes. The natural frequency of the SDOF system is determined using linear sloshing frequency (Bauer 1984), and the effective mass is used as the mass of the SDOF system.

This chapter presents the performance of TLDs in terms of effective damping, efficiency and robustness. A structure-TLD system with a rectangular, vertical-cylindrical or horizontal-cylindrical TLD, respectively, is investigated utilizing the equivalent mechanical model constructed in Chapter 2. The definition sketches for these TLDs are given in Figures 2.2, 2.3 and 2.6b. Tait (2004) introduced a scheme to study the performance of TLDs, in which performance charts for structure-TLD systems are developed. These performance charts, which were originally developed for TMDs (Vickery and Davenport 1970), consider the effects of tuning ratio, structural response motion, mass ratio and liquid depth. The contour lines in a performance chart represent the effective damping, efficiency or the RMS relative motion ratio of free surface liquid at the end-wall of the tank. The parameters and basic concepts will be introduced first,

followed by the influence of various parameters on the performance of TLDs and comparisons of the performance between the different TLDs.

5.1 Parameters of a Structure-TLD System

5.1.1 Modelling of a Structure-TLD System

The performance of TLDs is investigated using a structure-TLD system under random excitation. A structure-TLD system with the TLD mounted at the top the structure is shown in Figure 5.1a. Often one response mode of a structure dominates, therefore, the structure can be modelled as a generalized SDOF system. As illustrated in Figure 5.1b, M^* is the generalized mass of the primary structure for the vibration mode being suppressed; K^*, C^* and x_s are the generalized stiffness, damping and motion of the primary structure, respectively. The nonlinear TLD is modelled here as an equivalent mechanical system (i.e. equivalent TMD), which has been studied and is well understood. This permits the complex sloshing motion in an excited TLD to be greatly simplified and allows the performance of a TLD to be determined using formulas developed for a TMD. The TMD representation of a TLD, discussed in the previous chapter, is employed in this study of structure-TLD systems as shown in Figure 5.1c. The dynamic properties of a TLD are amplitude dependent, that is, the natural frequency, damping ratio and effective mass vary with amplitude (Sun 1995). However, for a TLD equipped with screen(s), the amplitude dependency of the natural frequency is considered to be negligible for wind-induced serviceability response levels (Tait 2004). In addition, this mechanical model of

the TLD has been developed for small response amplitudes. Therefore, the natural frequency and effective mass are assumed to remain constant.

5.1.2 Description of Parameters

The parameters affecting the response of a structure include mass ratio μ, tuning ratio Ω, TLD damping ratio ζ and structure damping ratio ζ_s.

- TLD mass ratio

$$\mu = \frac{\phi^2 m_{eff}}{M_s} \tag{5.1}$$

$$M_s = M^* + (m_w - m_{eff}) = M^* + m_0 \tag{5.2}$$

where ϕ is the mode shape value at the damper location, corresponding to the structural mode being targeted (it is assumed that the TLD is located at the top of the building and ϕ has a value of unity), m_w is the total liquid mass, m_{eff} is the effective mass of a TLD and M_s is defined as the mass of the structure, which takes account of the inactive mass of liquid, m_0, inside the tank (Vandiver and Mitone 1979).

- tuning ratio

$$\Omega = \frac{f_{TLD}}{f_s} \tag{5.3}$$

where f_{TLD} is the natural frequency of a TLD, and f_s denotes the natural frequency of the structure. Based on potential flow theory and linear long wave theory, f_{TLD} has been derived for TLDs with different tank geometries in Chapters 2 and 3, respectively. The natural frequency of a structure can be expressed as

$$f_s = \frac{1}{2\pi}\sqrt{\frac{K^*}{M_s}} \tag{5.4}$$

- TLD damping ratio

$$\zeta = \frac{c}{4\pi m f_{TLD}} \tag{5.5}$$

for random excitation the damping ratio is expressed as

$$\zeta = \sqrt{\frac{1}{2\pi}}\frac{C_L \rho \Delta \Xi}{m^*}\sigma_\eta \tag{5.6}$$

which is given in Equation 2.22

- structural damping ratio

$$\zeta_s = \frac{C^*}{4\pi M^* f_s} \tag{5.7}$$

where C^* is the equivalent generalized viscous damping of the primary structure. The value of the structural damping ratio is usually small for civil structures, typically 1 % to 5 %, and its influence on the performance of a TLD is often negligible (Warburton 1982). Thus, the structural damping ratio is assumed to be zero in this study when determining the efficiency of a TLD. However, the total damping of the structure-TLD system can be estimated as (Luft 1979)

$$\zeta_{TOT} = 0.8\zeta_s + \zeta_{eff} \tag{5.8}$$

The performance of a TLD attached to a structure can be evaluated by its effective damping, ζ_{eff}, efficiency, Ψ, and robustness. Effective damping of a TLD is defined as the additional damping provided by the TLD to a SDOF system with the same dynamic properties as the original primary structure in the structure-TLD system (Vickery and

Davenport 1970). It can be calculated by equating the response of the structure-TLD system to that of a SDOF system shown in Figure 5.1d. McNamara (1977) gave a closed form solution to determine the effective damping for both undamped and damped structures.

For undamped structures,

$$\zeta_{eff} = \frac{\Omega\mu\zeta}{(1+\mu)^2\Omega^4 + 2(1+\mu)\Omega^2(2\zeta^2 - 1) + \Omega^2\mu + 1} \tag{5.9}$$

Efficiency, Ψ, of a TLD is defined here as the ratio of effective damping of a TLD to that of an equivalent optimized linear TMD with the same liquid mass ratio μ_w.

$$\Psi = \frac{\zeta_{eff}}{\zeta_{eff-opt}} \times 100 \tag{5.10}$$

where $\zeta_{eff\text{-}opt}$ is the optimal effective damping for a linear TMD with

$$\mu_w = \frac{m_w}{M^*} \tag{5.11}$$

Robustness is more difficult to quantify. It is defined here as the insensitivity of efficiency or effective damping to variations in the tuning ratio and (or) level of applied excitation.

Freeboard is an important parameter that must be considered in TLD design. It is defined here as the distance between the still liquid depth and the tank lid height. Freeboard thus places a physical limit on the maximum wave amplitude. For a TLD, R_η is defined as the ratio between the RMS free surface motion at the end-wall, σ_η, and the RMS primary structural response motion, σ_s. In addition, it can be determined for an undamped structure (Gerges 2003) as follows

$$R_\eta = \Gamma \sqrt{\frac{1}{(1+\mu)^2\Omega^4 + 2(1+\mu)\Omega^2(2\zeta^2 - 1) + \Omega^2\mu + 1}} \tag{5.12}$$

The required amount of freeboard can be calculated by computing R_η and applying a peak factor, *PF*, to determine the maximum response amplitude. As the first approximation, *PF* can be estimated by (Davenport 1964 and Tait 2004)

$$PF = \sqrt{2\ln(\nu T_0)} + \frac{0.5772}{\sqrt{2\ln(\nu T_0)}} \tag{5.13}$$

where ν is the cycling frequency and T_0 is the averaging time.

To minimize the response of a structure under external excitation, a TLD is required to be properly designed. In order to achieve the maximum performance, the effective damping, tuning ratio and TLD damping ratio values must be optimized. Optimal values are formulated by Warburton (1982) for a structure-TMD system with $\zeta_s = 0$ under random excitation, and are given as

- optimal tuning ratio

$$\Omega_{opt} = \sqrt{\frac{1 + \frac{\mu}{2}}{1+\mu}} \tag{5.14}$$

- optimal TLD damping ratio

$$\zeta_{opt} = \frac{1}{4}\sqrt{\frac{\mu + \frac{3\mu^2}{4}}{4 + 6\mu + 2\mu^2}} \tag{5.15}$$

- optimal effective damping

By substituting Equation 5.14 and 5.15 into Equation 5.9, the optimal effective damping can be determined as

$$\zeta_{eff-opt} = \frac{1}{4}\sqrt{\frac{\mu+\mu^2}{1+\frac{3\mu}{4}}} \tag{5.16}$$

- ratio of root-mean-square (RMS) relative motion ratio for an optimally designed absorber

Similarly, substitution of Ω_{opt} and ζ_{opt} into Equation 5.12 leads to

$$\frac{R_{opt}}{\Gamma} = \frac{1+\mu}{\sqrt{2\mu+\frac{3\mu^2}{2}}} \tag{5.17}$$

All of the above expressions are a function of the mass ratio. Since the TLDs considered in this study are modelled as equivalent TMDs, these formulas are applicable to the proposed structure-TLD system for a particular target structural response amplitude, $\sigma_{s\text{-}target}$. As the absorber damping ratio is amplitude dependent, the optimal value will only be achieved for a particular σ_η value. As a result, the performance of a TLD is expected to be amplitude dependent.

5.2 Assessing the Effective Damping, Efficiency and Robustness of TLDs

A detailed parametric study is conducted in order to assess the effective damping, efficiency and robustness of TLDs with different tank geometries. Performance charts are utilized in this three part study, which is conducted to investigate the effect of Ω, $\sigma_s/\sigma_{s\text{-}target}$, h/L and μ on the performance of TLDs with different tank geometries.

- In Part 1 of this study, the performance of a TLD is investigated over a range of Ω and $\sigma_s/\sigma_{s\text{-}target}$ values for four μ_w values and three h/L values. The tuning ratio, Ω, is adjusted by changing K_s thus changing f_s while h/L and μ are held constant.
- In Part 2 of this study, Ω is varied by changing h while b is adjusted in order to maintain a constant μ_w value. This allows the influence of h/L to be investigated.
- In Part 3 of this study, h is varied in order to investigate the performance of TLDs when Ω, h/L, μ and μ_w are all varied simultaneously.

Part 1 and Part 3 are the variations which may be expected to occur in an actual TLD application.

A brief description of the procedure employed to develop a particular performance chart is provided as follows. For a certain mass ratio, μ, values of Ω_{opt} and ζ_{opt} are computed using Equations 5.14 and 5.15. The screen solidity ratio, S, of a TLD is subsequently selected to achieve the optimal effective damping ratio by applying Equation 5.6, where C_L is a function of S. In Part 1 of this study, the stiffness of the structure is varied to obtain different tuning ratio values ranging from 0.8 to 1.2, which is approximately a 20 % variation from the optimal tuning ratio value. The efficiency, Ψ, and relative motion ratio, R_η, are calculated for different tuning ratio and normalized structural response amplitude values, respectively. The value of $\sigma_s/\sigma_{s\text{-}target}$ is varied from 0.2 to 5 to demonstrate the influence of structural response motion on the performance of the TLD. Plotting the contours of various Ψ and R_η values produces a performance chart. Performance charts for parts 2 and 3 of this study are constructed in a similar manner while varying different parameters as described at the beginning of this section.

5.2.1 Influence of Mistuning

Part 1 of this study investigates the influence of mistuning due to a change in the natural frequency of the structure while other properties of the structure-TLD system remain constant. This mistuning case can result from the amplitude dependent natural frequency of a structure (Tamura and Suganuma 1996) and/or a change in the stiffness of a structure (i.e. cracked/uncracked concrete). Figure 5.3a shows a performance chart with Ψ contours for a horizontal-cylindrical TLD as a function of Ω and $\sigma_s/\sigma_{s\text{-}target}$. Figures 5.2a and 5.2b are extracted from Figure 5.3a to show the efficiency of a horizontal-cylindrical TLD at particular tuning ratio, Ω, or normalized structural response values, $\sigma_s/\sigma_{s\text{-}target}$, respectively. It is found in Figure 5.2a that for all cases of normalized structural response motion, the efficiency decreases when the TLD is mistuned. Figure 5.2b shows the variation of efficiency as a function of $\sigma_s/\sigma_{s\text{-}target}$ for different tuning ratio values. Although the efficiency is less sensitive to variations in the structural response motion, it rapidly decreases as the TLD is mistuned. These observations indicate that TLD efficiency is highly dependent on the tuning ratio. For example, a 5% variation in the tuning ratio results in approximately a 40% reduction in the efficiency at $\sigma_s/\sigma_{s\text{-}target} = 1$. This behaviour can also be observed by examining the distance between the contour lines at a certain normalized structural response amplitude in Figure 5.3a. Since the equivalent mechanical model of a TLD is constructed with the assumption of small response amplitude, further investigation on the validity of these charts is required for the large normalized structural response region.

5.2.2 Influence of Structural Response Motion ($\sigma_s/\sigma_{s\text{-}target}$)

The damping ratio for the TLDs studied here is amplitude dependent as determined in Chapter 2. When $\sigma_s/\sigma_{s\text{-}target}$ is small, the amount of TLD damping is insufficient. This leads to an under-damped system, which is defined as a TLD with $\zeta < \zeta_{opt}$. Therefore, an under-damped system occurs when $\sigma_s/\sigma_{s\text{-}target}$ is less than unity. In addition, excessive TLD damping results in an over-damped structure-TLD system, which is defined as a TLD with $\zeta > \zeta_{opt}$. This is found to occur when $\sigma_s/\sigma_{s\text{-}target}$ is greater than unity. It can also be observed from Figure 5.2a that the range of tuning ratio values for a certain level of efficiency is reduced in an under-damped system. However, in an over-damped system, the efficiency decreases while the range of tuning ratio values increases for a particular value of Ψ. The efficiency decreases as the normalized structural response motion is adjusted away from its target value, which is shown in Figure 5.2b. In this figure, the efficiency is found to decrease more rapidly in the direction of small structural response motion (under-damped system) than in the direction of large response motion (over-damped system) for the case of $\Omega \approx \Omega_{opt}$ ($\Omega = 1$). These observations demonstrate that an over-damped TLD is a more robust dynamic vibration absorber (DVA) compared to an under-damped DVA (McNamara 1977). These findings combined with those found in Section 5.2.1 demonstrate that there is a trade-off between TLD efficiency and robustness, which agrees with previous studies on a specific structure-TLD system with a rectangular TLD (Tait 2004).

5.2.3 Influence of Mass Ratio (μ *and* μ_w)

To examine the performance of TLDs at different mass ratio values, Part 1 is repeated for μ_w = 0.01, 0.02 and 0.05, respectively. The μ_w value is adjusted by varying the mass of the structure such that the properties of the TLD are held constant. Since not all of the liquid participates in the sloshing motion, μ is always smaller than μ_w but still affects the performance of a TLD in the same manner as μ_w. It is shown in Figures 5.3a to 5.3d that for a certain value of h/L, as μ_w is increased, the level of efficiency can be retained in a comparable range of $\sigma_s/\sigma_{s\text{-}target}$ values but over a wider range of tuning ratio values, i.e., the robustness is improved. For example, for $\Psi > 90\%$, the range of $\sigma_s/\sigma_{s\text{-}target}$ values is found to be approximately 0.6 to 2.0 for all μ_w value considered. However, the range of tuning ratio values, $\Delta\Omega$, increases from 0.04 (for μ_w = 0.005) to 0.09 for (for μ_w = 0.05).

5.2.4 Influence of Liquid Depth Ratio (h/L)

Using the same tank, additional performance charts are developed for TLDs with h/L = 0.15 and 0.2, respectively, by adjusting h. In order to hold μ_w constant, M_s is varied. Figures 5.3d to 5.3f show the efficiency of an attached horizontal-cylindrical TLD with μ_w = 0.05 at h/L = 0.1, 0.15 and 0.2, respectively. It is found that an increase in the liquid depth ratio results in a reduction in both the Ω and $\sigma_s/\sigma_{s\text{-}target}$ ranges for a given Ψ contour line. This is attributed to a reduction in normalized effective mass, m_{eff}/m_w, as h/L increases, that is, a smaller percentage of total liquid mass participates in the sloshing motion. Results indicate that the robustness of a TLD can be improved by a reduction in

the liquid depth ratio. However, an increase in the nonlinear response behaviour of the TLD is expected to occur for small h/L values.

In Part 2 of this study, Ω and ζ_{eff} for a structure-TLD system with $\mu_w = 0.02$ are optimized at $h/L = 0.15$. The tank width b is adjusted to hold μ_w constant so that the influence of h/L can be investigated. Since a vertical-cylindrical tank does not possess the dimension of b, only rectangular and horizontal-cylindrical TLDs are investigated in this part of the study. Figures 5.4 and 5.6 show the performance charts for rectangular and horizontal-cylindrical TLD, respectively. The solid lines, dotted lines and dashed lines correspond to Part 1, Part 2 and Part 3 of this study, respectively. Figures 5.4a and 5.6a show the effective damping for structure-TLD systems equipped with rectangular and horizontal-cylindrical TLDs, respectively. It should be noted that the effective damping of the TLD in Part 1 can be calculated by multiplying the efficiency by the effective damping of a corresponding optimized TMD.

As determined in Chapter 2, an increase in h/L results in a decrease in the normalized effective mass. As a result, as h/L is increased, μ decreases, since μ_w is held constant in this part of the study. Therefore, it is expected that the effective damping will also decrease as h/L is increased. The TLD damping ratio, which is another parameter that influences the effective damping value, decreases as h/L is increased.

A performance chart can be divided into four regions, namely, OD, OI, UI and UD, based on the level of TLD damping, as shown in Figure 5.4a. The letters U and O represent an under-damped system and over-damped system, respectively, for a TLD having a constant liquid depth ratio as described in Part 1. The letters D and I denote a

decrease or an increase, respectively, in TLD damping due to a change in h (and corresponding h/L). The contours in region OI correspond to an over-damped system and the contours in region UD correspond to an under-damped system. However, the TLD may be under-damped or over-damped in the UI and OD regions, depending on the effects of $\sigma_s/\sigma_{s\text{-}target}$ and h/L on ζ. Consequently a change in h/L will influence both μ and ζ, and both of the parameters affect ζ_{eff}. In some cases, μ will have a greater influence on ζ_{eff}; in other cases, ζ will have greater influence on ζ_{eff}.

For the structure-TLD system with a rectangular TLD, as shown in Figure 5.4a, the influence of the mass ratio, μ, has a greater influence in region UI. Therefore, for a particular $\sigma_s/\sigma_{s\text{-}target}$ value, the effective damping increases as h/L is increased up to $\Omega = \Omega_{opt}$ and decreases thereafter. However, ζ has a greater influence on the effective damping for the structure-TLD system with a horizontal-cylindrical TLD as shown in regions UI and OI in Figure 5.6a. Excessive damping at $h/L = 0.02$ (corresponding to $\Omega = 0.97$ and regions UI and OI) leads to an over-damped structure-TLD system. Unlike the case of a structure-TLD system with a rectangular TLD, the effective damping deceases compared to that found in Part 1 of this study when $\Omega < \Omega_{opt}$. When $\Omega > \Omega_{opt}$, as h/L is increased, μ and ζ_{TLD} both decrease, therefore, the effective damping is reduced compared to the values found in Part 1.

The increased influence of ζ on the structure-TLD system with a horizontal-cylindrical TLD is attributed to the significant change in h/L, which is varied from 0.020 to 0.618. However, the h/L values are only varied from 0.093 to 0.246 for the system with a rectangular TLD. It is noted that for the horizontal-cylindrical TLD with a radius of

23.5 m considered here, the lowest attainable tuning ratio is 0.97 based on Equations 5.3 and 2.84. This is attributed to the insensitivity of the natural frequency of a horizontal-cylindrical TLD to $h/2R$ as shown in Figure 2.10b. In order to match Ω of a structure-TLD system with a horizontal-cylindrical TLD to a structure-TLD system with a rectangular TLD, h/L requires significantly greater adjustment. As a result, the effect of h/L on effective damping is greater for a horizontal-cylindrical TLD than for a rectangular TLD.

5.2.5 Influence of Liquid Depth (h)

Part 3 of this study represents the case of a loss/ or the addition of liquid in a TLD tank. First, the TLDs are optimally tuned and damped for $h/L = 0.15$, $\mu_w = 0.02$ and $\sigma_s/\sigma_{s\text{-}target} = 1$. This corresponds to certain Ω_{opt}, ζ_{opt} and $\zeta_{eff\text{-}opt}$ values for each TLD. Next, h is adjusted, and ζ_{eff} is determined for different $\sigma_s/\sigma_{s\text{-}target}$. For comparative purposes, the contours are plotted in the same domains as those in Part 1 and Part 2 of this study, and additional axes of h/L and μ are attached in Figures 5.4 to 5.6. The adjustment of h results in a change in h/L, Ω, ζ and μ. In this part of the study, μ increases with h (and h/L), which is a direct result of an increase in effective mass, although the normalized effective mass, m_{eff}/m_w, decreases as h/L increases.

Comparing the results from parts 1 and 3 of this study in Figures 5.4a and 5.5a, the effective damping is found to decrease when $\Omega < \Omega_{opt}$, and increase when $\Omega > \Omega_{opt}$ for a rectangular and a vertical-cylindrical TLD. This is attributed to the significant increase in μ as h is increased. Generally, the efficiency of the structure-TLD system has the same trend as the effective damping for both rectangular and vertical-cylindrical TLDs, as

shown in Figure 5.4b and 5.5b. For a rectangular TLD, the total liquid mass increases more rapidly than the effective mass as h/L is increased above the value of 0.15 (corresponding to Ω_{opt}). As a result, the efficiency decreases compared to that found in Part 1 in region UD and a portion of region OD. These same trends are also observed in Figure 5.5b for a structure-TLD system with a vertical-cylindrical TLD.

As previously mentioned, the natural frequency of a horizontal-cylindrical TLD is found to be weakly dependent on h/L over a large range of $h/2R$ values. Thus, to adjust the tuning ratio, h has to be varied significantly, resulting in a large change in the mass ratio. Fortunately, in most practical application, a change of h for a tuned horizontal-cylindrical TLD by this large amount would be considered rare. It is also noted that for the same level of change in h, due to evaporation or spillage of liquid in a tank, the tuning ratio of a structure-TLD system with a horizontal-cylindrical TLD is affected less than a system using a rectangular or vertical-cylindrical TLD. The influence of h on effective damping of a horizontal-cylindrical TLD is shown in Figure 5.6a. The small liquid depth ratio at $\Omega = 0.97$ causes significant over-damping. As h/L increases, the mass ratio increases, thus the effective damping increases, however it is still less than ζ_{eff} in Part 1 due to an under-damped system in region UD. It is interesting to note that an effective damping value larger than $\zeta_{eff\text{-}opt}$ occurs at $\Omega \approx$ 1-1.04 and $\sigma_s/\sigma_{s\text{-}target} \approx$ 1.4-5 due to a significant increase in the mass ratio; however, it does not lead to a system with higher efficiency because of the corresponding increase in the total liquid mass as shown in Figure 5.6b. Figures 5.4 to 5.6, which show results from all three parts of this study, indicate that the influences of liquid depth and mass ratio on the effective damping and

efficiency are greater than the influence of liquid depth ratio for the particular TLDs studied.

5.2.6 Relative Motion Ratio of Structure-TLD Systems

As mentioned previously, freeboard is defined as the air space between the still free surface of the liquid and the lid or top of a tank. It is one of the physical limitations that must be considered in TLD design. For example, building storey height may limit the over all height of a tank. Required freeboard can be computed based on the relative motion ratio R_η. Part 1 of this study is used to investigate the influence of Ω, $\sigma_s/\sigma_{s\text{-}target}$, μ and h/L on the relative motion ratio of the free surface, R_η. It is found that R_η and Ψ have a similar trend as the parameters Ω, $\sigma_s/\sigma_{s\text{-}target}$, h/L and μ are varied, which is indicated by the similarity of Equations 5.9 and 5.12. Figure 5.7a shows that R_η decreases with an increase in $\sigma_s/\sigma_{s\text{-}target}$, which is a result of increased damping. R_η is also found to be less sensitive to the normalized structural response motion when the TLD is mistuned. For a certain value of h/L, an increase in the mass ratio causes a decrease in R_η and also the rate of decrease in R_η as shown in Figures 5.7a to 5.7d. The influence of h/L is presented in Figures 5.7d to 5.7f. For a certain value of μ_w, R_η and the rate of decrease in R_η are found to increase as h/L increases. These can be attributed to the influence of the effective mass and the total liquid mass as discussed in Sections 5.2.3 and 5.2.4. These observations indicate that a small liquid depth ratio value and a large mass ratio can lead to a structure-TLD system with a small value of R_η having reduced sensitivity to Ω and $\sigma_s/\sigma_{s\text{-}target}$.

5.3 Comparison of Efficiency of TLDs

In Part 1, a study has also been conducted on both rectangular and vertical-cylindrical TLDs with different values of h/L and μ_w in order to compare the performance of various TLDs considered in this study. The same efficiency and relative motion ratio trend as those discussed in Sections 5.2.1, 5.2.2 and 5.2.6 are found for the rectangular and vertical-cylindrical TLDs. Figure 5.8 shows the efficiency of all three TLDs with μ_w = 0.02 at h/L = 0.1, 0.15 and 0.2, respectively. It is found that the efficiency of a vertical-cylindrical TLD is slightly higher than that of a rectangular TLD for the cases of h/L = 0.1 and 0.15. However, it is slightly lower than the efficiency of a rectangular TLD as h/L approaches 0.2.

Results also show that within the range of $\sigma_s/\sigma_{s\text{-}target} \approx$ 0.2-1.8 and $\Omega \approx$ 0.9-1.1, the efficiency of a horizontal-cylindrical TLD is approximately 10% larger than the efficiency of a rectangular or vertical-cylindrical TLD; while for other ranges of Ω and $\sigma_s/\sigma_{s\text{-}target}$, the efficiency of a horizontal-cylindrical TLD remains at least 6% greater than the rectangular and vertical-cylindrical TLDs. The optimal efficiency of the three TLDs studied is given in Table 5.1. In this table, Ψ_r, Ψ_{vc}, Ψ_{hc} denote the efficiency of an installed rectangular, vertical-cylindrical and horizontal-cylindrical TLD, respectively. The difference in efficiency values between these TLDs greatly reflects the effective mass of the TLDs with changes in h/L. A large effective mass, leading to a large mass ratio, results in a high effective damping value. Observing the value of the contours for the same level of efficiency, a horizontal-cylindrical TLD is found to be more robust than both rectangular and vertical-cylindrical TLDs.

The relative motion ratio between the free surface and the structure, R_η, of these three TLDs is shown in Figure 5.9. Within the examined ranges of the parameters Ω and $\sigma_s/\sigma_{s\text{-}target}$, $R_{\eta\text{-}hc}$ is the smallest, followed by $R_{\eta\text{-}r}$ and $R_{\eta\text{-}vc}$ ($R_{\eta\text{-}r}$, $R_{\eta\text{-}vc}$ and $R_{\eta\text{-}hc}$ denote the relative motion ratio between free surface and the structure of structure-TLD systems with a rectangular, vertical-cylindrical and horizontal-cylindrical TLD, respectively). The values of R_η of the three optimized structure-TLD systems are provided in Table 5.2 for h/L = 0.1, 0.15 and 0.2. As h/L increases, the difference between $R_{\eta\text{-}hc}$ and $R_{\eta\text{-}r}$ increases from -11.1% to -11.9%, while the difference between $R_{\eta\text{-}hc}$ and $R_{\eta\text{-}vc}$ decreases from -55.1% to -53.2%. Comparing the distance between contours for each TLD shows that the sensitivity of R_η to Ω and $\sigma_s/\sigma_{s\text{-}target}$ are in the order of $R_{\eta\text{-}hc} < R_{\eta\text{-}vc} < R_{\eta\text{-}r}$. In other words, Ω and $\sigma_s/\sigma_{s\text{-}target}$ have the smallest influence on the relative motion ratio of a horizontal-cylindrical TLD for the three TLDs studied. It is noted that the calculated values of $R_{\eta\text{-}hc}$ are based on the wave amplitude at the edge of the tank corresponding to the still liquid, and not the wave amplitude at the end-wall, q^*, which is larger than the utilized wave amplitude, q, as shown in Figure 2.6b. The free surface mode shape $\varphi(x)$ obtained using Equation 2.105 is similar to that found by Budiansky (1960). Figure 5.10 shows half of the axis-symmetric mode shape for different h/L values. It can be seen that in general q underestimates q^*. However, as h/L increases, the difference between q^* and q becomes insignificant. Therefore, the results of relative motion ratio discussed above are considered valid.

5.4 Summary

The effective damping, efficiency and robustness of a rectangular, vertical-cylindrical and horizontal-cylindrical TLD installed in a structure have been investigated. The structure is modelled as a generalized SDOF system and the TLD is modelled as an equivalent mechanical SDOF system. The performance of TLDs, including the relative motion ratio, are examined by varying the structural response motion, tuning ratio, mass ratio, liquid depth ratio and liquid depth. It is found that when the values of Ω and $\sigma_s/\sigma_{s\text{-}target}$ are adjusted away from their optimum values, the TLDs become less effective but, in some cases, more robust dynamic vibration absorbers. Also, small liquid depth ratio and large mass ratio can lead to a robust structure-TLD system with a small value of R_η. However, it must be emphasised that the influence of nonlinearities (i.e. hardening, etc.) was not considered. The performance charts demonstrate that a loss or gain of a certain amount of liquid in a TLD tank influences a horizontal-cylindrical TLD less than a rectangular or vertical-cylindrical TLD. Due to the insensitivity of the natural frequency of a horizontal-cylindrical TLD to $h/2R$, the tuning ratio of a structure-TLD system with a horizontal-cylindrical TLD is more constant than the other two systems in terms of the influence of liquid depth. In addition, comparisons of performance between these three TLDs are made. The horizontal-cylindrical TLD is approximately 10% more efficient than the rectangular or vertical-cylindrical TLDs in the typical design and operational ranges of Ω, $\sigma_s/\sigma_{s\text{-}target}$ and h/L. For the case of $\mu_w = 0.02$, the relative motion ratio of an optimally designed horizontal-cylindrical TLD is approximately 12% less than a rectangular TLD and 54% less than a vertical-cylindrical TLD at $h/L = 0.1$ to 0.2. For

other μ_w values, the relative motion ratio of a structure-TLD system with a horizontal-cylindrical TLD is also found to be the smallest. Results from this study indicate that a horizontal-cylindrical TLD is the most robust and effective TLD of the TLDs investigated. Since the equivalent mechanical model of a TLD is constructed with the assumption of small response amplitude, further investigation on the validity of the performance charts is required for the larger response region.

Table 5.1 Efficiency of Installed TLDs with Different Tank Geometries with $\mu_w = 0.02$ at Ω_{opt} and $\sigma_{s\text{-}target}$

h/L	Ψ_r	Ψ_{vc}	Ψ_{hc}	$(\Psi_{hc}-\Psi_r)/\Psi_{hc}$%	$(\Psi_{hc}-\Psi_{vc})/\Psi_{hc}$%
0.1	88.4%	89.3%	98.4%	10.2%	9.3%
0.15	86.7%	87.0%	96.5%	10.2%	9.9%
0.2	84.5%	84.1%	94.1%	10.2%	10.6%

Table 5.2 Relative Motion Ratio between the Free Surface and the Structure with $\mu_w = 0.02$ at Ω_{opt} and $\sigma_{s\text{-}target}$

h/L	$R_{\eta\text{-}r}$	$R_{\eta\text{-}vc}$	$R_{\eta\text{-}hc}$	$(R_{\eta\text{-}hc}-R_{\eta\text{-}r})/R_{\eta\text{-}hc}$%	$(R_{\eta\text{-}hc}-R_{\eta\text{-}vc})/R_{\eta\text{-}hc}$%
0.1	2.2	3.07	1.98	-11.1%	-55.1%
0.15	3.25	4.49	2.98	-11.7%	-54.3%
0.2	4.23	5.79	3.78	-11.9%	-53.2%

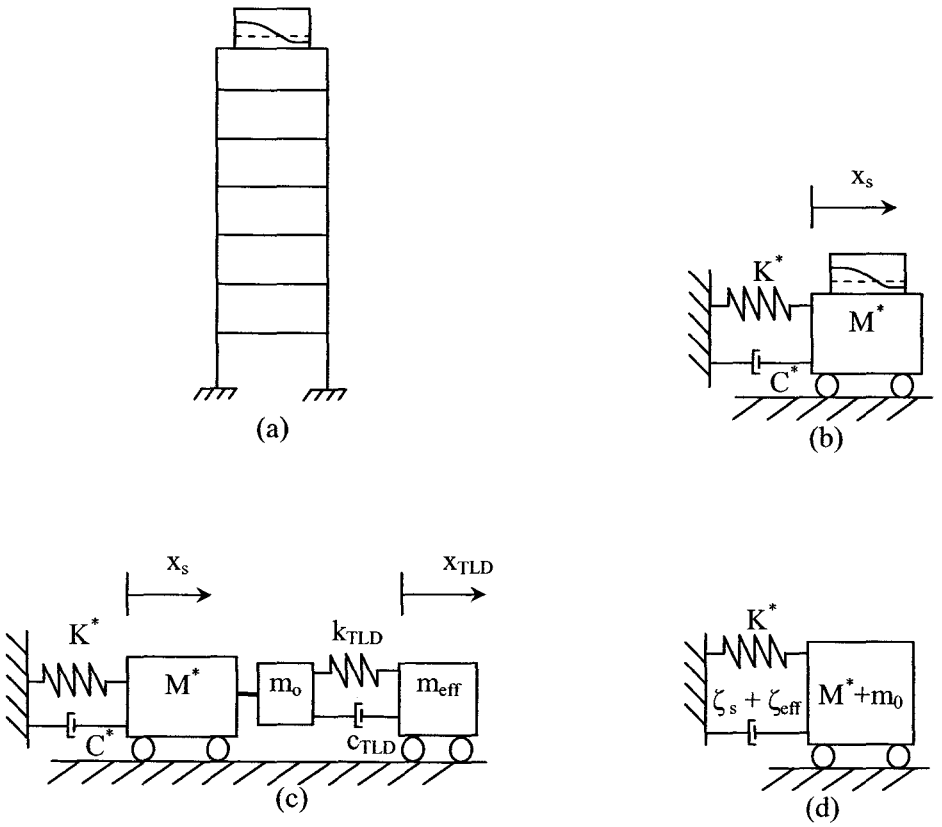

Figure 5.1 (a) Structure-TLD (b) Theoretical Representation (c) TMD Analogy (d) Equivalent Single-Degree-of-Freedom System

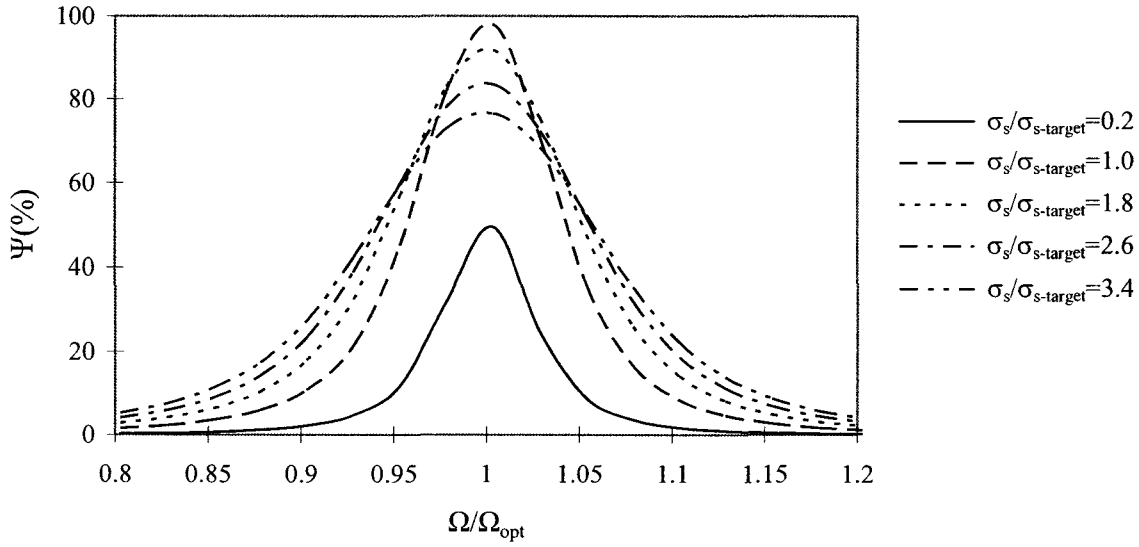

(a)

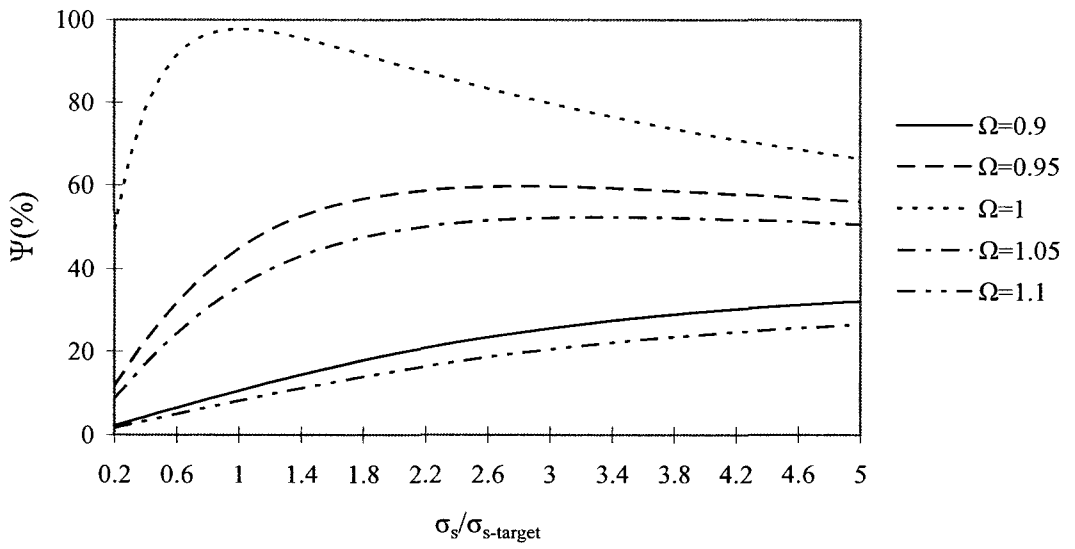

(b)

Figure 5.2 Efficiency of a Horizontal-Cylindrical TLD with $\Omega_{opt} = 0.996$

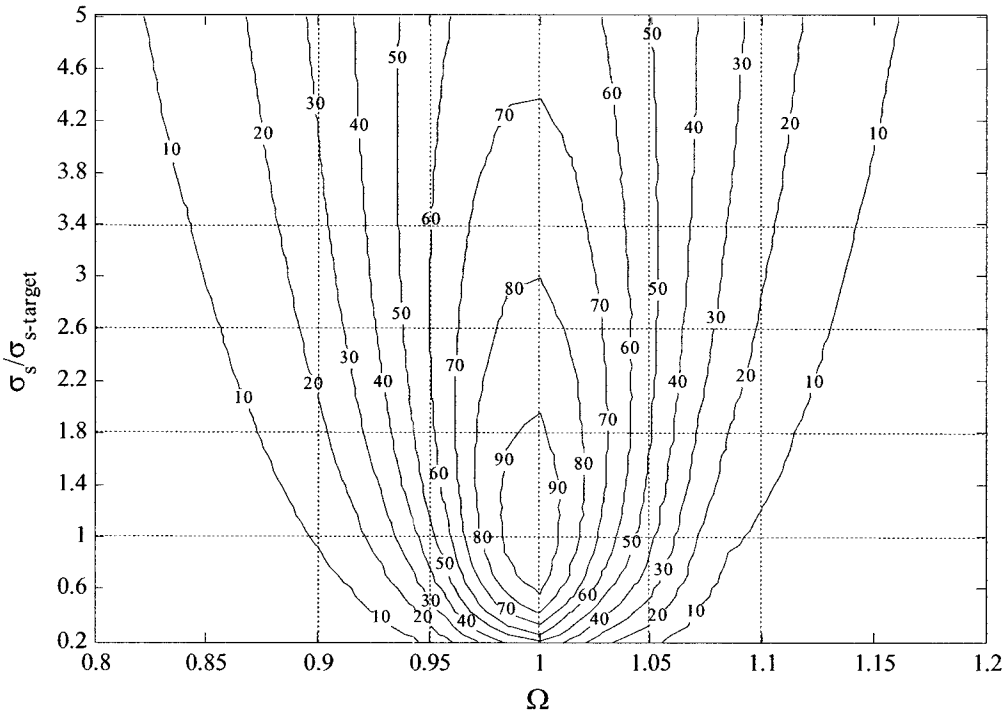

(a) $\mu_w = 0.005$, $\Psi = 98\%$, h/L = 0.1

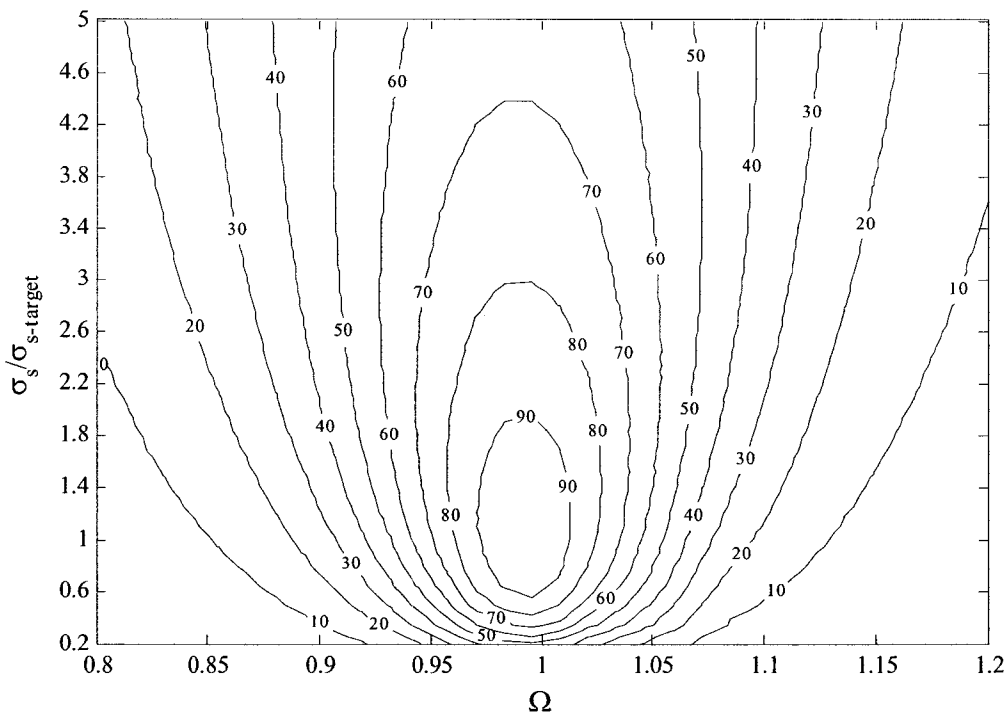

(b) $\mu_w = 0.01$, $\Psi = 98\%$, h/L = 0.1

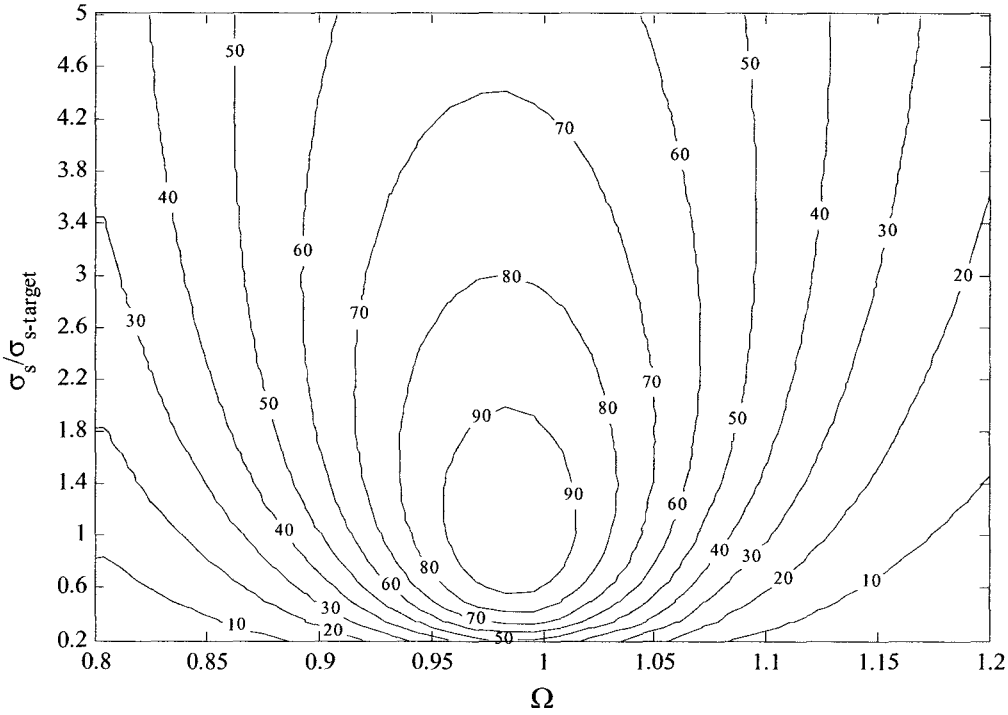

(c) $\mu_w = 0.02$, $\Psi = 98\%$, $h/L = 0.1$

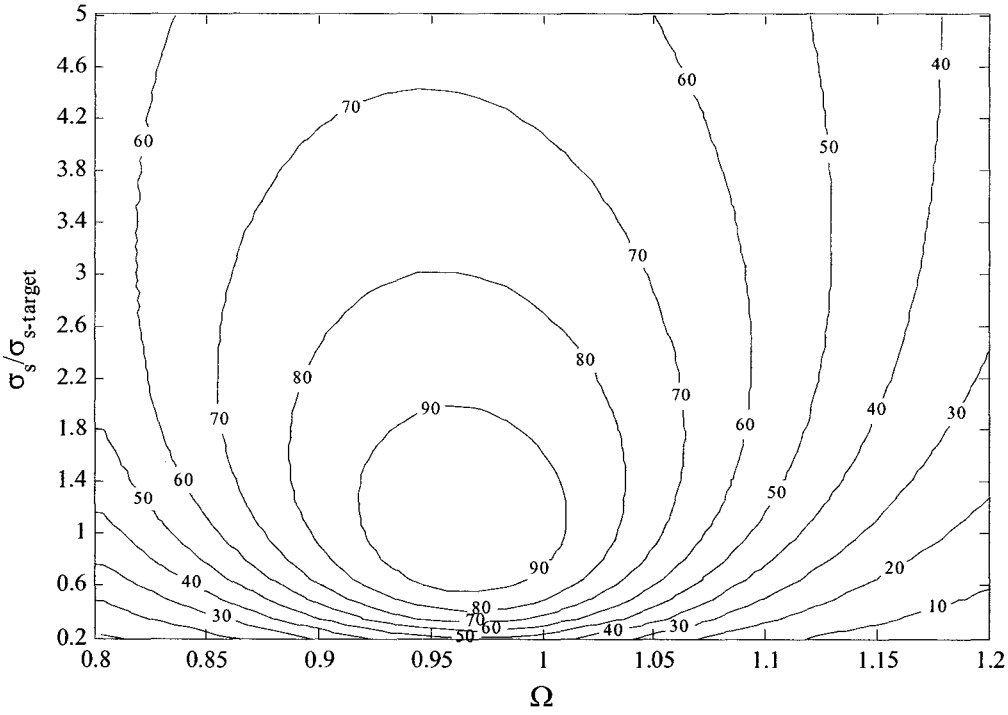

(d) $\mu_w = 0.05$, $\Psi = 98\%$, $h/L = 0.1$

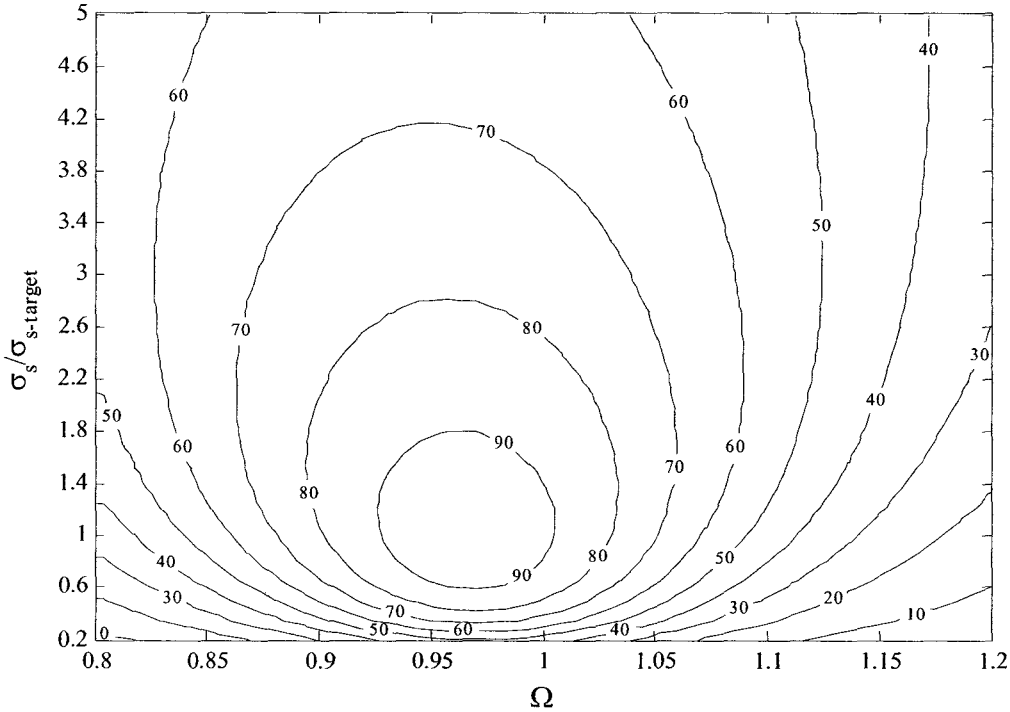

(e) $\mu_w = 0.05$, $\Psi = 96\%$, h/L = 0.15

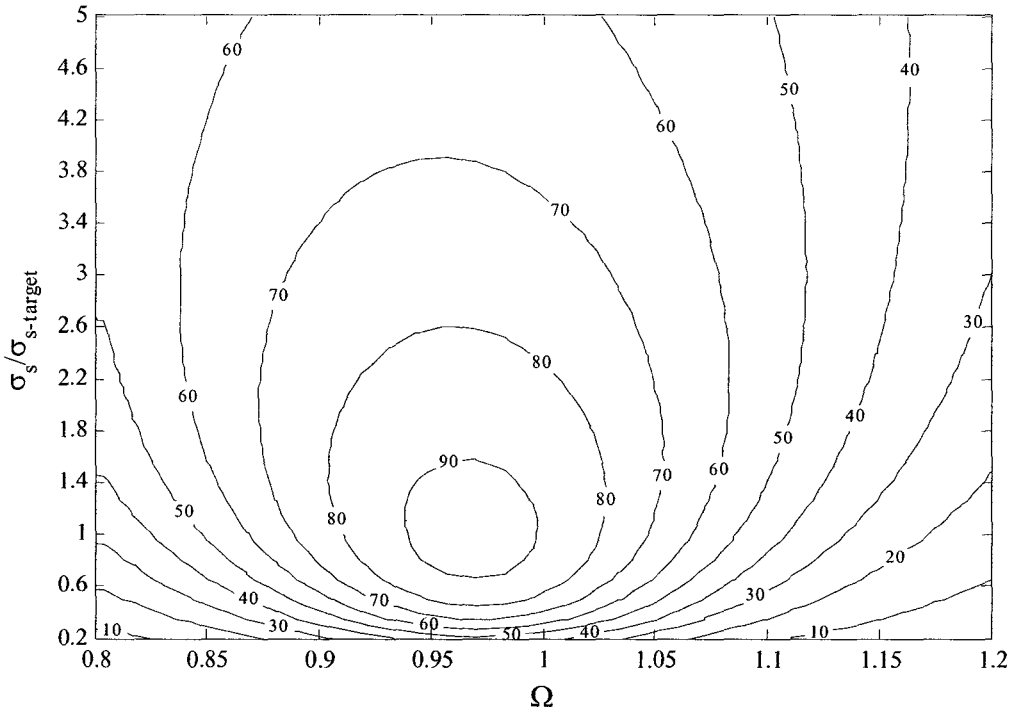

(f) $\mu_w = 0.05$, $\Psi = 94\%$, h/L = 0.2

Figure 5.3 Influence of Ω, h/L and μ_w on Ψ of a Horizontal-Cylindrical TLD

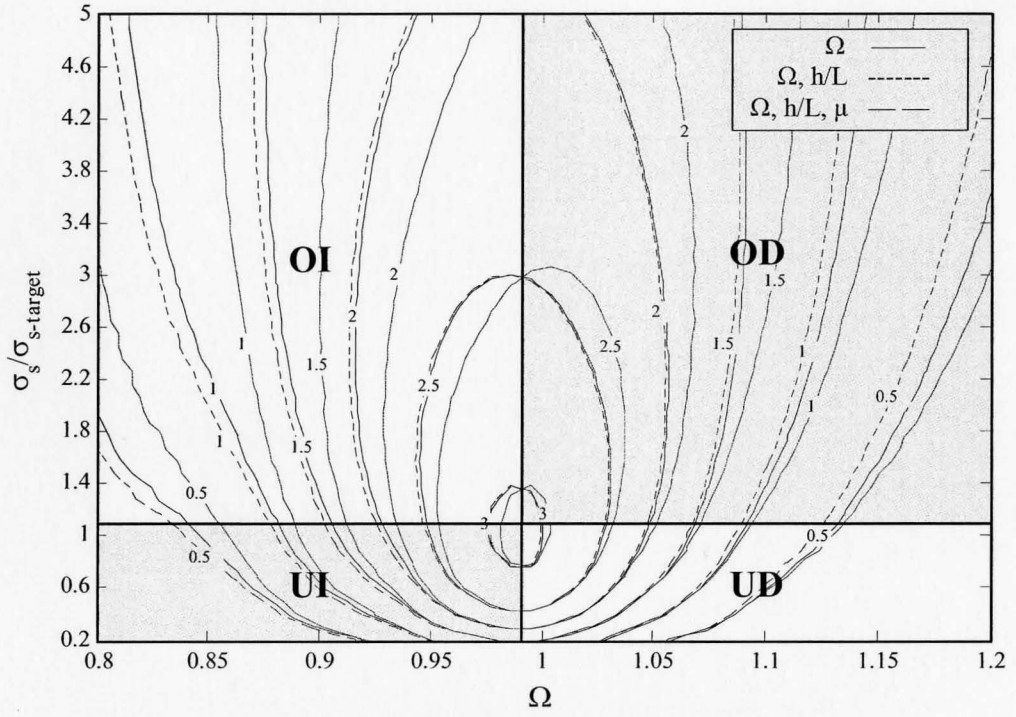

(a) ζ_{eff} ($\mu_w = 0.02$, h/L = 0.15 at Ω_{opt} and $\sigma_{s\text{-target}}$)

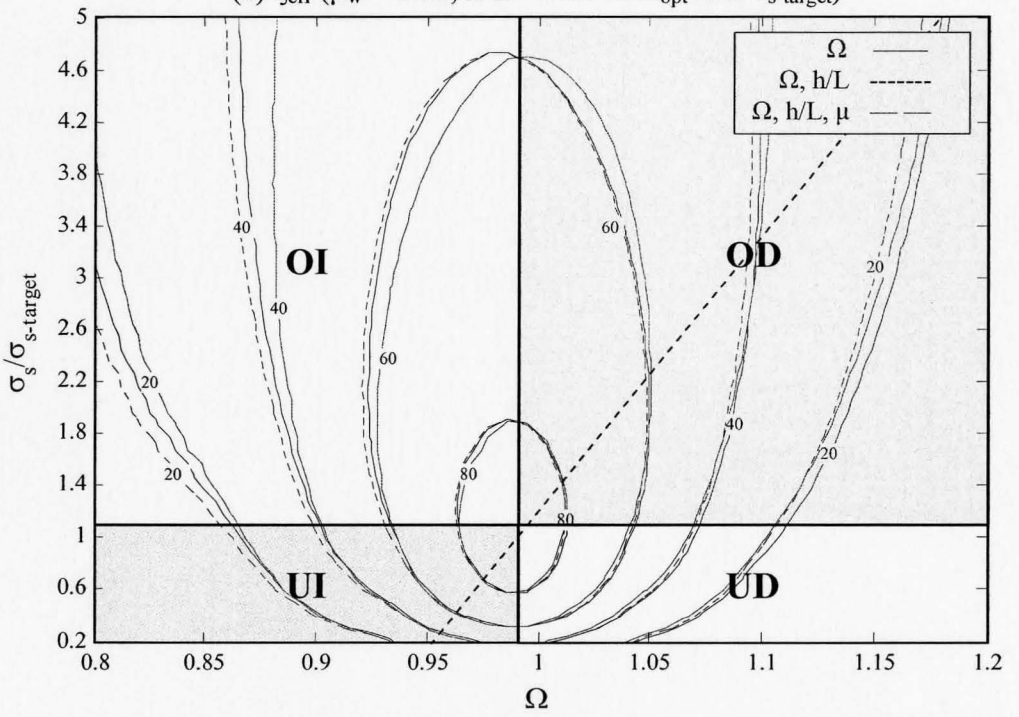

μ	0.010	0.011	0.012	0.014	0.015	0.017	0.019	0.020	0.022
h/L	0.093	0.106	0.120	0.136	0.153	0.172	0.194	0.218	0.246

(b) Ψ ($\mu_w = 0.02$, h/L = 0.15 at Ω_{opt} and $\sigma_{s\text{-target}}$)

Figure 5.4 Influence of *Ω*, *h/L* and *μ* on Performance of a Rectangular TLD

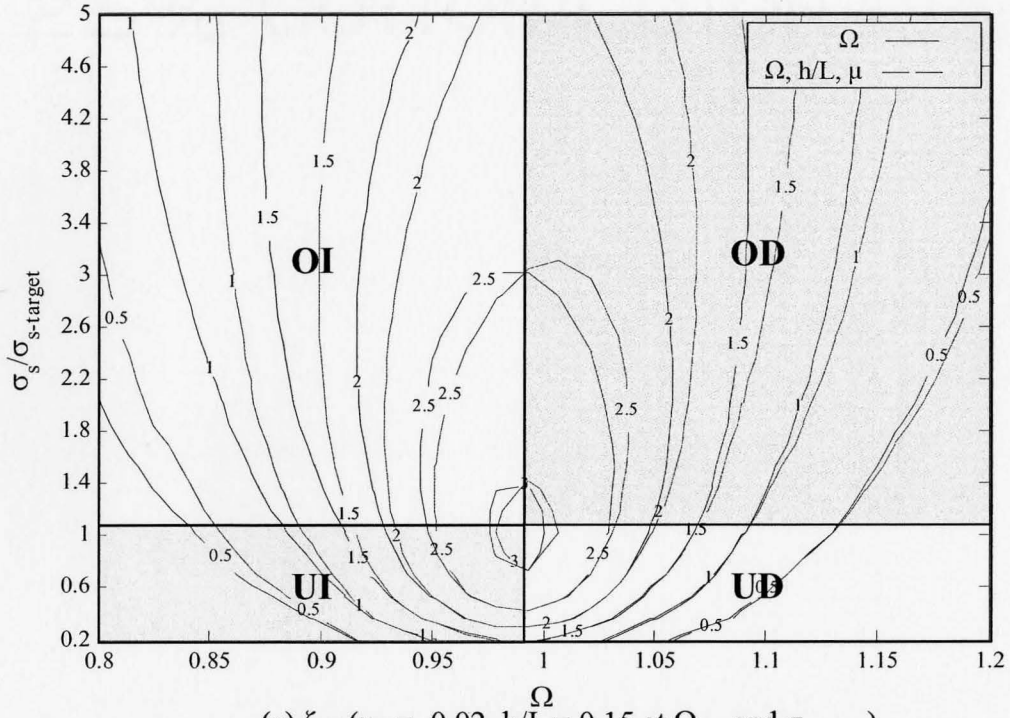

(a) ζ_{eff} (μ_w = 0.02, h/L = 0.15 at Ω_{opt} and $\sigma_{s\text{-target}}$)

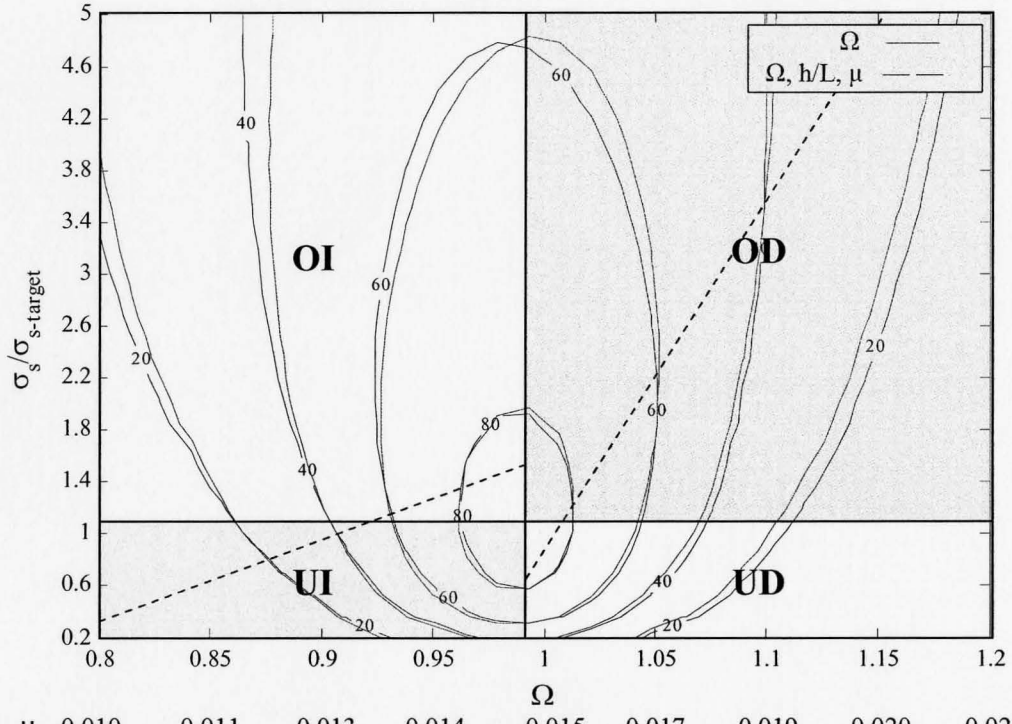

μ	0.010	0.011	0.013	0.014	0.015	0.017	0.019	0.020	0.022
h/L	0.092	0.106	0.120	0.136	0.153	0.173	0.196	0.222	0.253

(b) Ψ (μ_w = 0.02, h/L = 0.15 at Ω_{opt} and $\sigma_{s\text{-target}}$)

Figure 5.5 Influence of *Ω*, *h/L* and *μ* on Performance of a Vertical-Cylindrical TLD

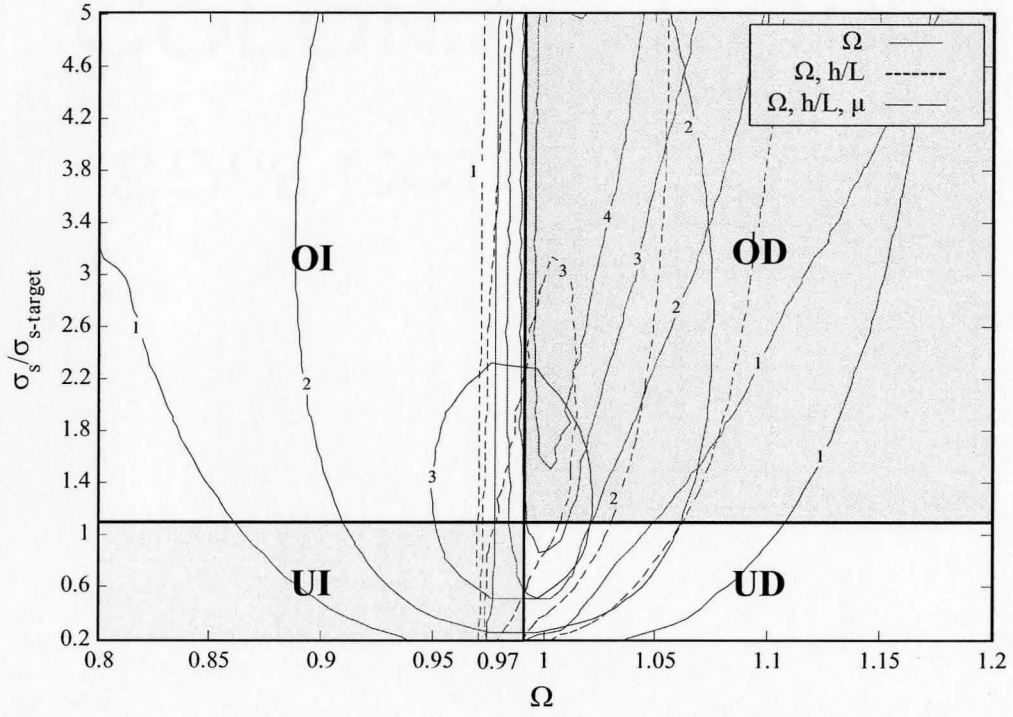

μ	-	-	-	-	0.035	0.085	0.113	0.126	0.131
$(h/L)_{h.b}$	-	-	-	-	0.197	0.332	0.435	0.529	0.618
$(h/L)_h$	-	-	-	- 0.020	0.195	0.307	0.387	0.451	0.513

(a) ζ_{eff} ($\mu_w = 0.02$, $h/L = 0.15$ at Ω_{opt} and $\sigma_{s\text{-target}}$)

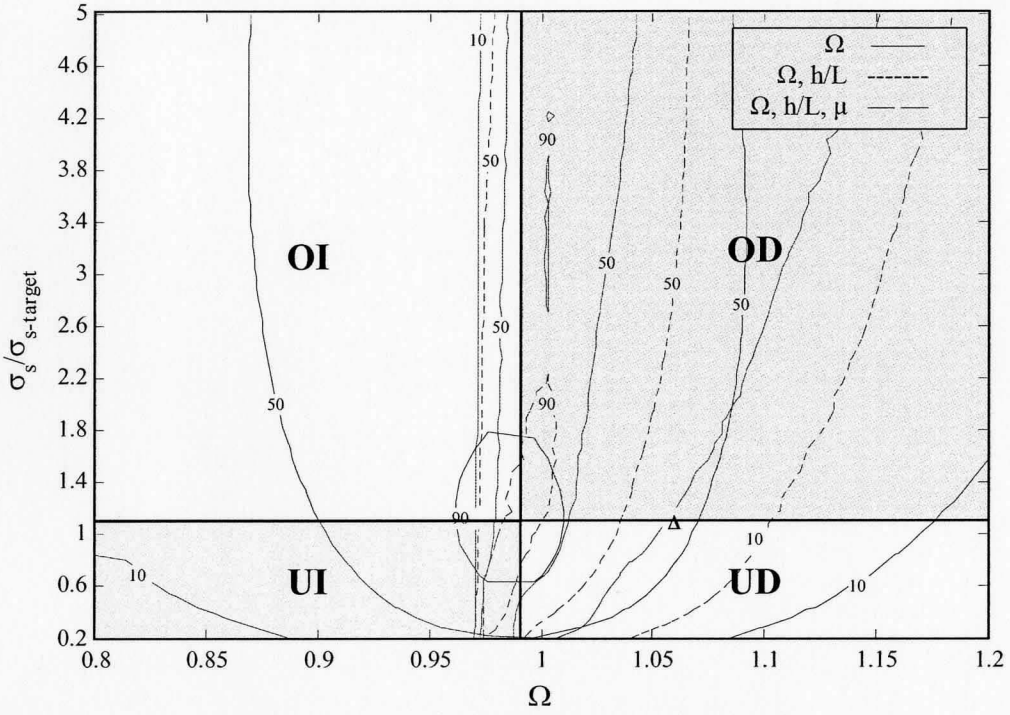

μ	-	-	-	-	0.035	0.085	0.113	0.126	0.131
$(h/L)_{h.b}$	-	-	-	-	0.197	0.332	0.435	0.529	0.618
$(h/L)_h$	-	-	-	-	0.195	0.307	0.387	0.451	0.513

(b) Ψ ($\mu_w = 0.02$, h/L = 0.15 at Ω_{opt} and $\sigma_{s\text{-target}}$)

Figure 5.6 Influence of *Ω*, *h/L* and *μ* on Performance of a Horizontal-Cylindrical TLD

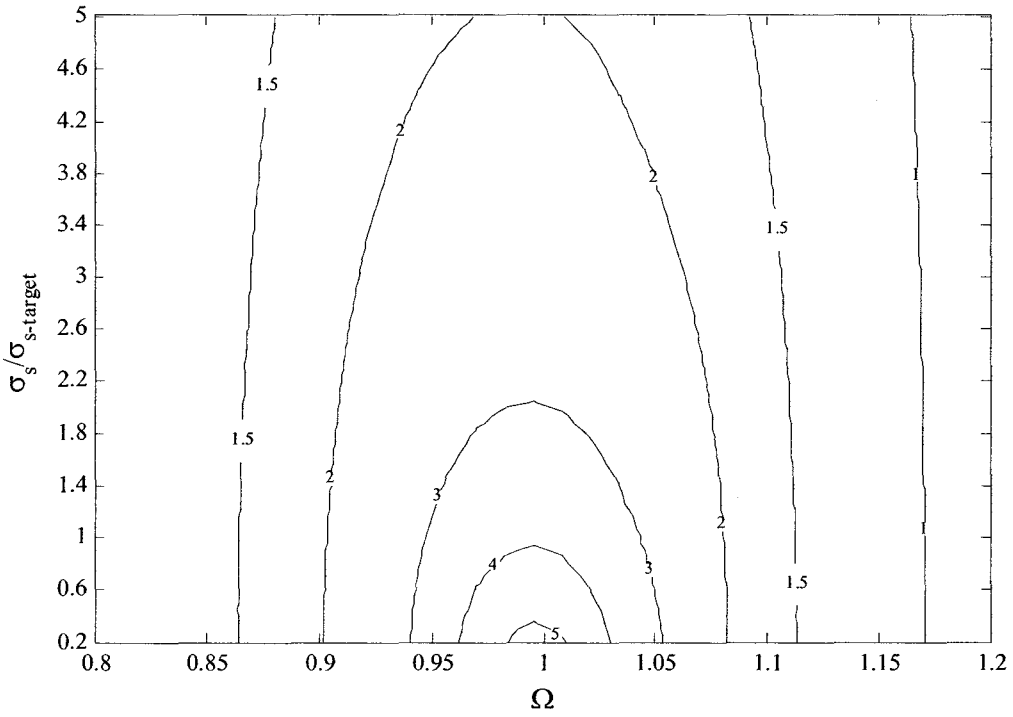

(a) $\mu_w = 0.005$, h/L = 0.1

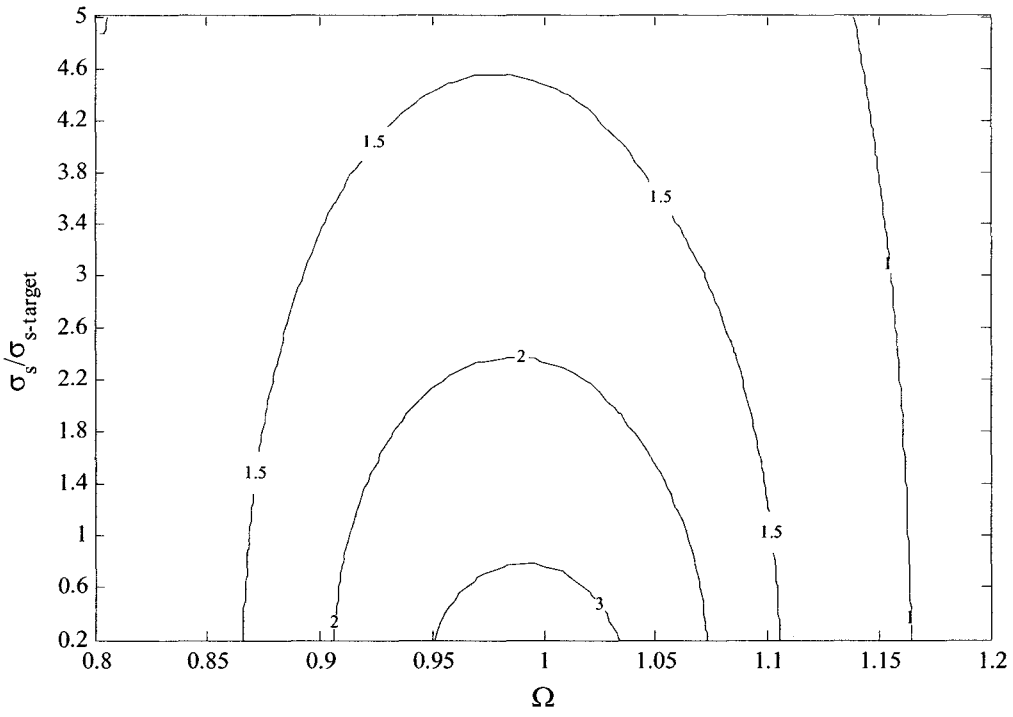

(b) $\mu_w = 0.01$, h/L = 0.1

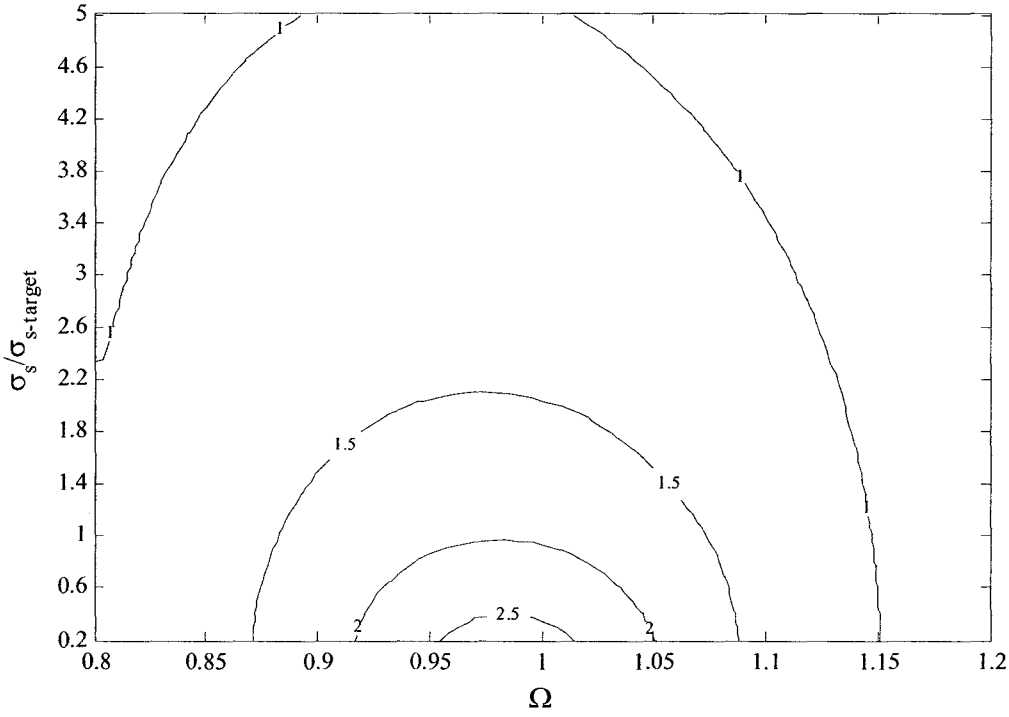

(c) $\mu_w = 0.02$, h/L = 0.1

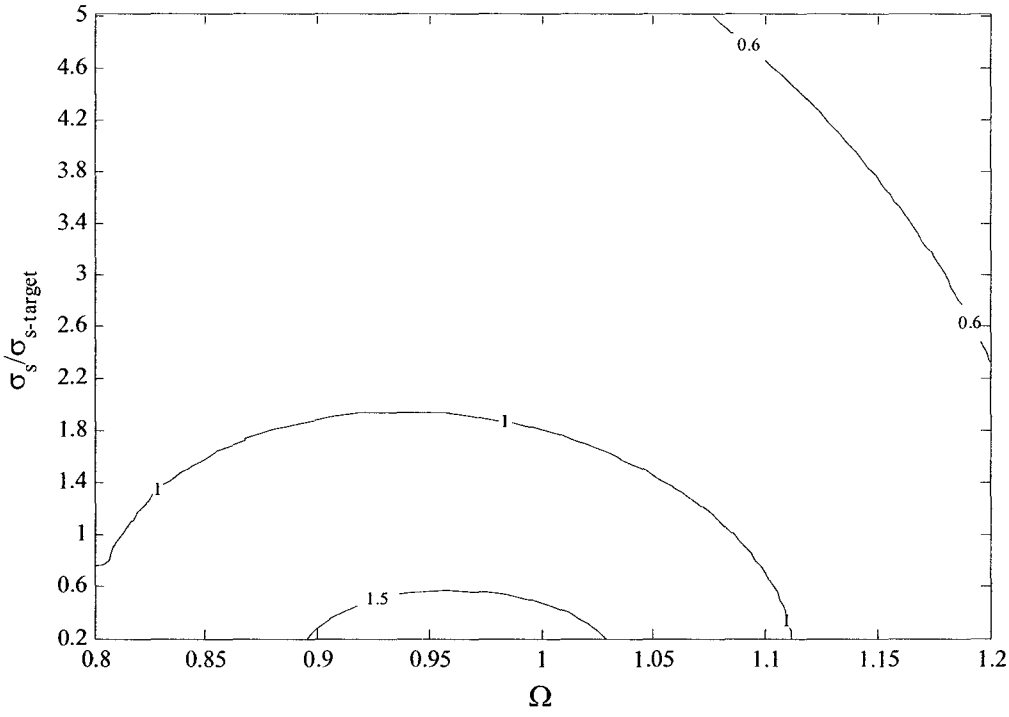

(d) $\mu_w = 0.05$, h/L = 0.1

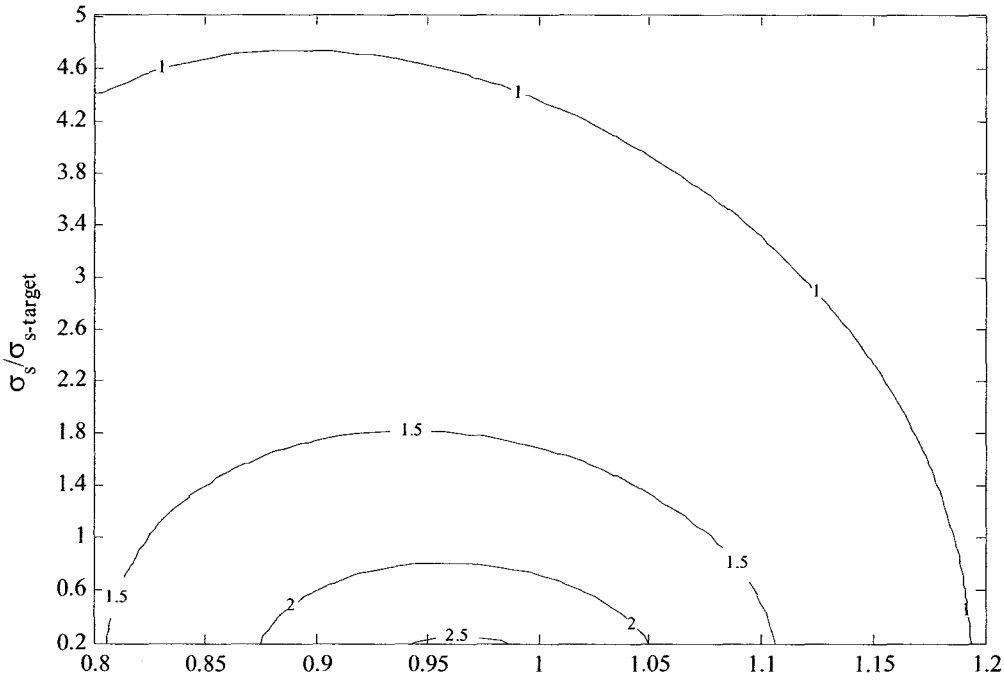

(e) $\mu_w = 0.05$, h/L = 0.15

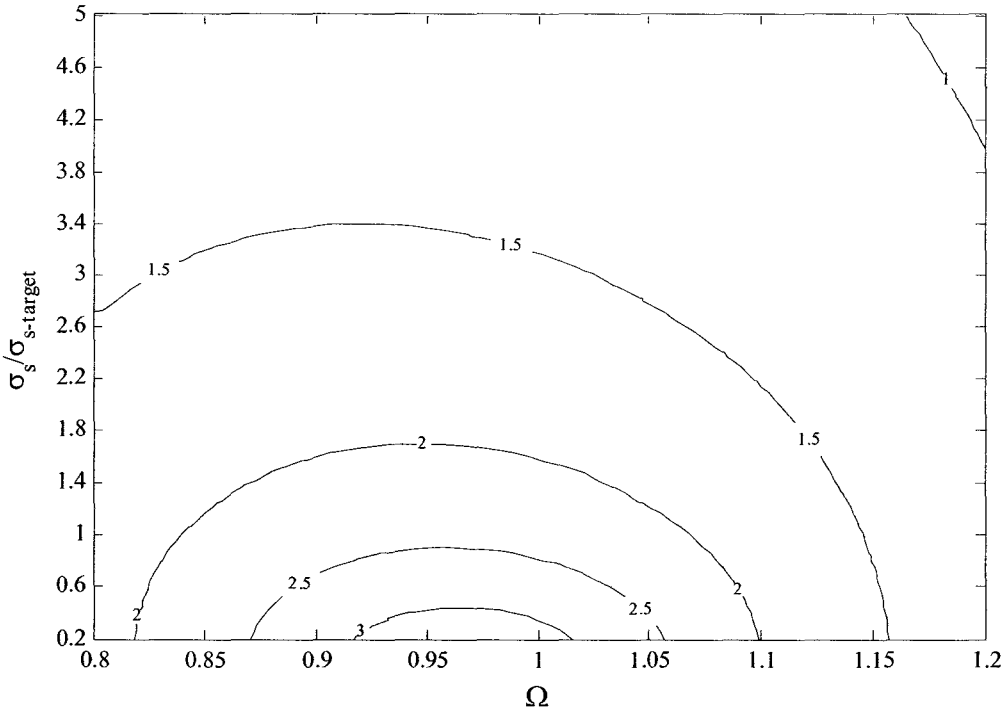

(f) $\mu_w = 0.05$, h/L = 0.2

Figure 5.7 Influence of Ω, h/L and μ_w on Relative Motion Ratio of a Horizontal-Cylindrical TLD

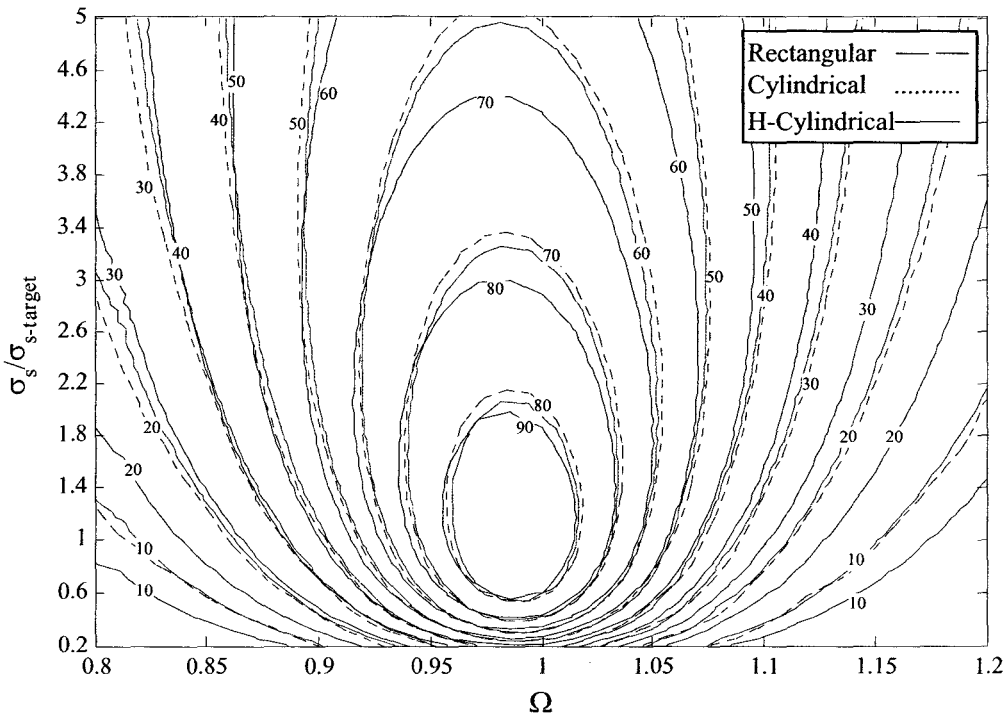

(a) $\mu_w = 0.02$, h/L = 0.1

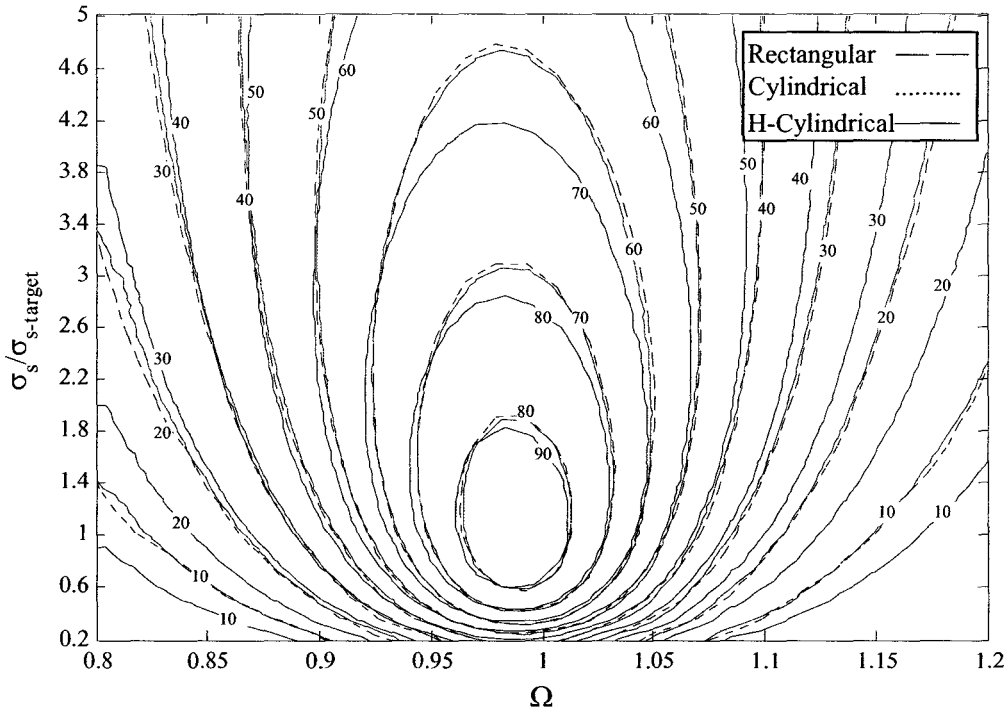

(b) $\mu_w = 0.02$, h/L = 0.15

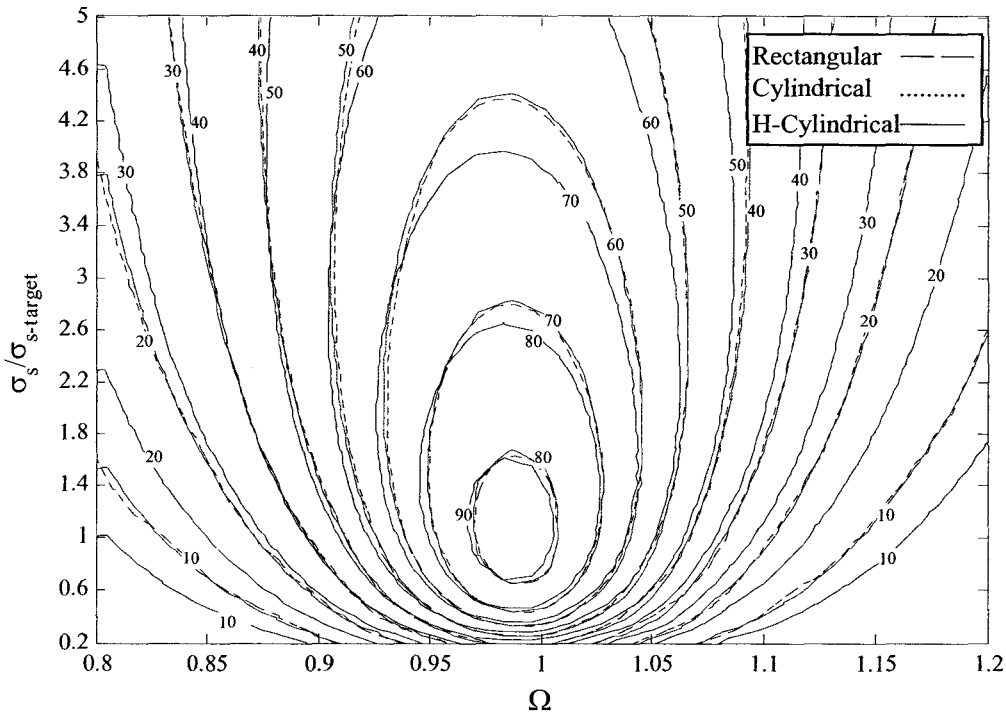

(c) $\mu_w = 0.02$, h/L = 0.2

Figure 5.8 Comparison of TLD Efficiency Values

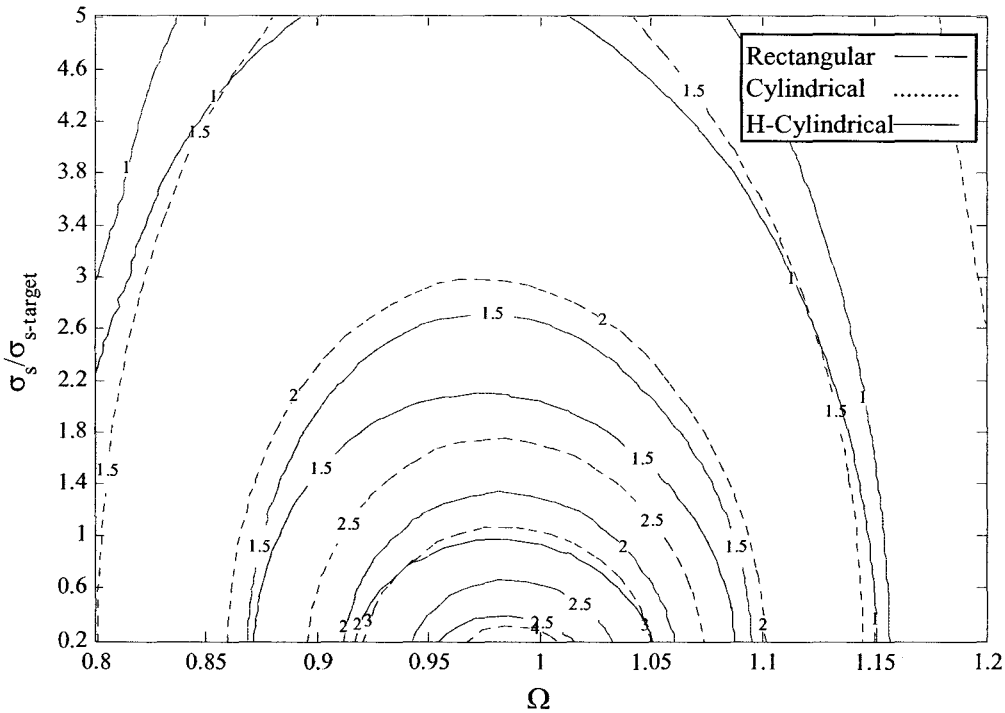

(a) $\mu_w = 0.02$, h/L = 0.1

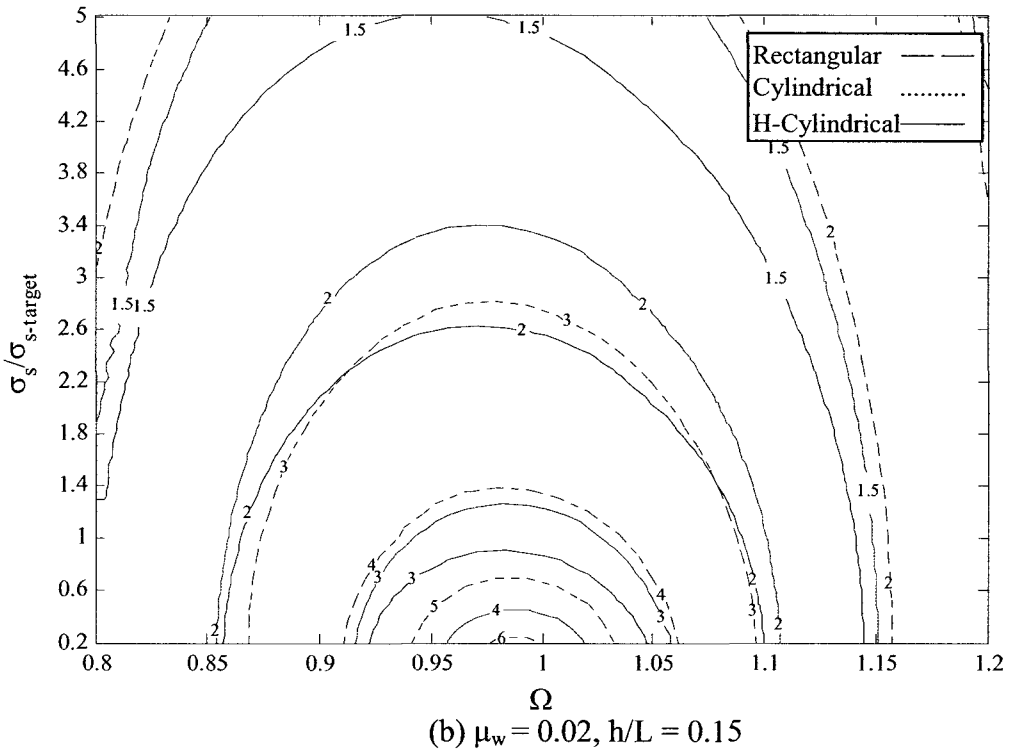

(b) $\mu_w = 0.02$, h/L = 0.15

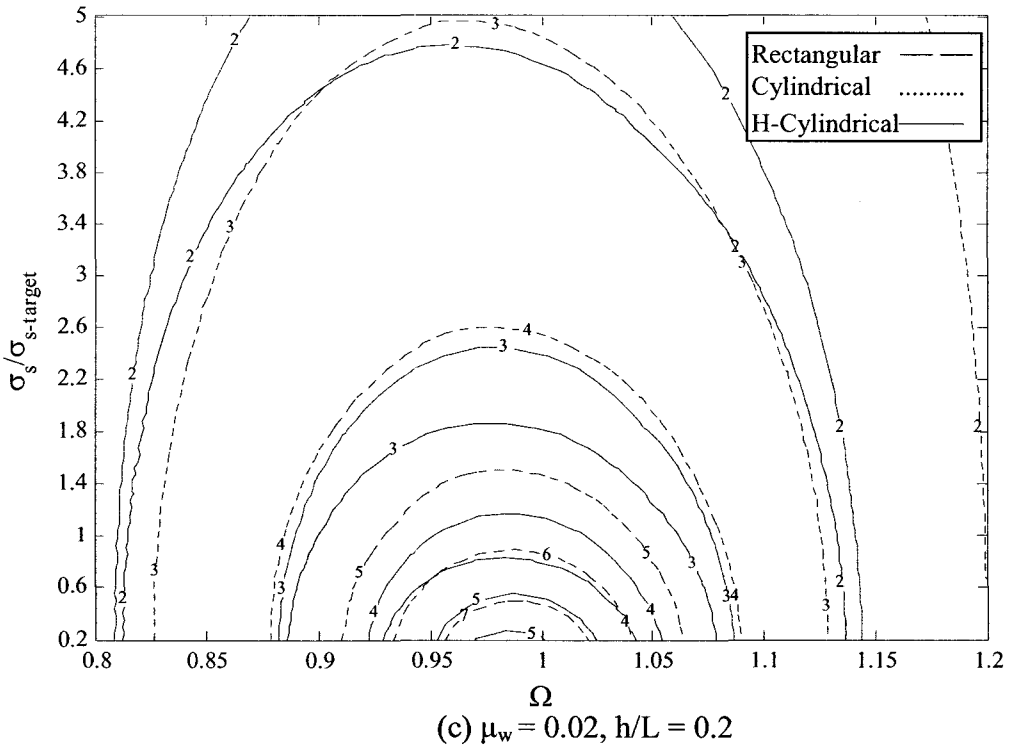

(c) $\mu_w = 0.02$, h/L = 0.2

Figure 5.9 Comparison of Relative Motion Ratio $R\eta$

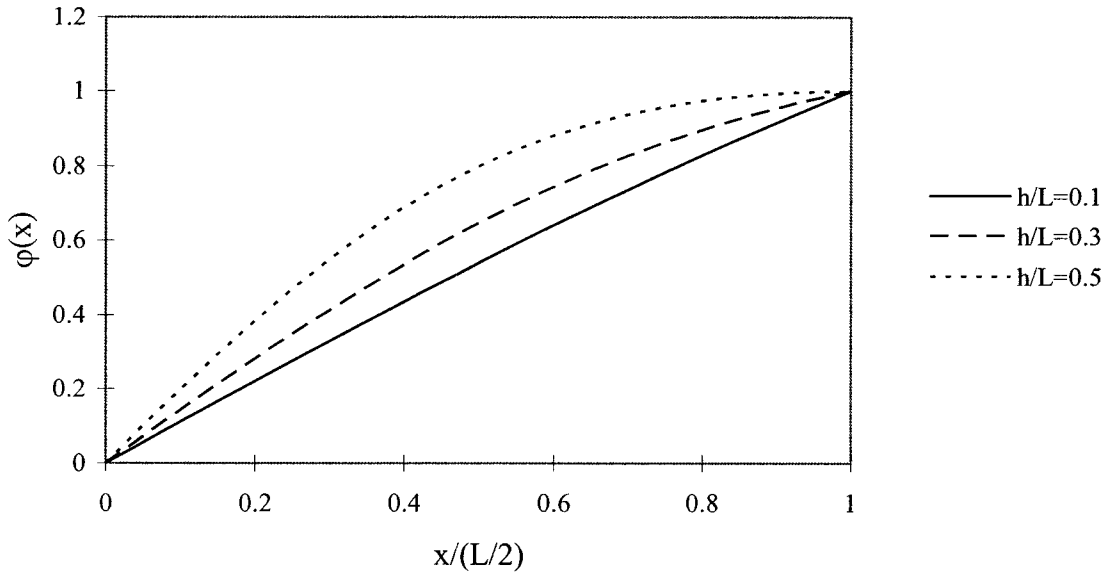

Figure 5.10 Mode Shape of the Free Surface in a Horizontal-Cylindrical Tank

Chapter 6 Conclusions and Recommendations

The research work conducted in this thesis includes the development of an equivalent mechanical model for TLDs with seven different tank geometries, investigation of the dynamic characteristics of a rectangular, vertical-cylindrical and horizontal-cylindrical TLD, respectively, and the performance of these three TLDs installed on a structure. The major conclusions of this thesis are presented below, followed by recommendations for future work.

6.1 Conclusions

The parameters of an equivalent mechanical model, which are the effective mass, damping ratio, and natural frequency, are derived for TLDs with rectangular, vertical-cylindrical, horizontal-cylindrical and hyperboloid tanks, respectively. Lagrange's equations, Morison's formula and the method of virtual work are applied in the derivations. The natural sloshing frequency and effective mass for each tank obtained using the potential flow theory agree with the results previously found by Graham and Rodriguez (1952), Bauer (1964) and Budiansky (1960). The additional damping introduced due to screens for different tanks is formulated utilizing the approach given by Tait (2007). The parameters of an equivalent mechanical model are compared for the studied tanks. It is found that for all tank geometries considered, as the liquid depth ratio increases, the normalized effective mass of the TLD decreases, and the natural frequency of the TLD increases.

From results obtained using potential flow theory, the values of the natural frequency, effective mass and damping ratio of the studied TLDs have the following

relationships for the common design range of h/L = 0.1 to 0.2. For the sloshing frequency values, $f_{hc} > f_{vc} > f_r > f_h$; for the effective mass values, $m_{hc} > m_h > m_r \approx m_{vc}$, and for the normalized equivalent viscous damping values, $\zeta_r/C_L > \zeta_{vc}/C_L \approx \zeta_{hc}/C_L > \zeta_h/C_L$, i.e. the horizontal-cylindrical TLD has the highest natural frequency and effective mass but the lowest normalized damping. The high natural frequency value is attributed to a short equivalent tank length. Additionally, the amount of effective mass for a tank is relative to its ability to eliminate inactive liquid. Although the normalized damping ratio is different between the tanks, ζ/C_L can be easily adjusted by selecting appropriate screens.

In order to construct an equivalent mechanical model for tanks with different geometries, where a suitable velocity potential function is not available, linear long wave theory is applied to obtain the velocity of sloshing liquid while Lagrange's equations, Morison's formula and the method of virtual work are utilized, as previously outlined in Chapter 2. The parameters of an equivalent mechanical model for triangular, sloped-bottom, parabolic and rectangular tank are obtained. The following trends are observed: for the sloshing frequency values, $f_{rl} > f_s > f_t > f_p$, for the effective mass values, $m_p > m_s > m_t > m_{rl}$; and for the normalized equivalent viscous damping values, $\zeta_{rl}/C_L > \zeta_p/C_L \approx \zeta_s/C_L > \zeta_t/C_L$.

These equivalent mechanical SDOF models are limited to small wave amplitudes such that potential flow theory or linear long wave theory is valid, and that the effective mass and natural frequency are regarded as amplitude-independent parameters.

Equivalent mechanical models for a rectangular, vertical-cylindrical and horizontal-cylindrical TLD are constructed and their dynamic characteristics are

investigated theoretically. First, the mechanical model for a rectangular TLD is validated from experimental shaking table tests conducted on a rectangular TLD. Subsequently, the model is utilized to investigate the dynamic characteristics of the different TLDs. It is observed that both the normalized sloshing force and energy dissipation decrease with an increase in excitation amplitude as a result of the amplitude-dependent damping. Since the model only takes the fundamental sloshing mode into account, the nonlinear free surface response behaviour cannot be captured. The study shows that to achieve the same magnitude of sloshing force, a horizontal-cylindrical TLD requires less liquid mass than a rectangular or vertical-cylindrical TLD. However, a horizontal-cylindrical TLD requires more installation volume than a rectangular or vertical-cylindrical TLD. In addition, it is confirmed theoretically that the viscous damping due to the boundaries of a tank can be neglected for large tanks.

The performance of rectangular, vertical-cylindrical and horizontal-cylindrical TLDs has been investigated using a mechanical model of structure-TLD system, where the TLDs are modelled as SDOF equivalent mechanical absorbers (Chapter 2) and the structure is modelled as a generalized SDOF system. The performance of the three TLDs is investigated under various response amplitudes, tuning ratio values, liquid depth values and mass ratio values using performance charts. When the values of Ω and $\sigma_s/\sigma_{s\text{-}target}$ are adjusted away from their optimal values, the TLDs are found to be less effective but in some cases more robust dynamic vibration absorbers. Also, it is shown that small liquid depth ratio and large mass ratio values can lead to a robust structure-TLD system with a small value of R_η. Results from this study indicate that the performance of TLDs is

strongly dependent on the tuning ratio, response amplitude, liquid depth and mass ratio. The results also show that the influence of liquid depth and mass ratio on the effective damping and efficiency are greater than the influence of liquid depth ratio. Furthermore, the performance of these three TLDs is compared. The horizontal-cylindrical TLD is approximately 10% more efficient than the rectangular or vertical-cylindrical TLDs in typical operational ranges of Ω, $\sigma_s/\sigma_{s\text{-}target}$ and h/L. These findings are attributed to the fact that horizontal-cylindrical TLDs possess larger effective mass values than rectangular and vertical-cylindrical TLDs. The relative motion ratio of a structure-TLD system with a horizontal-cylindrical TLD is found to be the smallest. It can be concluded that the horizontal-cylindrical TLD is the most robust and effective TLD with the smallest relative motion ratio among the investigated TLDs, however, it also requires the largest installation space. The mechanical model parameters of a rectangular TLD (the parameters of other TLDs can be found in Appendix A) and the key absorber design parameters are summarized in Tables 6.1 and 6.2.

6.2 Recommendations for Further Studies

The following recommendations are suggested for future studies:

- Approximated functions of the velocity potential need to be postulated for other TLDs tank geometries, whose velocity potential function cannot be obtained by directly solving the Laplace equation. Thus, additional equivalent mechanical models for various tank geometries can be developed for all values of liquid depth ratio, and an optimal container geometry can be identified.

- Since the equivalent mechanical model of a TLD is constructed with the assumption of small free surface amplitude, further investigation of the validity of these results is required for large response amplitudes, which would permit the study of structure-TLD systems under earthquake excitation.
- Higher modes of sloshing motion can be investigated to capture the hardening phenomenon and to improve the accuracy of results of the TLDs' dynamic properties and performance.
- Experiments should be conducted on all different tank geometries considered in this study in order to verify the proposed TLD and structure-TLD system models presented in this thesis. Parameters which should be experimentally investigated include screen location, number of screens, liquid depth, excitation type and excitation amplitudes.

Table 6.1 Mechanical Model Parameters of a Rectangular TLD

Natural Frequency (Equation 2.41)	$f_{TLD} = \frac{1}{2}\sqrt{\frac{g}{\pi L}\tanh\frac{\pi h}{L}}$
Effective Mass (Equation 2.51)	$m_r = \frac{8\tanh(\pi\frac{h}{L})}{\pi^3\frac{h}{L}} m_w$
Damping for Sinusoidal Excitation (Equation 2.22)	$\zeta_{eq}^{\ *} = \frac{2}{3}\frac{C_L \rho \Delta \Xi}{\pi m^*} q_0$
Damping for Random Excitation (Equation 2.25)	$\zeta_{eq}^{\ *} = \sqrt{\frac{1}{2\pi}}\frac{C_L \rho \Delta \Xi}{m^*}\sigma_\eta$
Ξ (Equation 2.53)	$\Xi = \sum_{j=1}^{ns}\left[\sin(\frac{\pi x_j}{L})\right]^3$
Δ (Equation 2.54)	$\Delta = \frac{bL}{\pi}\left[\frac{1}{3} + \frac{1}{\sinh^2\left(\frac{\pi h}{L}\right)}\right]$
Generalized Mass (Equation 2.49)	$m^* = \frac{1}{2}\frac{\rho b L^2}{\pi\tanh(\frac{\pi h}{L})}$

Table 6.2 Key Absorber Design Parameters

TLD Mass Ratio (Equation 5.1)	$\mu = \frac{\phi^2 m_{eff}}{M_s}$
Tuning Ratio (Equation 5.3)	$\Omega = \frac{f_{TLD}}{f_s}$
Effective Damping (Equation 5.9)	$\zeta_{eff} = \frac{\Omega\mu\zeta}{(1+\mu)^2\Omega^4 + 2(1+\mu)\Omega^2(2\zeta^2-1)+\Omega^2\mu+1}$
Efficiency (Equation 5.10)	$\Psi = \frac{\zeta_{eff}}{\zeta_{eff-opt}} \times 100$
Total Mass Ratio (Equation 5.11)	$\mu_w = \frac{m_w}{M^*}$
RMS Relative Motion Ratio (Equation 5.12)	$R_\eta = \Gamma\sqrt{\frac{1}{(1+\mu)^2\Omega^4 + 2(1+\mu)\Omega^2(2\zeta^2-1)+\Omega^2\mu+1}}$
Optimal Tuning Ratio (Equation 5.14)	$\Omega_{opt} = \sqrt{\frac{1+\mu/2}{1+\mu}}$
Optimal TLD Damping Ratio (Equation 5.15)	$\zeta_{opt} = \frac{1}{4}\sqrt{\frac{\mu+3\mu^2/4}{4+6\mu+2\mu^2}}$
Optimal Effective Damping Ratio (Equation 5.16)	$\zeta_{eff-opt} = \frac{1}{4}\sqrt{\frac{\mu_{TMD}+\mu_{TMD}^2}{1+3\mu_{TMD}/4}}$
Optimal RMS Relative Motion Ratio (Equation 5.17)	$\frac{R_{opt}}{\Gamma} = \frac{1+\mu}{\sqrt{2\mu+3\mu^2/2}}$

References

Abramson, H.N. (1966). "The Dynamic Behaviour of Liquids in Moving Containers", NASA SP-106, National Aeronautics and Space Administration.

Bartkowiak, K., Gamper, B. and Siekmann, J. (1985). "On Liquid Motion in a Circular Cylinder with Horizontal Axis", *Acta Mechanica*, Volume 54, pp207-220.

Bauer, H.F. (1960). "Mechanical Model for the Description of the Liquid Motion in a Rectangular Container", Lockheed Company, RN ER-8559.

Bauer, H.F. (1961). "Mechanical Analogy of Fluid Oscillations in Cylindrical Tanks with Circular and Annular Cross-Section", MSFC, NASA, MTP-AERO61-4.

Bauer, H.F. (1962). "Mechanical Model of Fluid Oscillation in Cylindrical Containers and Introduction of Damping", MTP-AERO-62-16.

Bauer, H.F. (1964). "Fluid Oscillations in the Containers of a Space Vehicle and Their Influence on Stability", NASA TR-T-187.

Bauer, H.F. (1981). "Liquid Oscillations with a Free Surface in Wedge-Shaped Tanks", *Acta Mechanica*, Vol. 38, No. 1-2, 1981, pp31-54. In German.

Bauer, H.F. (1984). "Oscillations of Immiscible Liquids in a Rectangular Container: A New Damper for Excited Structures", *Journal of Sound and Vibration*, Vol. 93, pp.117-133

Budiansky, B. (1960). "Sloshing of Liquids in Circular Canals and Spherical Tanks", *Journal of the Aero/Space Sciences*, Vol. 27, No. 3, pp. 161-173.

Cai, D., Li, A. and Cheng, W. (1999). "Parametric Study of TLDs with Baffles", *Proceedings of the Second World Conference on Structural Control*, Chichester, New York: Wiley.

Carrier, G.F. and Miles, J.W. (1960). "On the Annular Damper for a Freely Precessing Gyroscope", *Journal of Applied Mechanics*, Vol. 27, pp. 237-240

Chang C.C. and Qu, W.L. (1998), "Unified Dynamic Absorber Design Formulas for Wind-induced Vibration Control of Tall Buildings", *Structural Design of Tall Buildings*, Vol. 7, pp.147-166.

Chester, W. (1968). "Resonant Oscillations of Water Waves", *Proceedings of Royal Society of London*, Vol. 306, pp.5-22.

Clough, R.W. and Penzien, J. (1993). "*Dynamics of Structures*", 2nd ed. McGraw-Hill Inc., NY.

Davenport, A.G. (1964). "Note on the Distribution of the Largest Value of a Random Function with Application to Gust Loading", *Institute for Civil Engineers*, Vol. 28, pp. 187-196.

Dean, R. G. and Dalrymple, R. A. (1984). "*Water Wave Mechanics for Engineers and Scientists*", Prentice-Hall, Inc., Englewood Cliffs, New Jersey.

Den Hartog, J.P. (1956). "*Mechanical Vibrations*", 4th Ed., McGraw-Hill Book Company: New York, NY, USA.

Fujino, Y., Pacheco, B.B., Chaiseri, P. and Sun, L.M. (1988). "Parametric Studies on Tuned Liquid Damper Using Circular Containers by Free Oscillation Experiments", *Structural Engineering/Earthquake Engineering*, JSCE, 5(2), pp.381s-391s.

Fujino, Y., Pacheco, B.M, Chaiseri, P., Sun, L. and Koga, K. (1990). "Understanding of TLD Properties Based on TMD Analogy", JSCE, *Journal of Structural Engineering*, Vol.36A, pp. 557-590. In Japanese.

Fujino, Y.; Yeh, H.; Sun, L.; Pacheco, B.M.; Chaiseri, P. (1992). "Tuned Liquid Damper for Suppressing Horizontal Motion of Structures", *Journal of Engineering Mechanics*, Vol. 118, No.10, pp. 435-447

Fediw, A.A., Isyumov, N. and Vickery, B.J. (1995). "Performance of a Tuned Sloshing Water Damper", *Wind Engineering and Industrial Aerodynamics*, Vol. 57, pp. 237-247.

Gao, H.; Kwok, K.C.S. and Samali, B. (1997) "Optimization of Tuned Liquid Column Dampers", *Engineering Structures*, Volume19, Number 6, pp. 476-486

Gardarsson, S., Yeh, H. and Reed, D.A. (2001). "The Behaviour of Sloped-Bottom Tuned Liquid Dampers", *Journal of Engineering Mechanics*, Vol. 127, (3), pp. 266-271.

Gardarsson, S. (1997). "*Shallow-water Sloshing*", Ph.D. Thesis, University of Washington, Department of Civil Engineering, Seattle, WA.

Gerges, R. R. and Vickery, B. J. (2003). "Wind Tunnel Study of the Across-Wind Response of a Slender Tower with a Nonlinear Tuned Mass Damper", *Journal of Wind Engineering and Industrial Aerodynamics*, Vol. 91, No. 8, pp. 1069-1092

Graham, E.W. (1951). "The Forces Produced by Fuel Oscillations in a Rectangular Tank", Douglas Aircraft Co, Sm-13748.

Graham, E. W. and Rodriguez, A.M. (1952). "The Characteristics of Fuel Motion Which Affect Airplane Dynamics", *Journal of Applied Mechanics*, Vol. 19, No.3, pp. 381-388.

Hamelin, J. (2007). Private communication: Experimental data.

Kaneko, S. and Ishikawa, M. (1999). "Modeling of Tuned Liquid Damper with Submerged Nets", *Journal of Pressure Vessel Technology*, Vol.121, pp. 334-343.

Kaneko, S. and Yoshida, O. (1999). "Modeling of Deepwater-Type Rectangular Tuned Liquid Damper with Submerged Nets", *Journal of Pressure Vessel Technology*, Vol.121, pp. 413-422.

Kareem, A. and Sun, W.J. (1987). "Stochastic Response of Structures with Fluid-Containing Appendages", *Journal of Sound and Vibration*, Vol. 119, No.3, pp. 389-408.

Lamb, H. (1932). "*Hydrodynamics*", The University Press, Cambridge, England.

Le Méhauté, B. (1976). "*An Introduction to Hydrodynamics and Water Waves*", Springer-Verlag, New York.

Lepelletier, T. G. and Raichlen, F. (1988). "Nonlinear Oscillations in Rectangular Tanks," *Journal of Engineering Mechanics*, ASCE, Vol. 114, No. 1.

Luft, R.W. (1979). "Optimal Tuned Mass Dampers for Building", *Journal of the Structural Division*, ASCE, Vol. 105, No.12, pp.2766-2772.

McCarty, J.L. and Stephens, D.D. (1960). "Investigation of the Natural Frequencies of Fluid in Spherical and Cylindrical Tanks", NASA TN D-252.

McNamara, R.J. (1977). "Tuned Mass Dampers for Buildings", *Journal of the Structural Division*, ASCE, Vol. 103, No. 9, pp. 1785-1798

Modi, V.J. and Welt, F. (1987). "Vibration Control Using Nutation Dampers", *International Conference of Flow Induced Vibrations*, England, pp. 369-376

Moiseev, N.N. and Petrov, A.A. (1968). "The Calculation of Free Oscillations of a Liquid in a Motionless Container", *Advances in Applied Mechanics*, Vol. 9, pp. 91-154.

Morison, J.R., O'Brien, M.P., Johnson, J.W. and Schaaf, S.A. (1950). "The Force Exerted by Surface Waves on Piles", *Petroleum Transactions*, AIME, Vol. 187, pp. 149-155.

Shimizu, T. and Hayama, S. (1987). "Nonlinear Response of Sloshing Based on the Shallow Water Wave Theory," *JSME International Journal, 30(263)*, 806–813.

Sun, L.M., Fujino, Y., Pacheco, B.M. and Chaiseri, P. (1992). "Modelling of Tuned Liquid Damper", Journal of Wind Engineering and Industrial Aerodynamics, Vol. 43, No.3, pp. 1883-1894.

Sun, L.M., Fujino, Y., Chaiseri, P. and Pacheco, B.M. (1995). "The Properties of Tuned Liquid Dampers Using a TMD Analogy", *Earthquake Engineering and Structural Dynamics*, Vol. 24, pp. 967-976

Tait, M. J. (2004). "*The Performance of 1-D and 2-D Tuned Liquid Dampers*", Ph.D. Thesis, the University of Western Ontario, London, Canada.

Tait, M. J. (2007). "Modelling and Preliminary Design of a Structure-TLD System", Submitted to *Engineering Structures*.

Tamura, Y. and Suganuma, S. (1996). "Evaluation of Amplitude-Dependent Damping and Natural Frequency of Buildings during Strong Winds", *Journal of Wind Engineering and Industrial Aerodynamics*, Vol. 59, pp. 115-130

Troesch, B.A. (1960). "Free Oscillations of a Fluid in a Container", *Boundary Problems in Differential Equations*, University of Wisconsin Press, Madison, pp. 279–299.

Vandiver, J.K., Mitone, S. (1979). "The Effect of Liquid Storage Tanks on the Dynamic Response of Offshore Platforms", *Journal of Petroleum Technology*, Vol.31, No. 10, pp.1231-1240.

Vickery, B.J., and Davenport, A.G. (1970). "An Investigation of the Behaviour in Wind of the Proposed Centrepoint Tower, in Sydney, Australia", *Research Report BLWT-1-70*, The Boundary Layer Wind Tunnel Laboratory, The University o f Western Ontario, London, Canada.

Vickery, B.J., Galsworthy, J.K., Gerges, R.R. (2001). "The Behaviour of Simple Nonlinear Tuned Mass Dampers", *Proceedings of the Sixth World Congress of the Council on Tall Buildings and Urban Habitat, Melbourne*, Australia.

Warburton, G.B. (1982). "Optimum Absorber Parameters for Various Combinations of response and Excitation Parameters", *Earthquake Engineering and Structural Dynamics*, Vol.10, pp. 381-401

Warnitchai, P. and Pinkaew, T. (1998). "Modelling of Liquid Sloshing in Rectangular Tanks with Flow-Dampening Devices", *Engineering Structures*, Vol. 20, No. 7, pp. 593-600(8).

White, F.M. (1999). "*Fluid Mechanics*"4th Ed., McGraw-Hill: Boston.

Xu, Y.L., Samali, B. and Kwok, K.C.S. (1992). "Control of Along Wind Response of Structures by Mass and Liquid Dampers", *Journal of Engineering Mechanics*, ASCE, Vol. 118(1), pp. 20-39.

Yu, J., Wakahara, T, Reed, D (1999). "A Non-linear Numerical Model of the Tuned Liquid Damper", *Earthquake Engineering and Structural Dynamics*, Vol. 28, pp. 671-686

Zelt, J.A. (1986). "Tsunamis: The Response of Harbours with Sloping Boundaries to Long Wave Excitation", W. M. Keck Lab. Rep. No. KH-R-47, California Institute of Technology, Pasadena, Calif.

Appendix A Properties for Equivalent Mechanical Model of TLDs

A1 Formulas Based on Potential Flow Theory

A1.1 Rectangular TLDs

- Natural frequency

$$f_r = \frac{1}{2}\sqrt{\frac{g}{\pi L}\tanh\frac{\pi h}{L}} \tag{A 1}$$

- Effective mass

$$m_r = \frac{8\tanh(\pi\frac{h}{L})}{\pi^3\frac{h}{L}} m_w \tag{A 2}$$

- Damping ratio

Sinusoidal

$$\zeta_{eq}^{\ *} = \frac{2}{3}\frac{C_L \rho A \Xi}{\pi m^*} q_0 \tag{A 3}$$

Random

$$\zeta_{eq}^{\ *} = \sqrt{\frac{1}{2\pi}}\frac{C_L \rho A \Xi}{m^*}\sigma_\eta \tag{A 4}$$

where

$$\Xi = \sum_{j=1}^{ns}\left[\sin(\frac{\pi x_j}{L})\right]^3 \tag{A 5}$$

$$\Delta = \frac{bL}{\pi}\left[\frac{1}{3} + \frac{1}{\sinh^2\left(\frac{\pi h}{L}\right)}\right] \tag{A 6}$$

$$m^* = \frac{1}{2}\frac{\rho b L^2}{\pi \tanh(\frac{\pi h}{L})} \tag{A 7}$$

A1.2 Vertical-Cylindrical TLDs

- Natural frequency

$$f_{vc} = \frac{1}{2\pi}\sqrt{\frac{1.841g}{a}\tanh\frac{1.841h}{a}} \tag{A 8}$$

- Effective mass

$$m_{vc} = \frac{2}{\xi(\xi^2 - 1)}\frac{a}{h}\left(\tanh\frac{\xi h}{a}\right)m_w \tag{A 9}$$

- Damping ratio

The damping ratio of all TLDs can be computed by substituting m^*, Δ and Ξ into Equations A1.3 and A1.4. The equations for these three parameters are provided as follows.

$$\Xi = \sum_{j=1}^{ns} 2\int_0^{\theta_j}\{\frac{\cosh\frac{\xi(z+h)}{a}}{J_1(\xi)\sinh(\frac{\xi h}{a})}\left[J_0(\xi\cdot r/a) - a/(\xi\cdot r)J_1(\xi\cdot r/a)\right]\cos^2\theta - \frac{\cosh\frac{\xi(z+h)}{a}}{\frac{1}{a}\sinh(\frac{\xi h}{a})}\frac{J_1(\xi\cdot r/a)}{\xi J_1(\xi) r/a}\sin^2\theta\}^3 a\cos\theta d\theta \tag{A 10}$$

$$\Delta = \int_{-h}^{0} \left[\frac{\cosh(\frac{\xi(z+h)}{a})}{\sinh(\frac{\xi h}{a})} \right]^3 dz = \frac{a}{\xi} \left[\frac{1}{3} + \frac{1}{\sinh^2(\frac{\xi \cdot h}{a})} \right] \quad \text{(A 11)}$$

where

$\xi = 1.841$

$$m^* = \frac{\xi^2 - 1}{2\xi^3} \rho\pi \cdot a^3 \coth\frac{\xi h}{a} \quad \text{(A 12)}$$

A1.3 Horizontal-Cylindrical TLDs

- Natural frequency

$$f_c = \frac{1}{2\pi}\sqrt{\frac{\lambda_n g}{R}} = \frac{1}{2\pi}\sqrt{\frac{2\lambda_n g}{L}} \quad \text{(A 13)}$$

- Effective mass

$$m_{hc} = \frac{2}{\pi}\rho(\lambda_1 a^3) B_1^{\,2} / A_1 \quad \text{(A 14)}$$

where

$A_1 = (1/3)(2.050)^{h/L}$

$B_1 = 0.339(1.392)^{h/L}$

- Damping ratio

$$\Delta = \left[\frac{g}{\omega^2} \frac{2R(R-H)}{\sqrt{R^2 - H^2}} \right]^3 \quad \text{(A 15)}$$

$$\Xi = \sum_{j=1}^{ns} \int_b \int_{-\sqrt{R^2-x^2}}^{-H} \left(\frac{(z-R)^2 - x_j^{\,2}}{\left[x_j^{\,2} + (z-R)^2\right]^2} \right)^3 dzdy \quad \text{(A 16)}$$

$$m^* = \frac{2\rho a A_1 R^2}{\lambda_1} \tag{A 17}$$

The properties of the equivalent mechanical model of a horizontal-cylindrical TLD can also be calculated by using the method discussed in Section 2.3.3.

A1.4 Hyperboloid TLDs

- Natural frequency

$$f_h = \frac{1}{2\pi}\sqrt{\frac{2hg}{R^2+h^2}} \tag{A 18}$$

- Effective mass

$$m_h = 45\{(64(h/L)^6 - 80(h/L)^4 + 100(h/L)^2 + 15][3 - 4(h/L)^2]\}^{-1} m_w \tag{A 19}$$

- Damping ratio

$$\Delta = 1 \tag{A 20}$$

$$\Xi = \sum_{j=1}^{ns} \frac{\begin{array}{c}[(-3 + a^2\lambda^2 + 2a^4\lambda^4)\sqrt{1/\lambda^2 - a^2} + (3h_j{}^4\lambda^4 + 18h_j{}^2\lambda^2 - h_j{}^2\lambda^4 a^2 \\ -12h_j{}^3\lambda^3 - 12h_j\lambda + 2h_j\lambda^3 a^2 - a^2\lambda^2 - 2a^4\lambda^4 + 3)\sqrt{(h_j - 1/\lambda)^2 - a^2}]\end{array}}{-15\lambda^4 R^3} \tag{A 21}$$

$$m^* = \frac{1}{120}\rho\pi\frac{15R^6 + 25R^4h^2 - 5R^2h^4 + h^6}{R^2 h} \tag{A 22}$$

The parameters λ, a, and h_j are given as

$$\lambda = \frac{2h}{R^2+h^2}$$

$$a = \sqrt{\left(\frac{1}{\lambda}\right)^2 - R^2}$$

$$h_j = \sqrt{a^2 - r^2} - 1/\lambda$$

A2 Formulas Based on Linear Long Wave Theory

A2.1 Triangular TLDs

- Natural frequency

$$f_t = \frac{1.023}{\pi L}\sqrt{gh} \tag{A 23}$$

- Effective mass

$$m_t = 95.7\% m_w \tag{A 24}$$

- Damping ratio

$$\Delta = \left[\frac{s}{\kappa h}\right]^3 \tag{A 25}$$

$$\Xi = \sum_{j=1}^{ns}\left[\frac{\partial \eta}{\partial x}\right]^3 h(x_j) = \sum_{j=1}^{ns}\left[\sqrt{\frac{\kappa}{x}} J_1(2\sqrt{\kappa x})\right]^3 \frac{h}{s} x_j \tag{A 26}$$

$$m^* = \frac{\rho}{h}\left(\frac{s}{\kappa}\right)^{3/2} [cJ_0{}^2(c) - 2J_0(c)J_1(c) + cJ_1{}^2(c)] \tag{A 27}$$

where

$\kappa = \omega^2 s / gh$

$c = 2\sqrt{ks}$

A2.2 Sloped-Bottom TLDs

- Natural frequency

$$f_s = \frac{\varepsilon}{2L}\sqrt{gh} \tag{A 28}$$

$$\varepsilon = \frac{f_s}{f_r} \tag{A 29}$$

- Effective mass

$$m_s = \frac{32\rho s^2 h^2 \left[-2J_1(c) + cJ_1(c)\sin c(1-1/s) + cJ_0(c)\cos c(1-1/s)\right]^2}{c^4 \begin{bmatrix} cJ_0^{\,2}(c) - 2J_0(c)J_1(c) + cJ_1^{\,2}(c) + cL_0J_1^{\,2}(c)/2s \\ -2J_0(c)J_1(c)\cos c(1-1/s) - J_1^{\,2}(c)\sin c(1-1/s) \\ +J_0^{\,2}(c)\sin c(1-1/s) + cL_0J_0^{\,2}(c)/s \end{bmatrix}} \tag{A 30}$$

- Damping ratio

$$\Xi = \sum_{j=1}^{ns}\left[\frac{\partial \eta}{\partial x}\right]^3 h(x_j) \tag{A 31}$$

$$\Delta = \left[\frac{s}{\kappa h}\right]^3 \tag{A 32}$$

$$m^* = 2\rho\left(\frac{s}{ch}\right)^2 \begin{bmatrix} cJ_0^{\,2}(c) - 2J_0(c)J_1(c) + cJ_1^{\,2}(c) + cL_0J_1^{\,2}(c)/2s \\ -2J_0(c)J_1(c)\cos c(1-1/s) - J_1^{\,2}(c)\sin c(1-1/s) \\ +J_0^{\,2}(c)\sin c(1-1/s) + cL_0J_0^{\,2}(c)/s \end{bmatrix} \tag{A 33}$$

where

$$\frac{\partial \eta}{\partial x} = -\sqrt{\frac{\kappa}{x}}J_1(2\kappa\sqrt{sx}) \qquad \text{for } x_j < s$$

$$\frac{\partial \eta}{\partial x} = -\sqrt{\frac{\kappa}{s}}\left[J_1(c)\cos\sqrt{\frac{\kappa}{s}}(x-s) + J_0(c)\sin\sqrt{\frac{\kappa}{s}}(x-s)\right] \qquad \text{for } s < x_j < L_0$$

$$h(x_j) = \begin{cases} hx_j/s & x_j < s \\ h & s \le x_j \le L_0 \end{cases}$$

A2.3 Parabolic TLDs

- Natural frequency

$$f_p = \frac{1}{\pi L}\sqrt{gh} \tag{A 34}$$

- Effective mass

$$m_t = m \tag{A 35}$$

- Damping ratio

$$\Xi = \sum_{j=0}^{ns} h(x_j) \tag{A 36}$$

$$\Delta = \left[\frac{s}{\kappa h}\right]^3 \tag{A 37}$$

$$m^* = \frac{1}{3}\frac{L_0{}^3 b}{h} \tag{A 38}$$

A2.4 Rectangular TLDs

- Natural frequency

$$f_{rl} = \frac{1}{2L}\sqrt{gh} \tag{A 39}$$

- Effective mass

$$m_{rl} = \frac{8}{\pi^2} m \tag{A 40}$$

- Damping ratio

$$\Xi = \sum_{j=1}^{ns}\left[\sin\left(\frac{\pi}{L}x_j\right)\right]^3 \tag{A 41}$$

$$\Delta = h\left[\frac{\pi g}{L}\right]^3 \tag{A 42}$$

$$m^* = \frac{1}{2}\frac{\rho L^3}{\pi^2 h} \tag{A 43}$$

Appendix B Derivation of Wave Height in Horizontal-Cylindrical Tank

The velocity potential of sloshing fluid in a horizontal-cylindrical tank is given as

$$\phi(x,z,t) = c_c \frac{x}{x^2 + (z-R)^2} \cos \omega t \tag{B 1}$$

Applying the linearized Bernoulli equation

$$\eta = -\frac{1}{g}\left(\frac{\partial \phi}{\partial t}\right)\Big|_{z=H} \tag{B 2}$$

to the velocity potential function (Equation B1) at the free surface

$$\eta = \frac{\omega}{g} c_c \frac{x}{x^2 + (H-R)^2} \sin \omega t \tag{B 3}$$

At point A, where the tank edge and the still liquid meet, as shown in Figure 2.6

$$x = -\sqrt{R^2 - H^2} \tag{B 4}$$

Based on Equation B4, a mode shape function, $\varphi(x)$, can be expressed as

$$\varphi(x) = \frac{2R(R-H)}{\sqrt{R^2 - H^2}} \frac{x}{x^2 + (H-R)^2} \tag{B 5}$$

Incorporating Equation B5 into B3

$$\eta(x,t) = -\frac{\omega c_c}{g} \frac{\sqrt{R^2 - H^2}}{2R(R-H)} \frac{2R(R-H)}{\sqrt{R^2 - H^2}} \frac{x}{x^2 + (H-R)^2} \sin \omega t \tag{B 6}$$

or

$$\eta(x,t) = q(t) \frac{2R(R-H)}{\sqrt{R^2 - H^2}} \frac{x}{x^2 + (H-R)^2} \tag{B 7}$$

where

$$q(t) = \frac{\omega c_c}{g} \frac{\sqrt{R^2 - H^2}}{2R(R-H)} \sin \omega t = q_0 \sin \omega t \qquad \text{(B 8)}$$

Appendix C Derivation of Horizontal Velocity Component of Liquid in a Triangular Tank

Momentum equation is given by Equation 3.2

$$b\frac{\partial u}{\partial t} = -gb\frac{\partial \eta}{\partial x}$$

The horizontal velocity component can be obtained by integrating the momentum equation (Equation 3.2) over time

$$\int \frac{\partial u}{\partial t} dt = \int -g\frac{\partial \eta(x,t)}{\partial x} dt$$

Substituting $\eta(x,t) = q_0 J_0(2\sqrt{\kappa x})\cos\omega t$ into the above equation leads to

$$u = \int -g\frac{\partial q_0 J_0(2\sqrt{\kappa x})\cos\omega t}{\partial x} dt$$

$$u = -g\frac{\partial J_0(2\sqrt{\kappa x})}{\partial x}\int q_0 \cos\omega t dt$$

$$u = -\frac{g}{\omega}\left[-\sqrt{\frac{\kappa}{x}}J_1(2\sqrt{\kappa x})\right] q_0 \sin\omega t$$

$$u = \frac{g}{\omega^2}\sqrt{\frac{\kappa}{x}}J_1(2\sqrt{\kappa x})\dot{q}(t)$$

or

$$u = \frac{s}{\kappa h}\sqrt{\frac{\kappa}{x}}J_1(2\sqrt{\kappa x})\dot{q}(t)$$